Faculté des Sciences Appliquées
Département ArGEnCo
Géomécanique et Géologie de l'ingénieur
Prof. R. CHARLIER

STUDY OF THE THERMO-HYDRO-MECHANICAL BEHAVIOUR OF A CLAY REPOSITORY

SCOPING CALCULATIONS

TIMODAZ PROJECT

G. Tyberghein, F. Collin & R. Charlier

June 2007

Université de Liège – ArGEnCo
www.argenco.ulg.ac.be/geo3

Institut de Mécanique et de Génie Civil, Chemin des Chevreuils 1, Bât. B52/3 B 4000
Liège 1 - Sart Tilman– Belgique
Tél.: 04/366.93.34 ; Fax: 04/366.93.26
E-mail : Robert.Charlier@ulg.ac.be

TABLE DES MATIERES

1 INTRODUCTION 3

2 MODELISATION OF THE CLAY REPOSITORY 4

2.1 GEOMETRY 4
2.2 CONSTITUTIVE MODEL AND PARAMETERS 4
2.3 INITIAL CONDITIONS 6
2.4 BOUNDARY CONDITIONS 6
2.5 THERMAL SOURCE THERMS 8
2.5.1 PC case 8
2.5.2 I1 case 10
2.5.3 I2 case 12
2.6 THERMO-HYDRO-MECHANICAL SOLICITATIONS 14

3 TEST CASE 1 : HEATING UNDER DRAINED CONDITION AT ROCK WALL 15

3.1 PC CASE 15
3.1.1 Results : reference case (PCA) 15
3.1.2 Comparison of results for different heat fluxes 24
3.2 I1 CASE 28
3.2.1 Results : reference case (I1A) 28
3.2.2 Comparison of results for different heat fluxes 35
3.3 I2 CASE 36
3.3.1 Results : reference case (I2A) 36
3.3.2 Comparison of results for different heat fluxes 43

4 TEST CASE 2 : HEATING UNDER UNDRAINED CONDITION 44

4.1 RESULTS FOR PC CLAY 44
4.1.1 Temperature 44
4.1.2 Pore pressure 44
4.1.3 Displacement 45
4.1.4 Stress paths 46
4.2 COMPARISON BETWEEN THE DRAINED AND UNDRAINED CASES 50
4.2.1 Pore pressure 50
4.2.2 Displacement 50
4.2.3 Stress paths 51
4.3 RESULTS FOR I1 CLAY 52
4.4 RESULTS FOR I2 CLAY 53

5 TEST CASE 3 : HEATING UNDER DRIPPING CONDITION 55

5.1 SATURATED CASE 56
5.2 UNSATURATED CASE 57

6 PARAMETRIC SENSITIVITY STUDY 58

6.1 THERMAL CONDUCTIVITY COEFFICIENT 58
6.1.1 PC 58
6.1.2 I1 60
6.2 DILATATION ANGLE (PC) 61
6.3 MECHANICAL PARAMETERS (C,Φ) (I2) 63
6.4 BIOT COEFFICIENT (I1) 65
6.5 PERMEABILITY (I2) 67
6.6 CONSTITUTIVE LAW SENSIBILITY STUDY (PC) 70
6.6.1 Van Eekelen 70
6.6.2 CapSol model with thermal softening 71

1 INTRODUCTION

During the review of the TIMODAZ project, we were asked to clarify how the present project could achieve the estimation of the ultimate thermal limits of the clays in the context of the long term performance of the repository design. It was then proposed in the meeting held in June at Liège to perform some scoping calculations to study this particular aspect.

Previous studies revealed that the Thermo-Hydro-Mechanical (THM) responses of a host formation in a repository depend highly on the boundary conditions, especially the hydraulic one. Moreover, thermal solicitations conditions (thermal sources terms : variable heat flux) influence too the THM responses of the host formation. Consequently, different numerical **tests cases** will be proposed.

We will not consider specifically some host formations, but try to evaluate the behaviours of a range of argillaceous formations, from plastic (PC) to indurated (I1, I2) clays, as representative of the main underground laboratories in clayey layers.

Taking into account the fact that there still exist uncertainties on some parameters (for example, the thermal conductivity of the PC), some parametric sensibility studies will be proposed too.

The objective of the scoping calculations is thus to study, numerically, the THM responses of the host formations under different conditions and thus to have an insight on the most critical conditions (important influencing factors) for the THM behaviour of the host formation including the thermal limits of it. These analyses are intended to be a guide, a first lighting, for the experimental tests to be conducted within the TIMODAZ project.

2 MODELISATION OF THE CLAY REPOSITORY

2.1 GEOMETRY

We propose to treat the problem as a one-dimensional problem (radial-axisymmetric) that is an idealization of the excavation of a cylindrical cavity in a porous isotropic infinite medium. The excavation will eventually be followed by a liner installation of thickness “e” which allows a given convergence α_{exc} and a heating phase corresponding to the injection of a given thermal flux at the lining. Let’s note that gravity is not considered in this modelling.

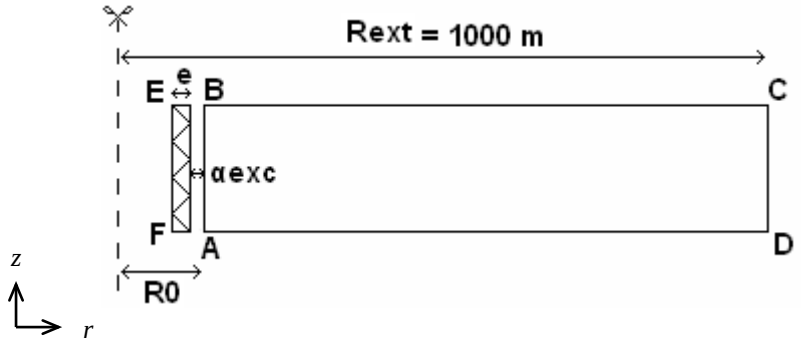

Figure 1 : Problem geometry

The segment AB represents the tunnel surface. The inner radius R_0 is equal to 2 m for PC clay, 0.35 m for I1 clay and 1.25 m for I2 clay. The external radius R_{ext} of the slice is chosen at least 100 times the tunnel radius to be sure that the stresses on the external boundary are not influenced, thus we chose R_{ext} = 1000 m for the three kinds of clay.

The clay repository is meshed in 80 isoparametric finite elements, that is 8 sections which are themselves divided in 10 elements. The liner is meshed in 10 finite elements. An interface element is placed between the liner and the gallery wall. It allows the passage of heat flux and water flow once the two elements are in contact.

2.2 CONSTITUTIVE MODEL AND PARAMETERS

We propose to use a Mohr-Coulomb model (elasto-perfect plasticity) and a thermo-hydraulic coupled law as the thermo-hydro-mechanical constitutive model of clay (reference case). In this model, the variation of temperature induces only elastic deformations. Alternatively, an internal friction model (Van Eekelen) as well as a model with thermal softening will be used. This will be explained later.

Here are the thermo-hydro-mechanical characteristics of the three clays constituting the repository (Table 1, 2 and 3). The properties are given for the initial temperature and pore water pressure. However, we suppose that the parameters are temperature independent.

Geomechanical characteristics		PC	I1	I2
Young's elastic modulus [MPa]	E'	300	5000	5000
Poisson's ratio [-]	υ'	0.125	0.3	0.27
Specific mass [kg/m³]	ρ	2026	2400	2340
Cohesion [MPa]	c'	0.3	3.5	8.6
Friction angle [°]	$\varnothing'$	18	25	24.6
Dilatation angle [°]	ψ	0	0	0
Coefficient of Biot [-]	b	1	1	1

Table 1 : Geomechanical characteristics

Hydraulic characteristics		PC	I1	I2
Porosity	n	0.39	0.18	0.137
Permeability [m/s]	$k_v = k_h$	4.10^{-12}	5.10^{-14}	2.10^{-13}
Fluid dynamic viscosity [Pa.s]	μ	10^{-3}	10^{-3}	10^{-3}
Liquid compressibility coefficient [MPa^{-1}]	χ_{fl}	5.10^{-4}	5.10^{-4}	5.10^{-4}

Table 2 : Hydraulic characteristics

Thermic characteristics		PC	I1	I2
Thermal conductivity [W/(mK)]	λ	1.35	1.75	1.5
Heat capacity [J/(kg.K)]	C_p	2300	1000	920
Solid thermal expansion coefficient [K^{-1}]	α_s	10^{-5}	10^{-5}	2.10^{-5}
Liquid thermal expansion coefficient [K^{-1}]	α_w	3.10^{-4}	3.10^{-4}	3.10^{-4}

Table 3 : Thermic characteristics

The liner is supposed to be elastic. Here are its thermo-hydro-mechanical characteristics for the three cases :

Liner properties		PC	I1	I2
Young's elastic modulus [GPa]	E	50	205	No liner
Poisson's ratio [-]	υ	0.2	0.3	
Thickness [cm]	e	30	2.5	
Porosity [-]	n	0.1	0.1	
Permeability [m/s]	$k_v = k_h$	4.10^{-10}	5.10^{-12}	
Thermal conductivity [W/(mK)]	λ	1.5	35	
Volumetric heat capacity [MJ/(m³K)]	c_v	1.8	3.925	
Solid thermal expansion coefficient [K^{-1}]	α_s	$1.2*10^{-5}$	$1.7*10^{-5}$	
Liquid thermal expansion coefficient [K^{-1}]	α_w	3.10^{-4}	3.10^{-4}	

Table 4 : Liner properties

Note : The liner is watertight, but, for the scoping calculation, in order to be able to take into account the different hydraulic conditions, we propose to consider that the liner is permeable.

Interface elements properties :

Thermal flow interface element properties		
Porosity	n_0	0.3
Transverse transmissivity	T_{T_c}	10^{10}
Hydraulic flow interface element properties		
Porosity	n_0	0.3
Transverse transmissivity	T_{H_c}	10^{-8}

Table 5 : Interface element properties

2.3 INITIAL CONDITIONS

The clay formation around the gallery is considered as homogeneous and isotropic. The initial stresses are supposed to be lithostatic ($\sigma_0 = \sigma_h = \sigma_v = \rho.g.z$, ρ is the material specific mass, g the gravity acceleration and z the depth). In addition, the modelling zone is supposed to be sufficiently deep so that the variation of the stresses and pore pressure with depth is neglected. The formation is supposed to be completely saturated. Initial conditions to be considered are listed in table 6 :

Initial state		**PC**	**I1**	**I2**
Total stresses [MPa]	σ_H	4.5	12	22.6
	σ_v	4.5	12	22.6
Pore pressure [MPa]	P_{w0}	2.25	5	5
Effective stresses [MPa]	σ'_H	2.25	5	17.6
	σ'_v	2.25	7	10.9
Temperature [°C]	T_0	16	22	38

Table 6 : Initial state – stresses, pore water pressure and temperature

2.4 BOUNDARY CONDITIONS

Mechanical boundary conditions are imposed such as :

- the axial displacements are fixed on the boundaries AD, DC and BC
- the radial stress is fixed equal to σ_H on the boundary CD

Hydraulic boundary conditions are imposed such as :

- the boundaries AD and BC are impermeable
- P_w is fixed equal to P_{w0} on the boundary CD

Thermal boundary conditions are imposed such as :

- the boundaries AD and BC are adiabatic
- T is fixed equal to T_0 on the boundary CD

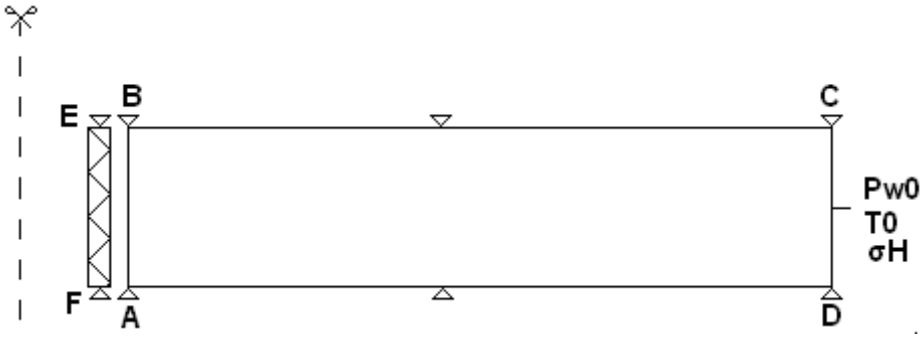

Figure 2 : Boundary conditions

To simulate the excavation, the total radial stresses and the water pressure at the tunnel face (AB) decrease linearly to 100 kPa (so that the effective stresses are equal to zero). If a liner is required (PC and I1 cases), the convergence of the gallery is controlled and the liner is placed to allow a given convergence α_{exc}. At the end of the excavation, the contact is realised between the soil and the liner. The excavation is then followed by a one-year open drift period during which the liner face EF (when there is a liner) or the gallery wall AB (when there is not a liner) is supposed to be under drained conditions (the pore water pressure is fixed to be equal to the atmospheric pressure) or dripping conditions.

During the heating phase, various boundary conditions are imposed on the liner inner face EF. These boundary conditions are of two types : a given decreasing heat flux and a hydraulic condition (drained, undrained or dripping). This will be explained in details in the following chapters.

2.5 THERMAL SOURCE THERMS

2.5.1 PC CASE

Concerning the thermal source terms for the scoping calculations of PC clay, we propose to study two kinds of wastes : VHLW and MOX55. The heat fluxes of these two wastes in function of the time after their production are given in the figure 3.

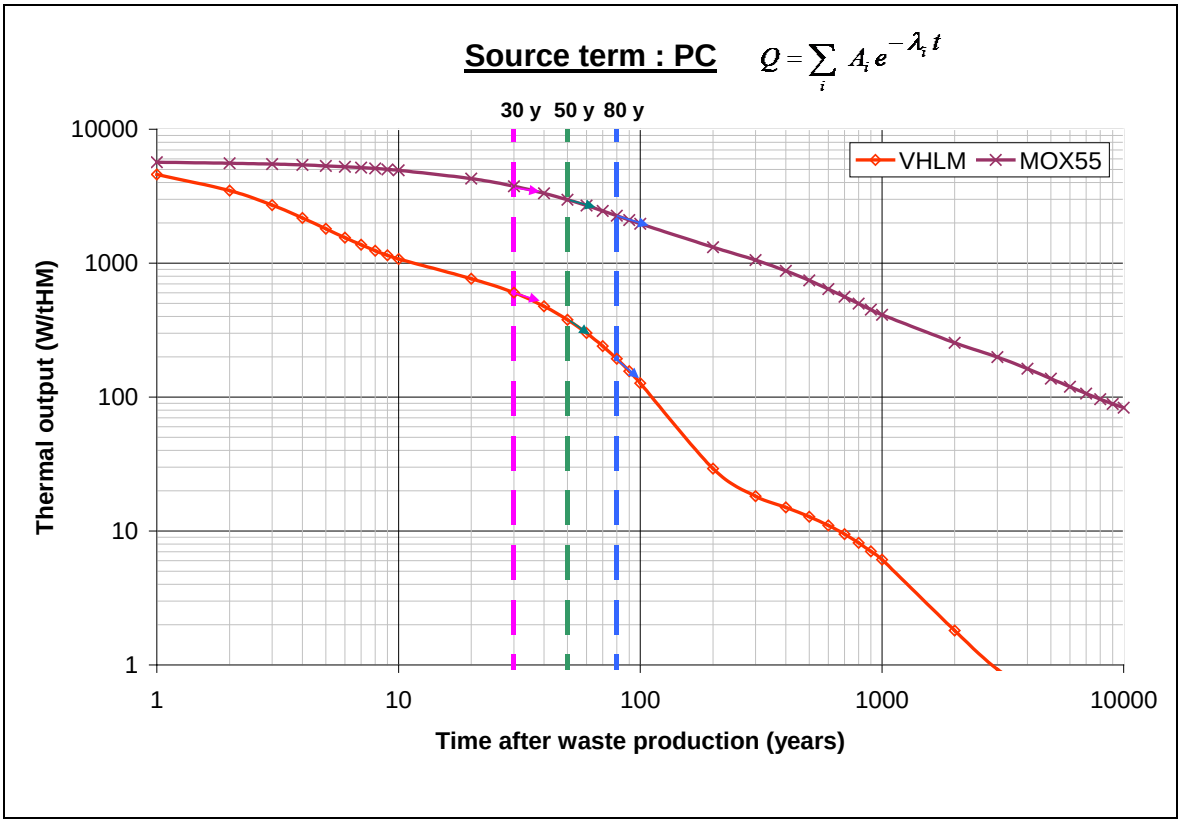

Figure 3 : Time evolution of heat flux (W/tHM) of two kinds of wastes after their production (PC case)

The heat production of the wastes is calculated thanks to the following equation :

$$Q = \sum_i A_i e^{-\lambda_i t}$$

where Q is expressed in W/tHM and t in years.

Note : tHM (tonnes Heavy Metal) refers to the initial mass of the wastes.

For the Vitrified High Level Waste (VHLW) :

Vitrified High Level Waste (VHLW)	**A1**	5021	**λ1**	0.3894
	A2	1205	**λ2**	0.02458
	A3	27.04	**λ3**	1.63E-03
	A4	0.7576	**λ4**	6.546E-05
	A5	0.1	**λ5**	0

For Spend Fuel – MOX55 :

Spent Fuel - MOX55	**A1**	3782	**λ1**	0.02273
	A2	1545	**λ2**	0.002844
	A3	326.4	**λ3**	0.000374
	A4	100.6	**λ4**	2.86E-05

For each of the wastes, three cases of degradation before storage in the gallery are considered :

- after 50 years of storage (**Reference case**) ;
- after 30 years of storage ;
- after 80 years of storage.

Totally, we have 6 thermal source terms to be applied directly on the gallery liner :

Wastes	Cooling time on surface		
	50 years	30 years (hot case)	80 years (cold case)
VHLW	**A (reference case)**	B	C
MOX50	D	E	F

Table 7 : Thermal source terms to be considered for PC case

For the scoping calculations, we need to express these thermal source terms in terms of linear thermal load density (W/m). The conversion depends on the repository designs.

For PC case, we consider the Supercontainer designs for both VHLW and Spent Fuel. The parameters are given in table 8 :

Wastes	tHM/canister	Linear thermal load density (axial)
SF : MOX 55	0.45665	1 canister/6.216 m
VHLW	1.33	2 canisters/4.2 m

Table 8 : Supercontainer design considered for PC case

This gives the linear thermal density (W/m) as shown in figure 4 below :

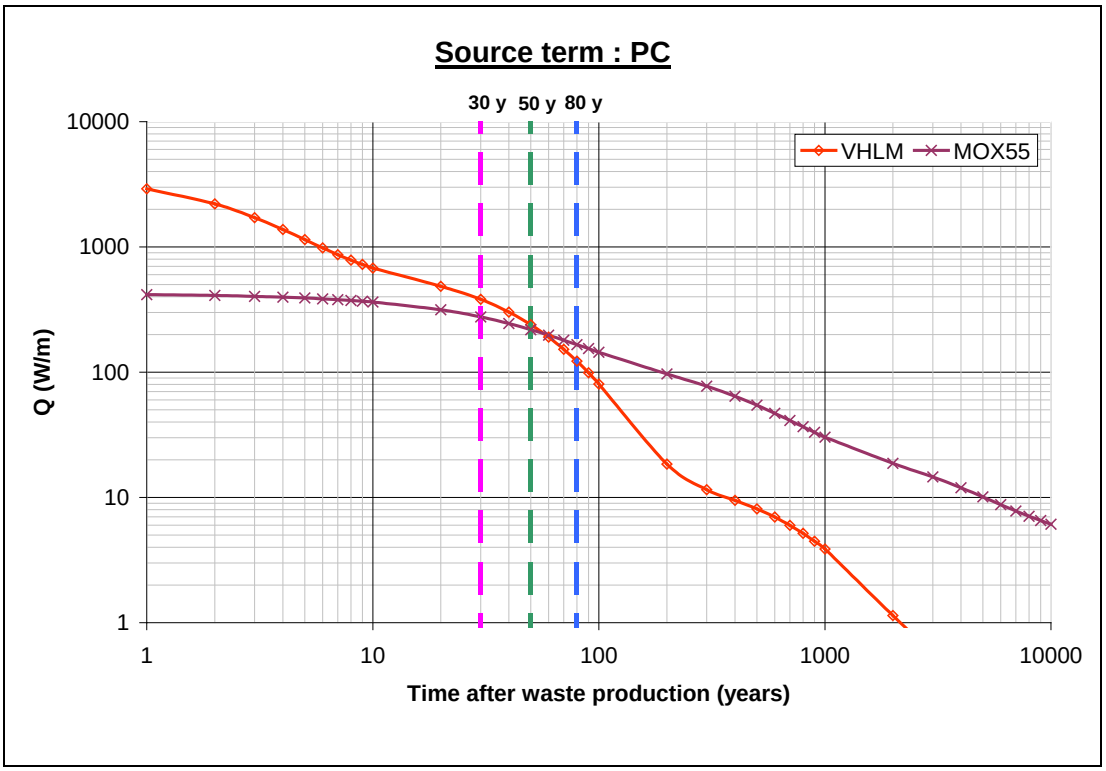

Figure 4 : Thermal flux evolution (W/m) of the Supercontainer design for PC case

2.5.2 I1 CASE

For I1 case, the vitrified HLW C1 will be considered. The evolution of the nominal thermal power in function of the time after its production is given at the Figure 5.

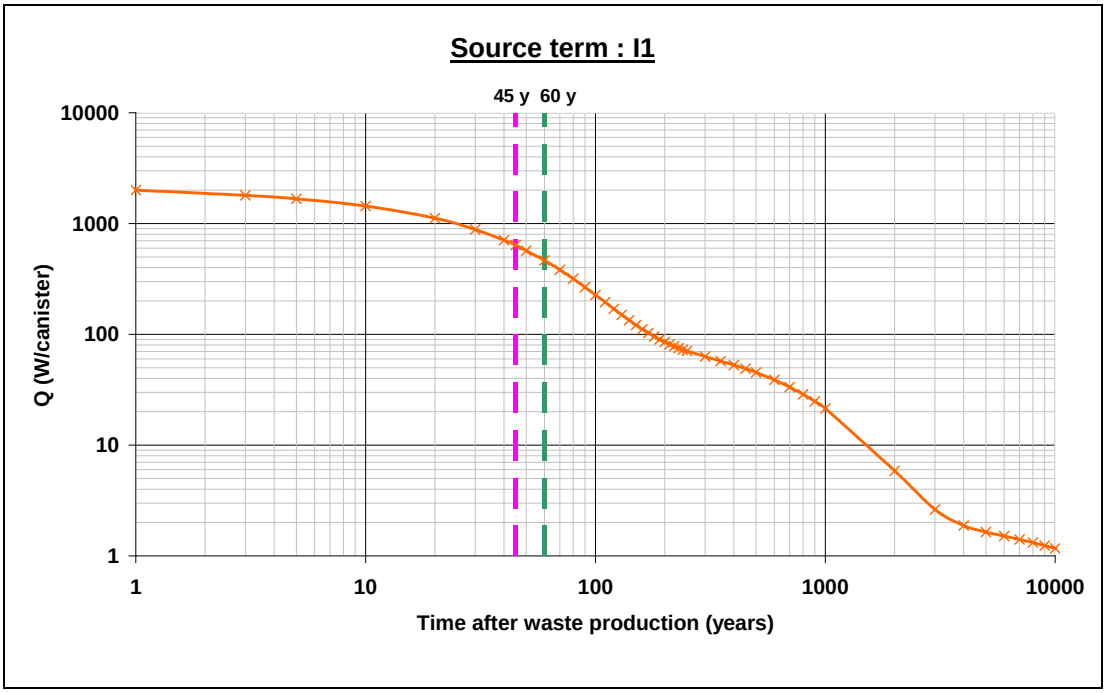

Figure 5 : Time evolution of the nominal thermal power of the HLW type C (W/canister) after unloading from reactor

The design schema (alvéole C) is given in Table 9.

Wastes	Linear thermal load density (axial)
HLW type C1	8 canisters/32 m

Table 9 : HLW type C1 repository design considered for I1 case

The heat flux of considered waste in function of the time after unloading from reactor is given in Figure 6. The intermediate storage time to be considered in the modelling will be 45 and 60 years (hot and normal case).

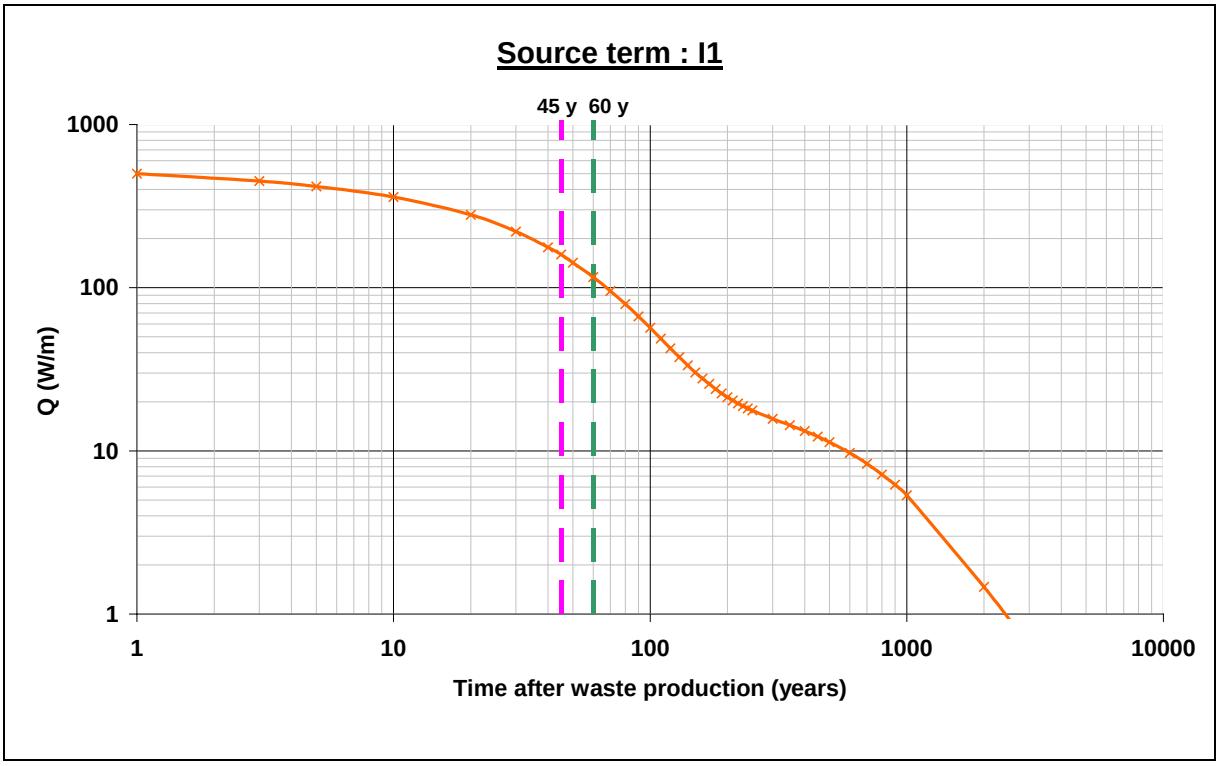

Figure 6 : Thermal flux evolution (W/m) of the HLW type C1 design for I1 case

2.5.3 I2 CASE

For I2 case, the spent fuel waste BE will be considered. The evolution of the nominal thermal power in function of the time after its production is given at the Figure 7.

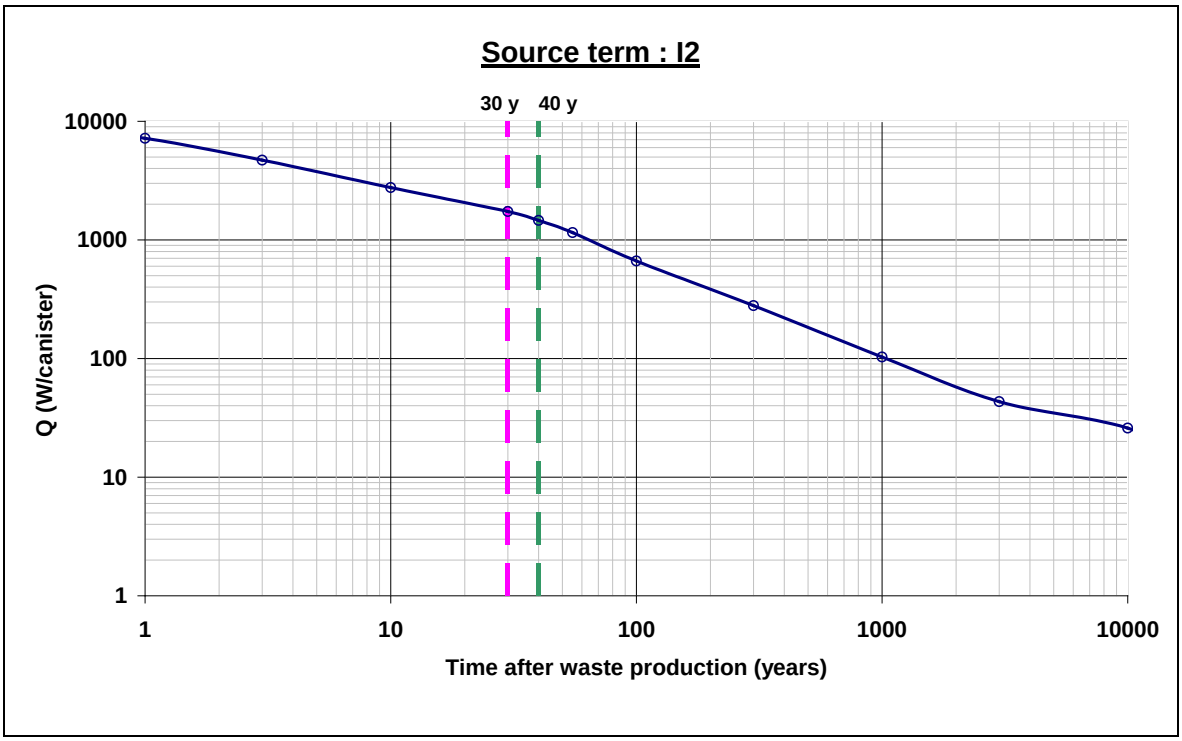

Figure 7 : Time evolution of the nominal thermal power of the Spent fuel BE (W/canister) after unloading from reactor

The design schema (BE container repository design) is given in Table 10.

Wastes	Linear thermal load density (axial)
Spent fuel (BE-3 PWR UO2 container)	1 container /7 m

Table 10 : The BE container repository design considered for I2 case

The heat flux of considered waste in function of the time after unloading from reactor is shown at Figure 8. The intermediate storage time to be considered in the modelling will be 30 and 40 years (hot and normal case).

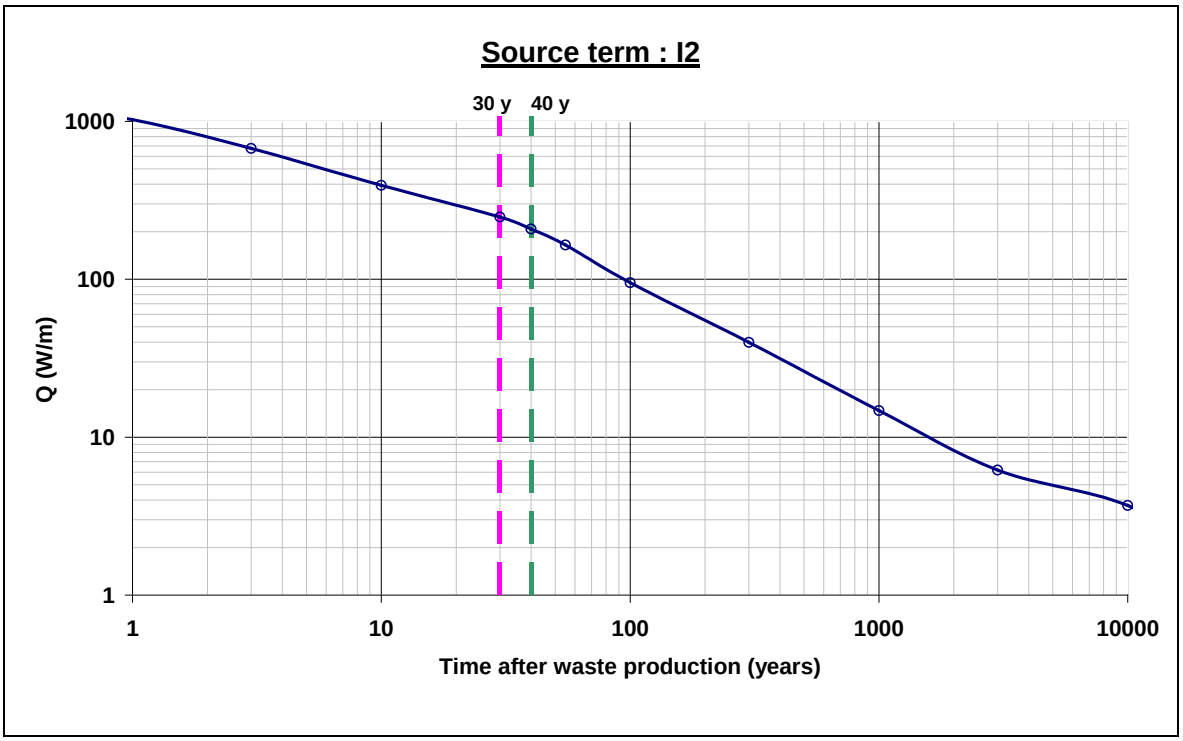

Figure 8 : Thermal flux evolution (W/m) of the Spent Fuel design for I2 case

2.6 THERMO-HYDRO-MECHANICAL SOLICITATIONS

Here is the general definition for the simulations where t_{exc} is the end time of excavation, t_{liner} the end time of the liner installation, $t_{drainage}$ is the open drift time after construction of the gallery during which the gallery is considered to be under drained or dripping conditions.

- Excavation (t_{exc}):

Excavation of the gallery is realized within t_{exc} days by reducing linearly the total radial stresses and the water pressure at the tunnel surface (AB) at the atmospheric pressure 0,1 MPa (so that the effective stresses are equal to zero).

  - PC : t_{exc} = 3 days
  - I1 : t_{exc} = 3 days
  - I2 : t_{exc} = 1 day

- Liner installation (t_{liner})

The liner allows a given convergence α_{exc} before contact with the host rock. Once the contact is realised, an interface element allows hydraulic and thermal fluxes between the host rock and the liner.

  - PC : immediate after excavation
  - I1 : immediate after excavation
  - I2 : no liner

- Open drift time after construction of the gallery ($t_{open\text{-}drift}$ = 1 year)

Two boundary conditions at the liner inner surface EF (liner) or at the gallery wall AB (no liner) are studied. The first one is to consider the gallery under drained condition during a year (test case 1 and 2) and the second one under dripping conditions (test case 3).

- Heating (t_{heat} = 1000 years)

Canisters are placed in the gallery and a decreasing heat flux is given out at the liner inner surface EF (liner) or at the gallery wall AB (no liner). The simulation duration is 1000 years.

During this phase, various hydraulic boundary conditions are imposed on the liner inner face EF (liner) or at the gallery wall AB (no liner) : drained conditions (test case 1), undrained conditions (test case 2) or dripping conditions (test case 3).

3 TEST CASE 1 : HEATING UNDER DRAINED CONDITION AT ROCK WALL

3.1 PC CASE

3.1.1 RESULTS : REFERENCE CASE (PCA)

The excavation of the gallery and the liner installation are realized within 3 days. The water pressure at the tunnel face (AB) decreases linearly to the atmospheric pressure. The convergence of the gallery (face AB) is controlled and the liner is placed to allow a convergence α_{exc} = 9 cm.

The excavation is followed by a one-year open drift period during which the liner face (EF) is supposed to be under drained conditions : the pore water pressure is fixed to be equal to the atmospheric pressure. During the thousand-years heating phase, the gallery is still supposed to be drained : the pressure remains at 100 kPa. The heat flux considered is the VHLW after 50 years. The conductibility parameter taken for the soil is λ = 1.35 W/(mK) and the dilatancy angle ψ = 0 °. The elasto-plastic model used is a Mohr-Coulomb model.

Temperature, displacements, pore pressures and stress state are analysed during the excavation of the test drift and over a thousand-year period after the excavation. In particular, stress state are computed at r = R_1, r = $2R_1$, r = $5R_1$ and r = $10R_1$.

3.1.1.1 Temperature

Figure 9 presents the evolution of flux and temperature at the gallery wall. The first year, there is no heat injection and temperature in clay remains constant (T = 16 °C). Once the decreasing heat flux is applied (Q_0 = 23.7 W/m²), temperatures in the rock mass progressively rise. At the gallery wall, the highest temperature (T_{max} = 68.3 °C) is reached after more or less 10 years of heating. Let's note that "two years" of simulation corresponds to "one year" of heating, "eleven years" to "ten years", etc.

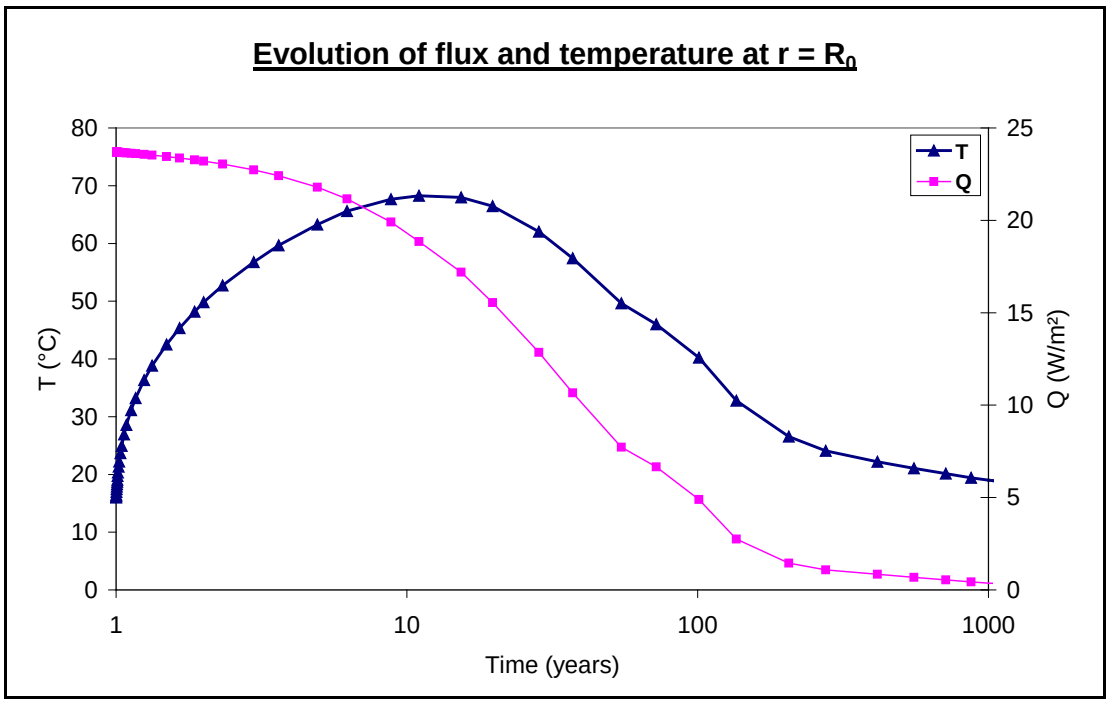

Figure 9 : Flux and temperature evolution at r = R_0 (semi-logarithmic scale)

Figure 10 presents temperature profile at different period of time during the heating stage. We note that significant changes in temperature are limited in space to a radius of 100 meters. Nevertheless, the far field is also slightly disturbed. At 1001 years, temperatures have nearly returned to their initial state (16°C) : the temperature at the gallery wall being equal to 19°C.

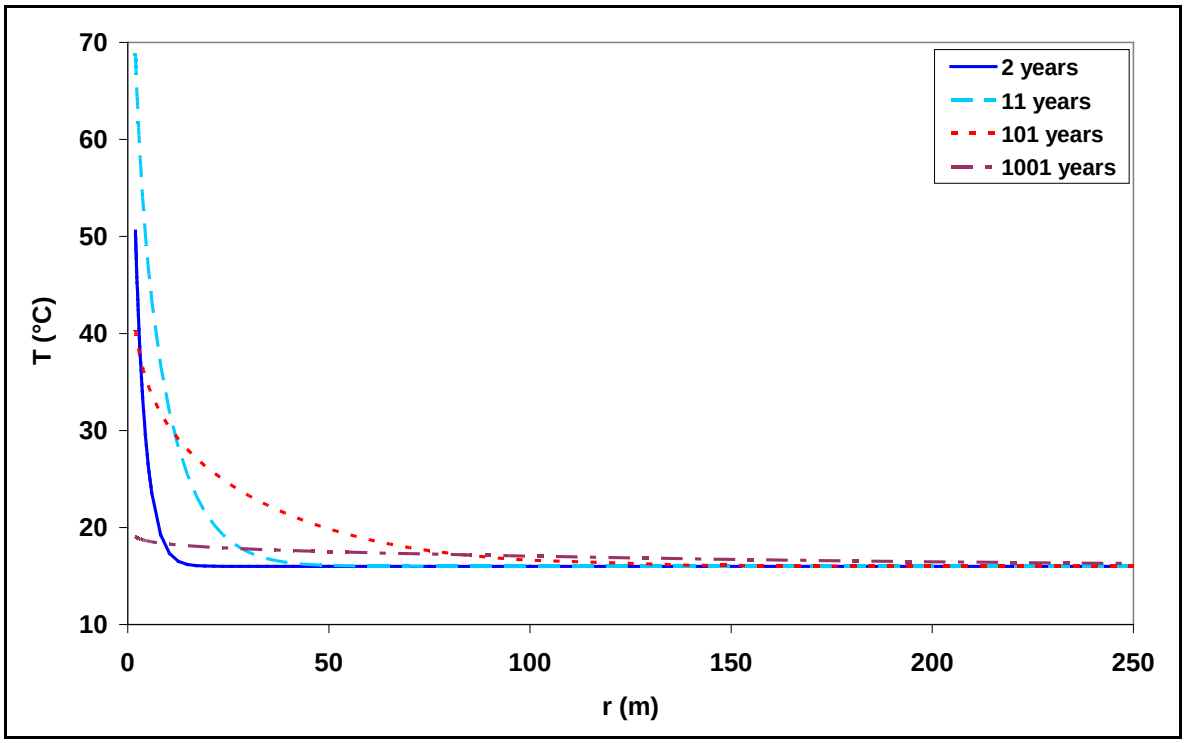

Figure 10 : Radial profile of temperature at different periods (heating)

3.1.1.2 Pore pressure

Figure 11 shows the radial profile of pore pressure during and at the end of excavation (3 days), after 15 days and 1 year of drained conditions a the lining. We note that during the excavation (day 1, 2 and 3), the pressure at the gallery wall decreases linearly to 100 kPa. With time, pore pressure distribution takes a profile corresponding to the fact that the gallery acts as a drain for the rock mass. In the far field (r > 13 meters), pore pressure distribution is not influenced.

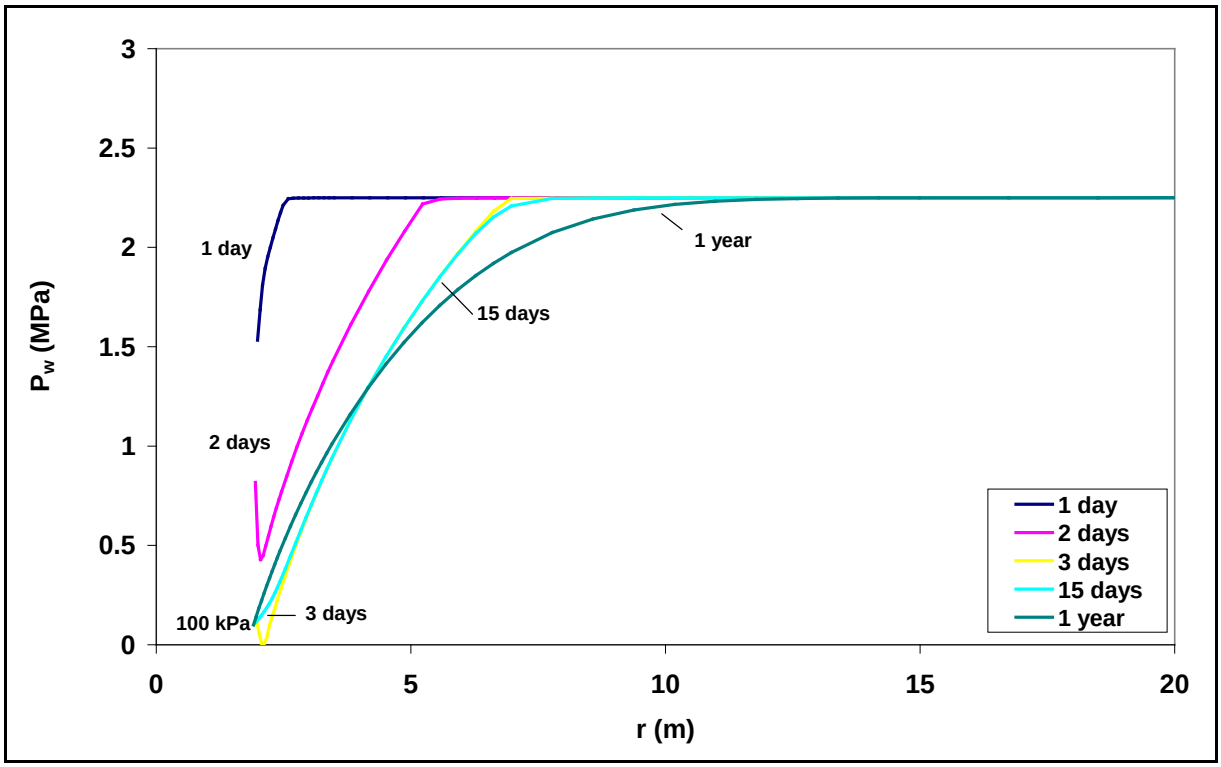

Figure 11 : Radial profile of pore water pressure at different periods during the excavation (3 days) and the drainage (1 year)

Figure 12 presents the radial profile of pore pressure at different periods (2 years, 11 years, 101 years and 1001 years) during the heating phase. Let's note that "two years" corresponds to "one year" of heating, "eleven years" to "ten years", etc. From 2 years to 11 years, pore pressure increases with time near the gallery wall. This is due to the rise of temperature which causes a dilatation of grains and water. Consequently, as there is less pore space and that the water dilates, the pressure increases. The largest overpressure (190 kPa) at the time steps considered is observed at a radius of 16 m after 10 years of heating. After this period, as the temperature is decreasing until returning to its initial state, the pore water pressure drops. The outline after 1000 years of heating confirms that the gallery acts as a drain for the clay. The hydraulic disturbed zone is limited in space and the influence can be observed until the 150 meters.

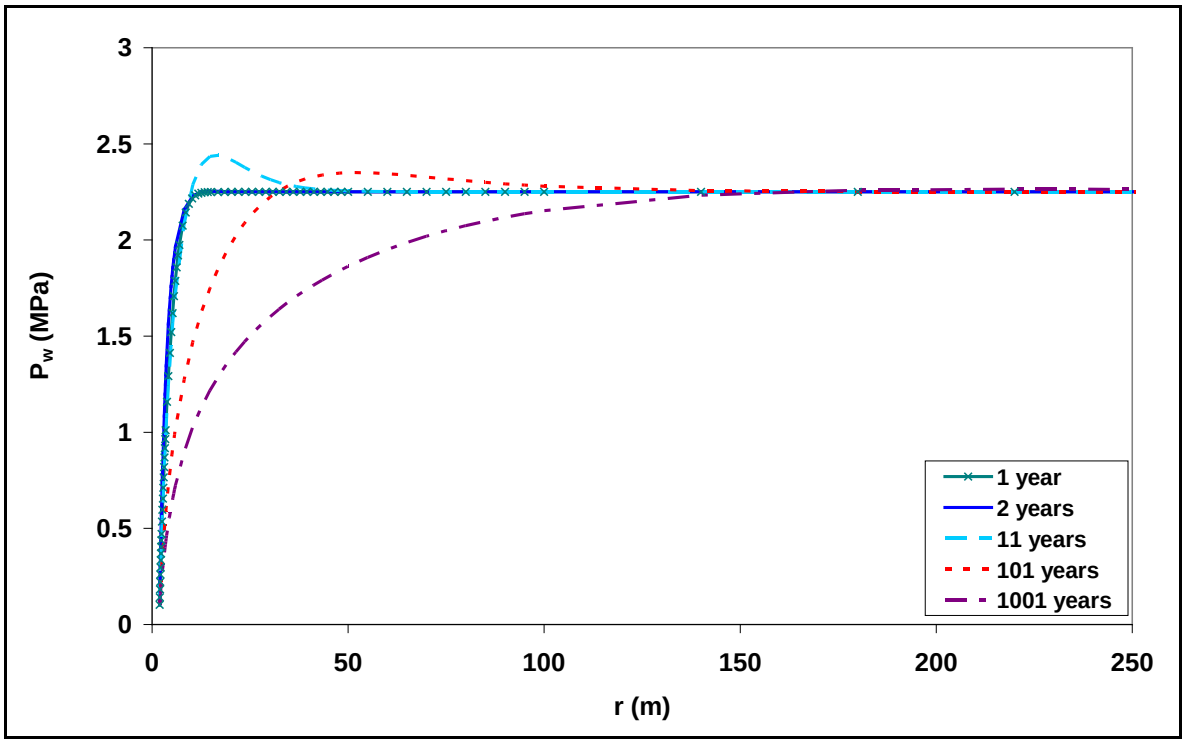

Figure 12 : Radial profile of pore water pressure at different periods during the heating phase

3.1.1.3 Displacement

When releasing total stress, the gallery wall converges and a negative radial displacement is measured until the clay comes in contact with the lining : α_{exc} = 9 cm (Figure 14). Once the contact is established, displacement rate drops down to zero until the end of excavation (3 days). During the one-year drainage phase, no major change in displacements is observed.

After 10 years of heating, we observe on Figure 14 small positive radial displacements from a radius of 30 meters until the far field which are due to the rise of temperature. Over 11 years, once the temperature decreases and given the pore pressure and effective stresses changes, we observe negative displacements. At first, these are limited at the near field (101 years) but then propagate to the whole rock mass (1001 years). The highest radial displacements (5.5 cm) are measured around 65 meters from the gallery.

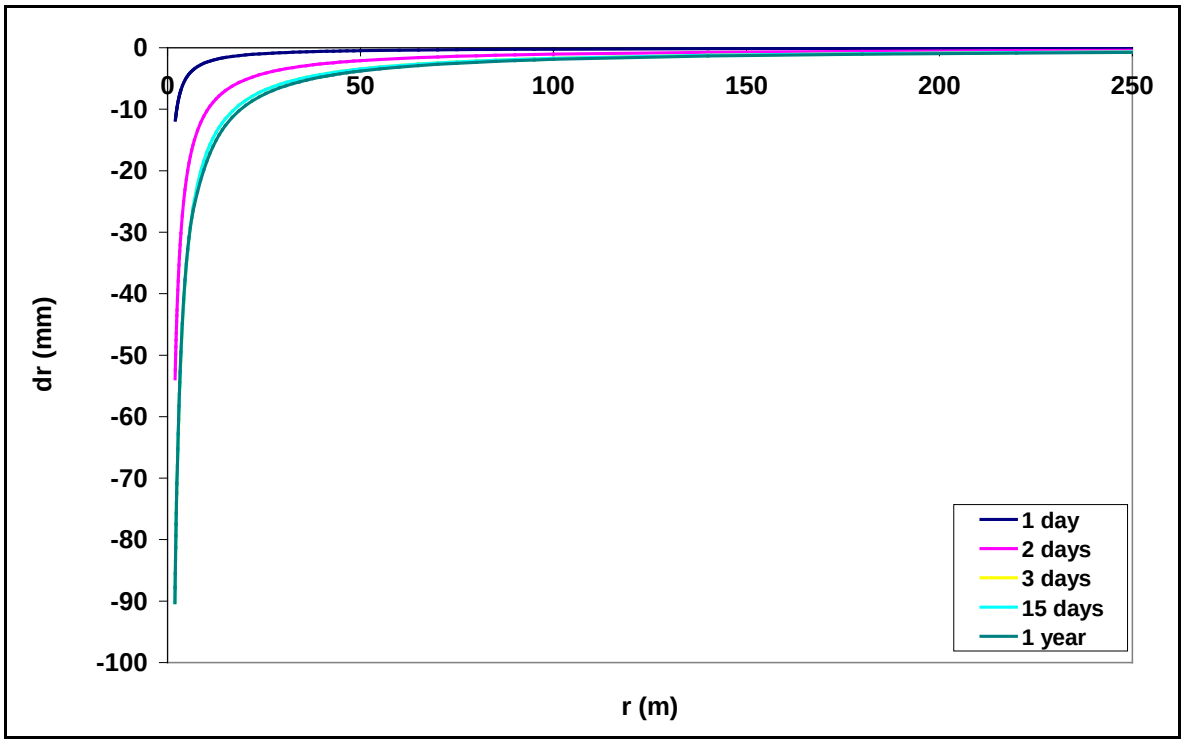

Figure 13 : Radial profile of radial displacement during excavation and open drift period

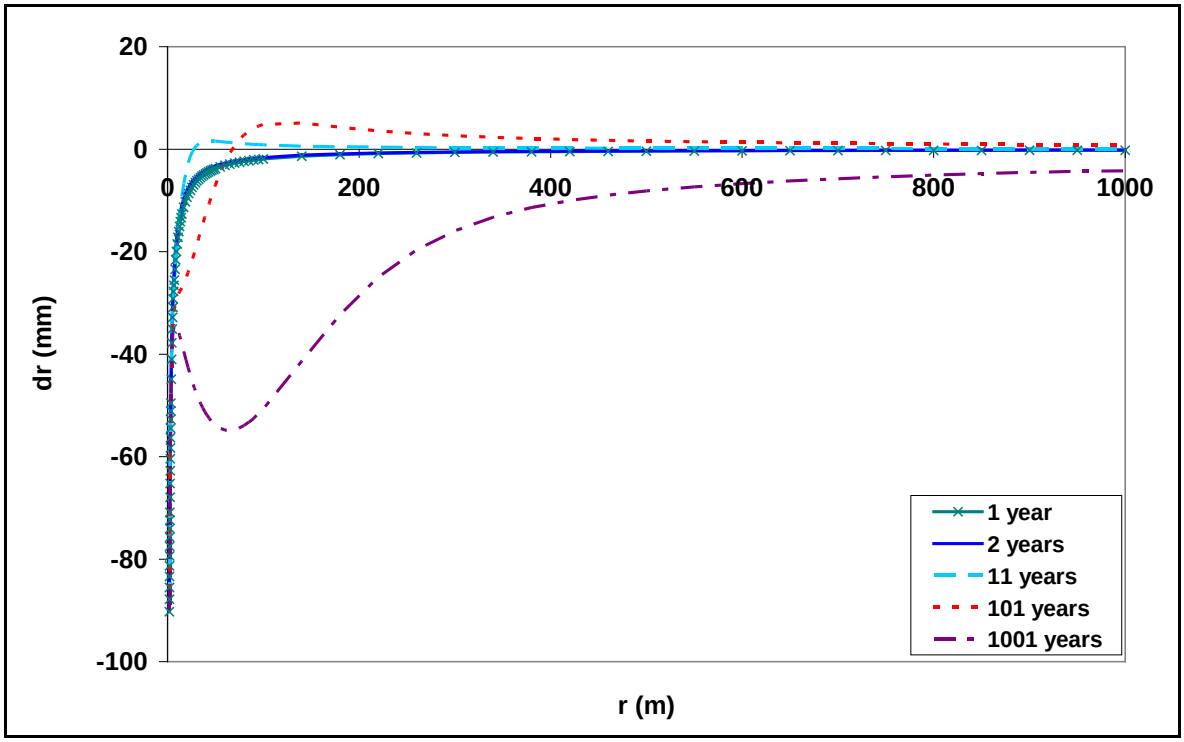

Figure 14 : Radial profile of radial displacement at different periods during heating phase

3.1.1.4 Stress paths

Figure 15 shows the deviatoric stress at the gallery wall in function of the time. Figure 16 and Figure 17 show radial profiles of radial and orthoradial effective stress at different periods.

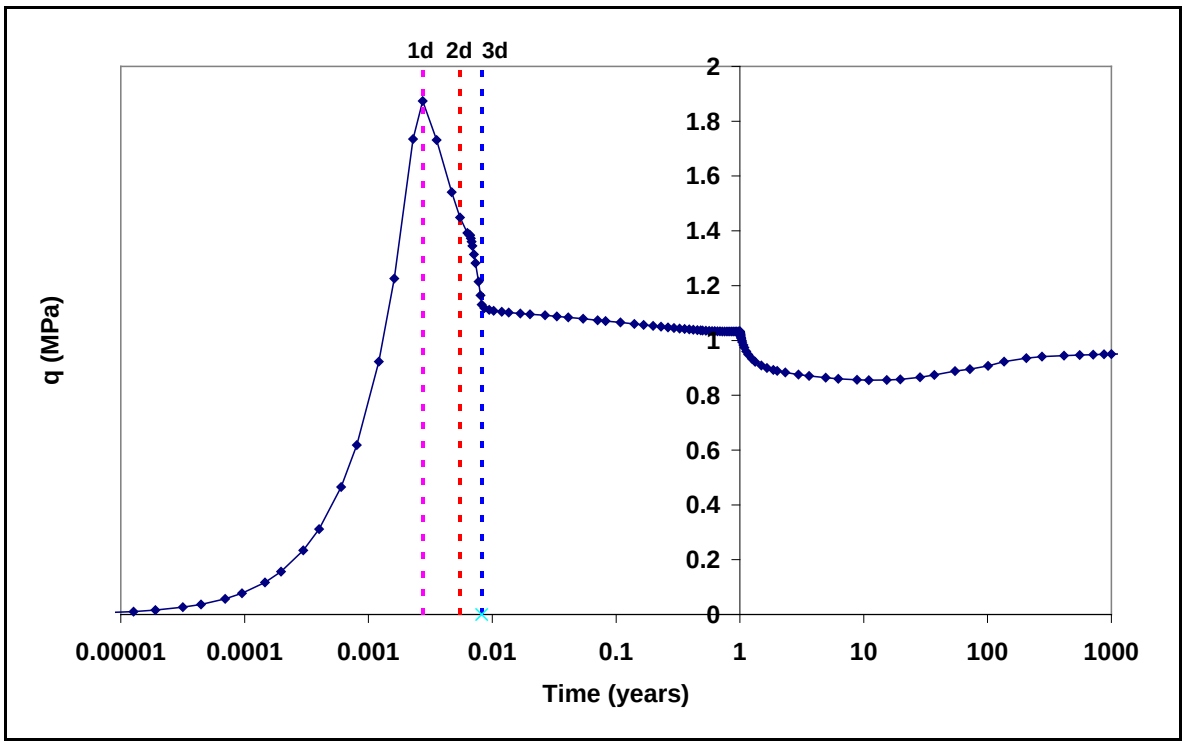

Figure 15 : Deviatoric stress at the gallery wall ($r = R_0$) in function of the time

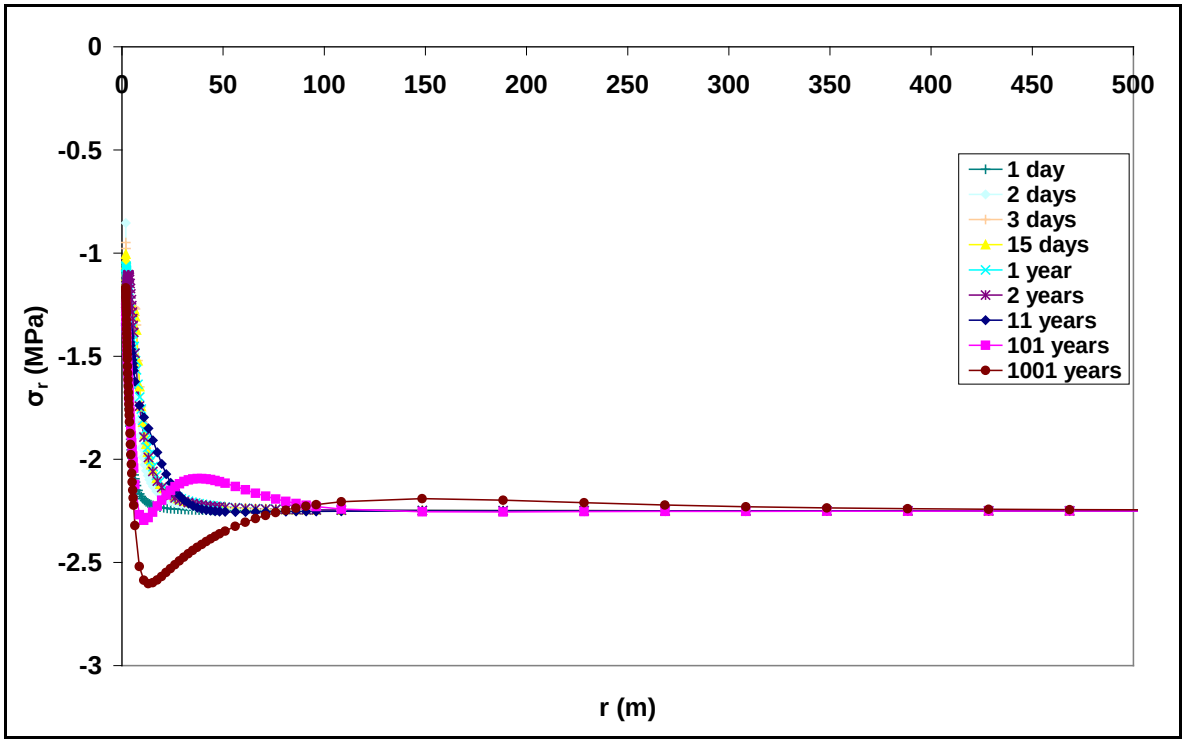

Figure 16 : Radial profile of radial effective stress at different periods

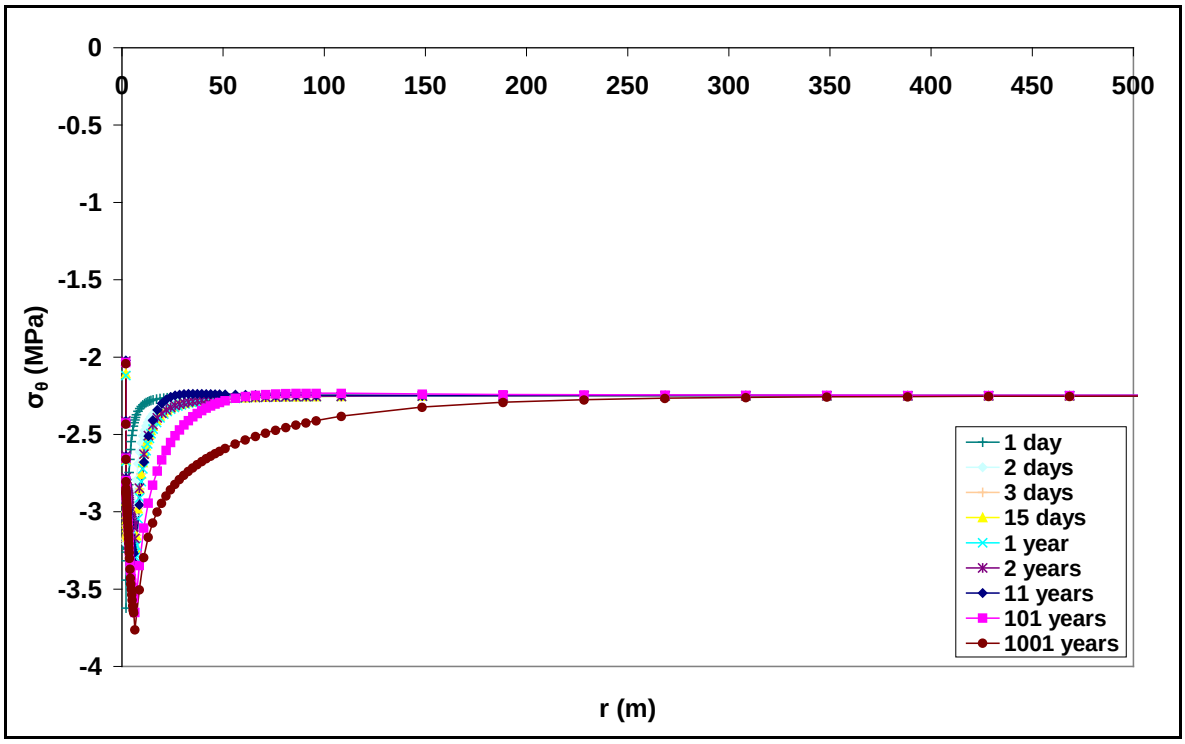

Figure 17 : Radial profile of orthoradial effective stress at different periods

Figure 18 and Figure 19 show the effective stress path of clay at different radius R_0 = 2m, 2 R_0, 5 R_0 and 10 R_0 in the (p', q) stresses plane. Figure 18 relates in details the stress evolution during the excavation (3 days), during the drainage of the gallery, during the increase of temperature and finally during the temperature decrease. Figure 19 summarizes the different stress paths on the same graph. The initial Mohr-Coulomb yield limit is also plotted.

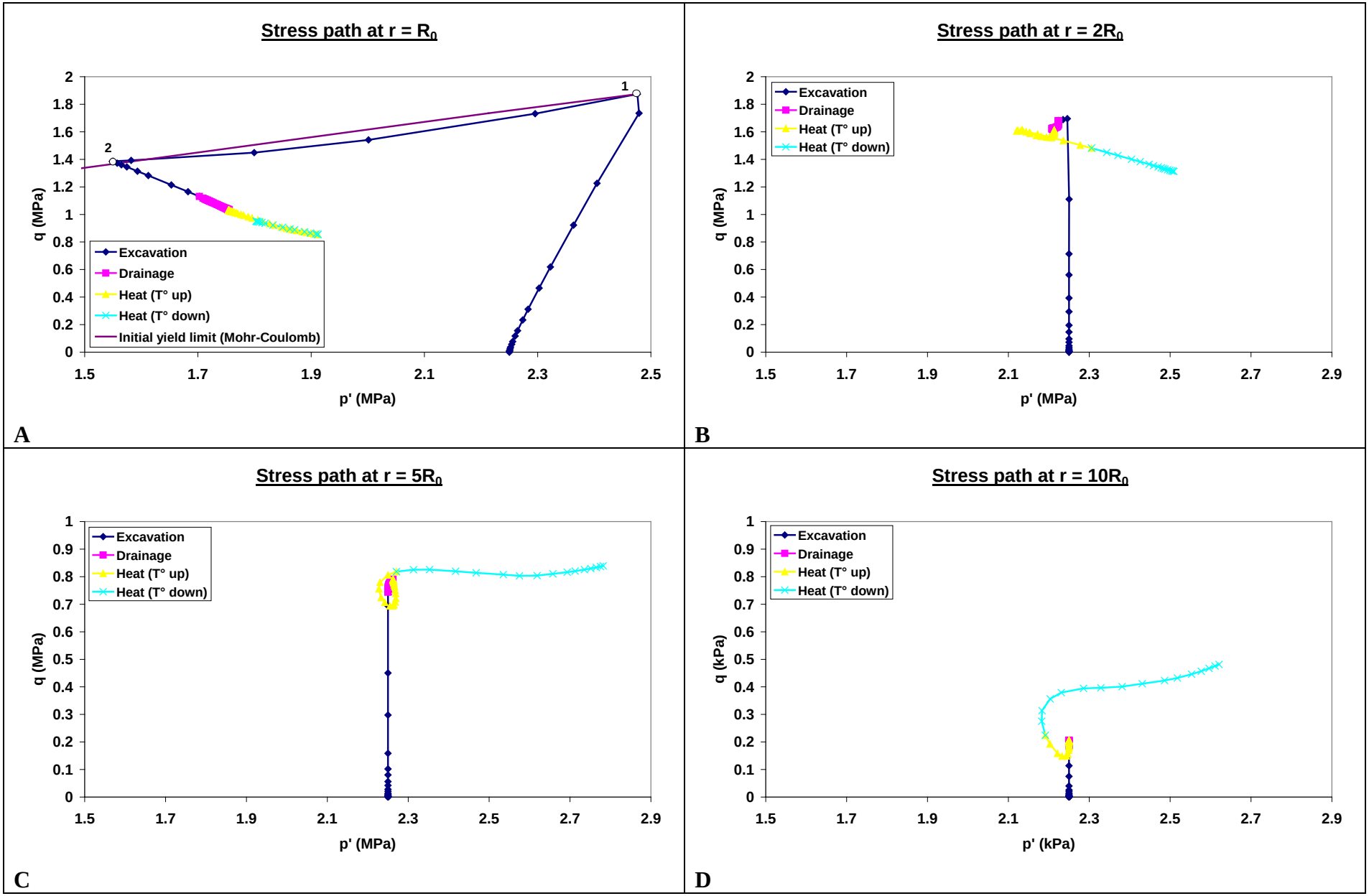

Figure 18 : Effective stress paths at r = R_0, r = $2R_0$, r = $5R_0$ and r = $10R_0$

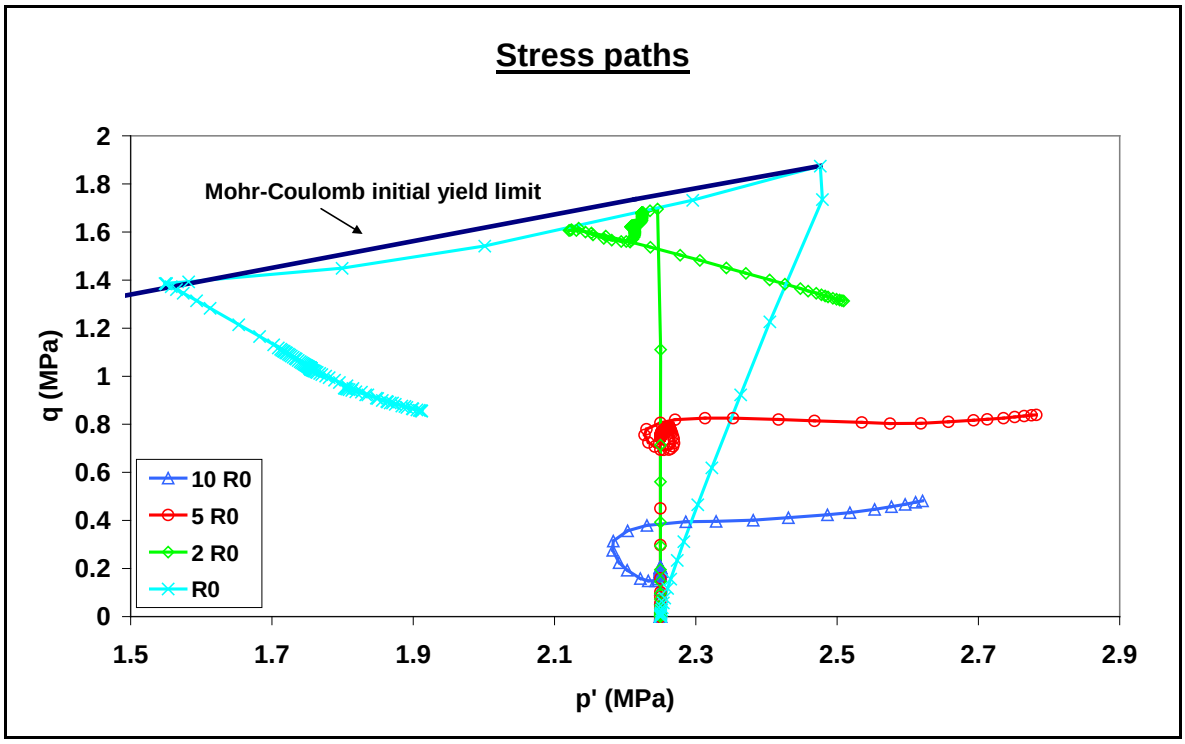

Figure 19 : Effective stress paths at r = R_0, r = $2R_0$, r = $5R_0$ and r = $10R_0$

The initial stress state is isotropic and located in the elastic domain as shown on Figure 19.

Figure 18A : When total stress and pore pressure on the gallery wall start decreasing (excavation), the mean stress increases and the deviatoric stress increases until the stress state reaches the yield limit (stage 1). As there is no hardening possible, the stress path is then obliged to follow the yield limit until the clay comes in contact with the lining (stage 2). At this stage the plastic radius reaches its maximum and is equal to 6.7 m. Let's note that only the initial yield limit is plotted and that this one changes in the (p', q) axes. Thus the clay is in a plastic state from 1 to 2. Once the contact with the liner is realised, there is a progressive stress release of the rock so that the stress state is elastic : the mean stress slightly increases and the deviatoric stress decreases. The drainage of the gallery (from 3 days to 1 year) is still characterised by a progressive stress release of the rock mass which continues while the temperature increases. When the temperature of clay decreases, the stresses follow the inverse way (reversibility).

Figure 18B C and D: The stress state at r = 2 R_0 is plastic at the end of the excavation but after that remains elastic. The stress states at r = 5 R_0 and 10 R_0 stay elastic during the whole mechanical and thermal loading.

3.1.2 COMPARISON OF RESULTS FOR DIFFERENT HEAT FLUXES

The modelling procedure is identical. Let's remind that it is divided in three stages. First, releasing the total radial stress and the pore pressure on the gallery wall down to zero simulates the excavation. Stress release lasts 3 days. Within these three days, the clay comes in contact to the rigid lining initially located at 9 cm far from the clay. In the second stage, the drainage of the gallery is modelled during 1 year. Finally, the third stage is the placing of the canister from which a heat flux is given off. As it has been mentioned before, calculations for six different thermal source terms are realized, that is Vitrified High Level Waste and Spent Fuel MOX55 after 30, 50 and 80 years of cooling on surface (Table 11).

Wastes	Cooling time on surface		
	50 years	30 years	80 years
VHLW	**A (reference case)**	B	C
MOX50	D	E	F

Table 11 : Thermal source terms to be considered

The evolutions of the input values (thermal flux) imposed at the gallery lining are shown on the Figure 20 below.

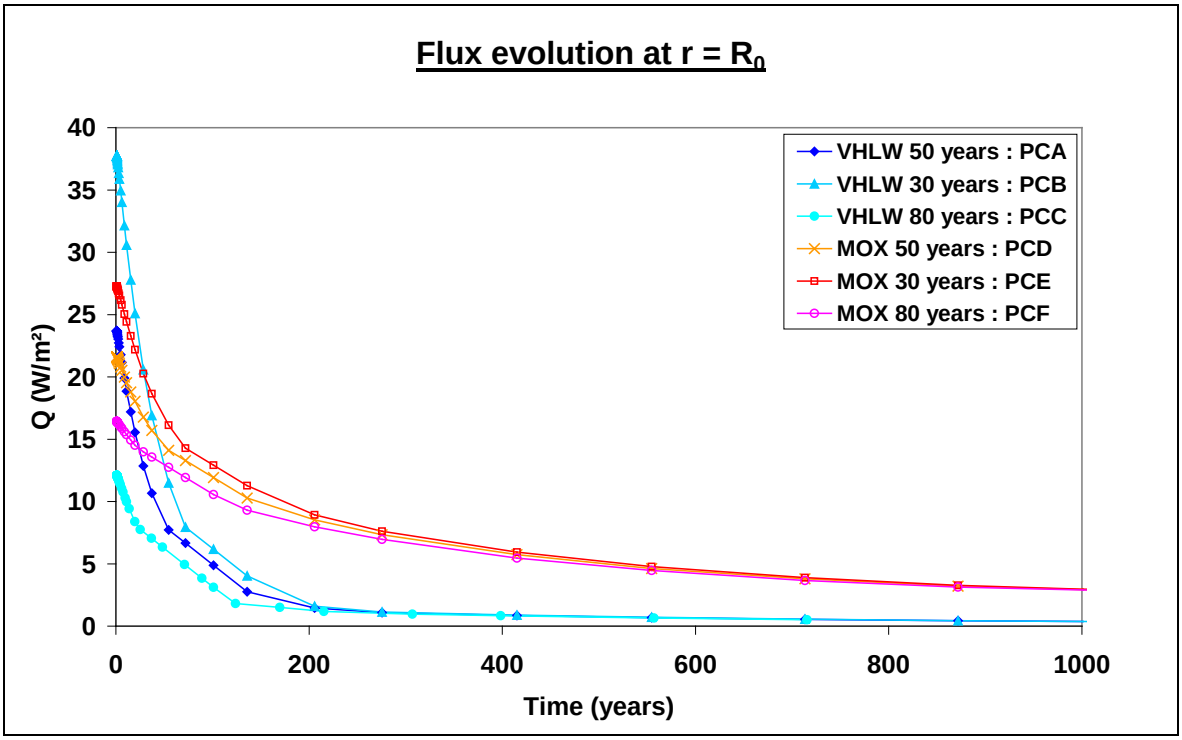

Figure 20 : Thermal heat sources comparison

3.1.2.1 Temperature

The evolution of temperature at the gallery wall is shown on the Figure 21 below. We observe two tendencies depending of the type of waste. For the MOX, the rise and decrease of temperature is slower than the VHLW. Moreover, the temperature after 1000 years of simulations stays relatively high for MOX (34°C) while for VHLW the temperature has nearly returned to its initial state (19°C).

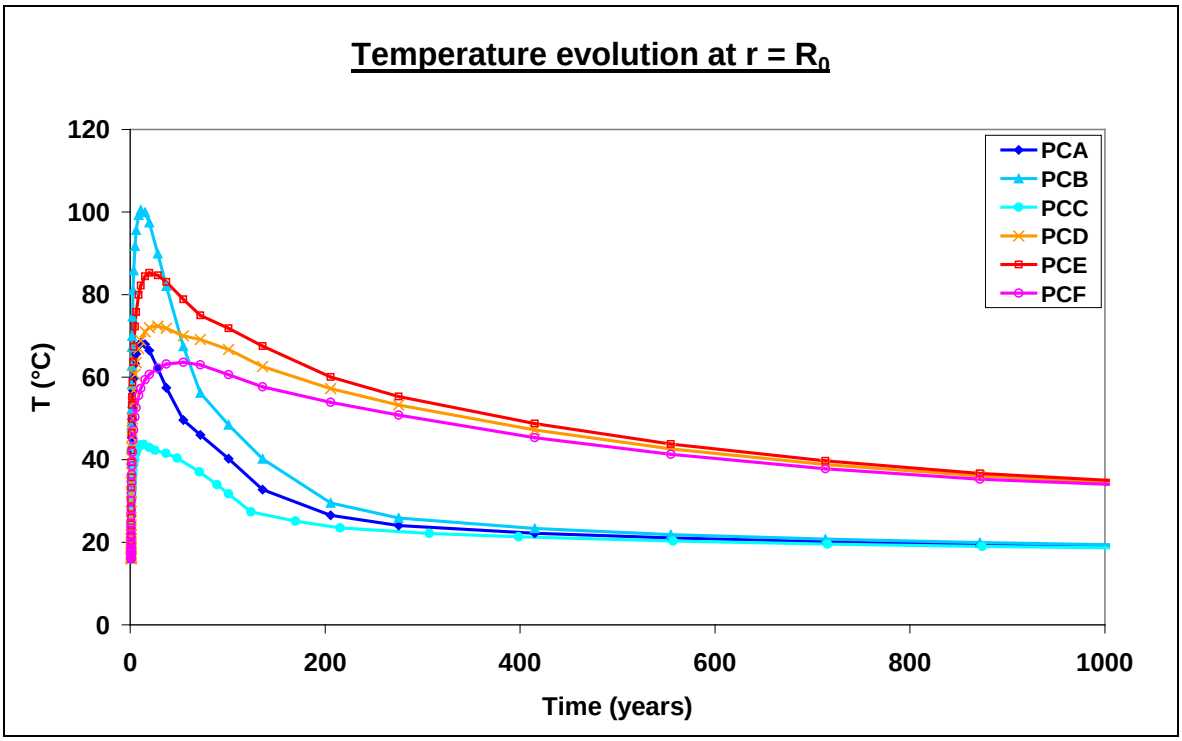

Figure 21 : Temperature evolution for 6 heat sources - Comparison

Table 12 recapitulates the highest temperatures reached at the gallery wall for the different types of wastes. This can be quite interesting if a maximum temperature criterion in the clay host rock is fixed. For example, if we allow a maximum temperature of 90 °C, we note that the VHLW after 30 years of cooling on surface would not be allowed in the clay repository.

	T_{max} (°C)	t (years)
PCA	68.3	11
PCB	100.5	11
PCC	43.7	13.9
PCD	72.4	28.5
PCE	85.3	19.7
PCF	63.6	54.6

Table 12 : Highest temperatures reached at the gallery wall - Comparison

3.1.2.2 Pore pressure

Figure 22 represents the pressure profile in function of the time during the heating phase for VHLW after 30, 50 and 80 years of cooling on surface. The pore pressures during the excavation and drainage are not shown on the figure since they are identical to the reference case.

The tendency for the 3 cases is similar. First from 2 years to 11 years, pore pressure increases with time near the gallery wall. The higher is the temperature, the larger is the overpressure (180 kPa for the reference case, 390 kPa for the VHLW 30 years and 60 kPa for VHLW 80 years). This confirms that the rise of temperature induces a diminution of pore space (solid dilatation) and a water dilatation, which causes an increase of water pressure. After this period, as the temperature is decreasing until returning to its initial state, the pore water pressure drops. The pore pressure remains higher for the case inducing higher temperature. After 1000 years of heating, as the temperatures are nearly identical in the 3 cases, pressure profiles are superposed.

The conclusions stay also true for the spent fuel MOX55.

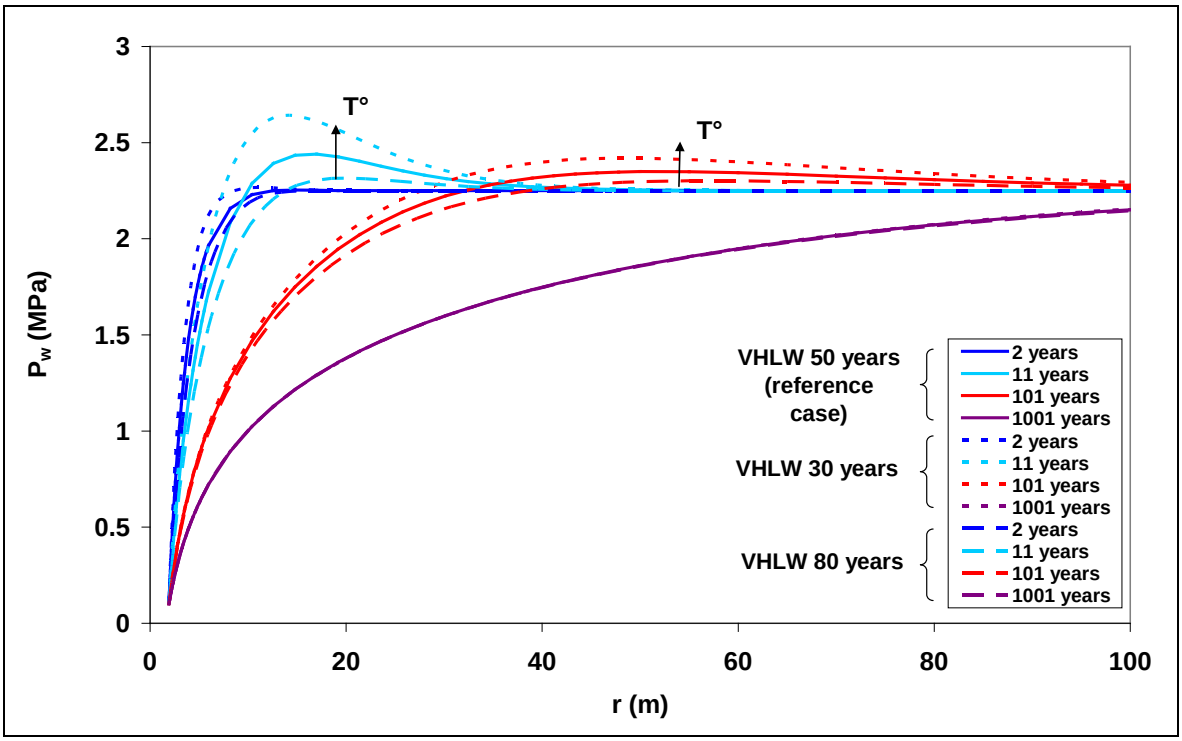

Figure 22 : Radial profile of pore water pressure for VHLW after 30, 50 and 80 years of cooling on surface

3.1.2.3 Displacement

Figure 23 represents the radial profile of displacement in function of the time during the heating phase for VHLW after 30, 50 and 80 years of cooling on surface. The displacements during the excavation and drainage are not shown on the figure since they are identical to the reference case.

Once again, the tendency for the 3 cases is similar. First, from 2 years to 11 years, we observe small positive radial displacements which are due to the rise of temperature. The higher is the temperature, the bigger is the positive displacement. After this period, once the temperature decreases, we observe negative displacements. At first, these are limited at the near field (101 years) but then propagate to the whole rock mass (1001 years). The positive displacements remain higher for the case inducing higher temperature. The conclusions stay also true for the spent fuel MOX55 (Figure 24).

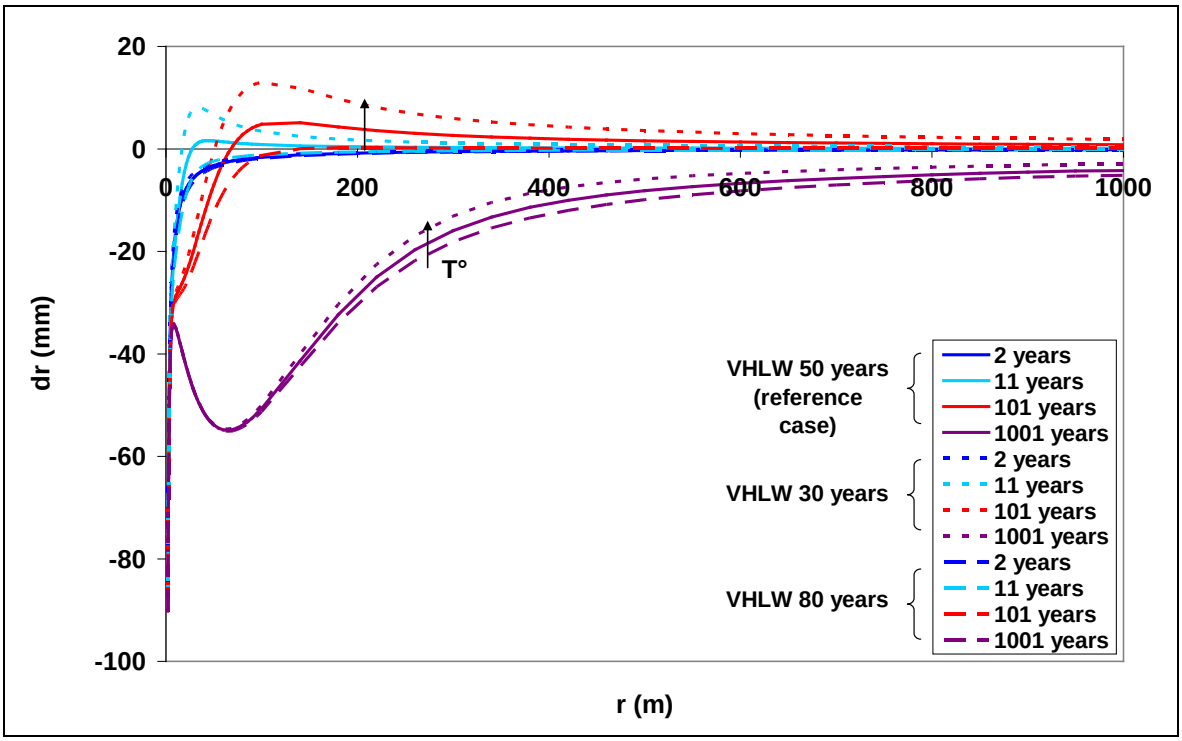

Figure 23 : Radial profile of displacement for VHLW after 30, 50 and 80 years of cooling

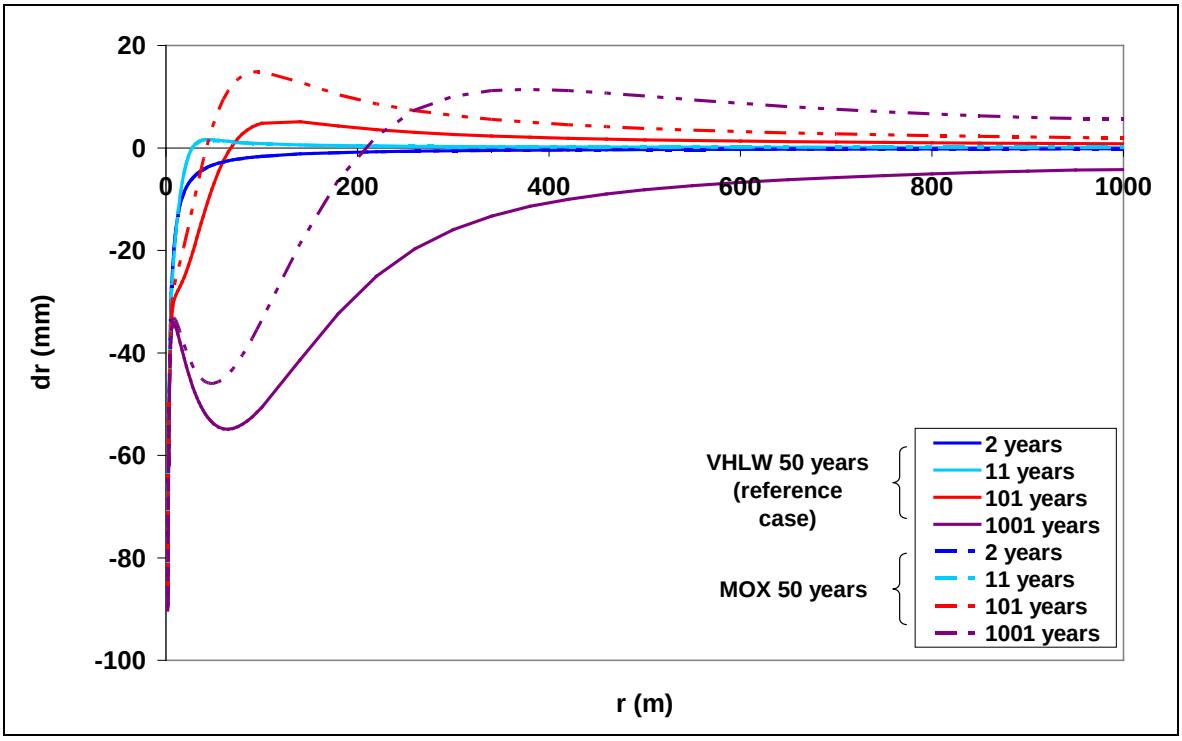

Figure 24 : Radial profile of displacement for VHLW and MOX after 50 years of cooling on surface

3.1.2.4 Stress path

Figure 25 represents the stress paths for VHLW placed after 30, 50 and 80 years of cooling at different radius. We observe that the extreme deviatoric and mean stresses are identical in all

cases : p_{min} = 1550 kPa, p_{max} = 2800 kPa, q_{min} = 0 kPa and q_{max} = 1840 kPa. We note that at the gallery wall the thermal loading and unloading induce reversible stress state and that the amplitude of the unloading is all the larger as the thermal variation is high.

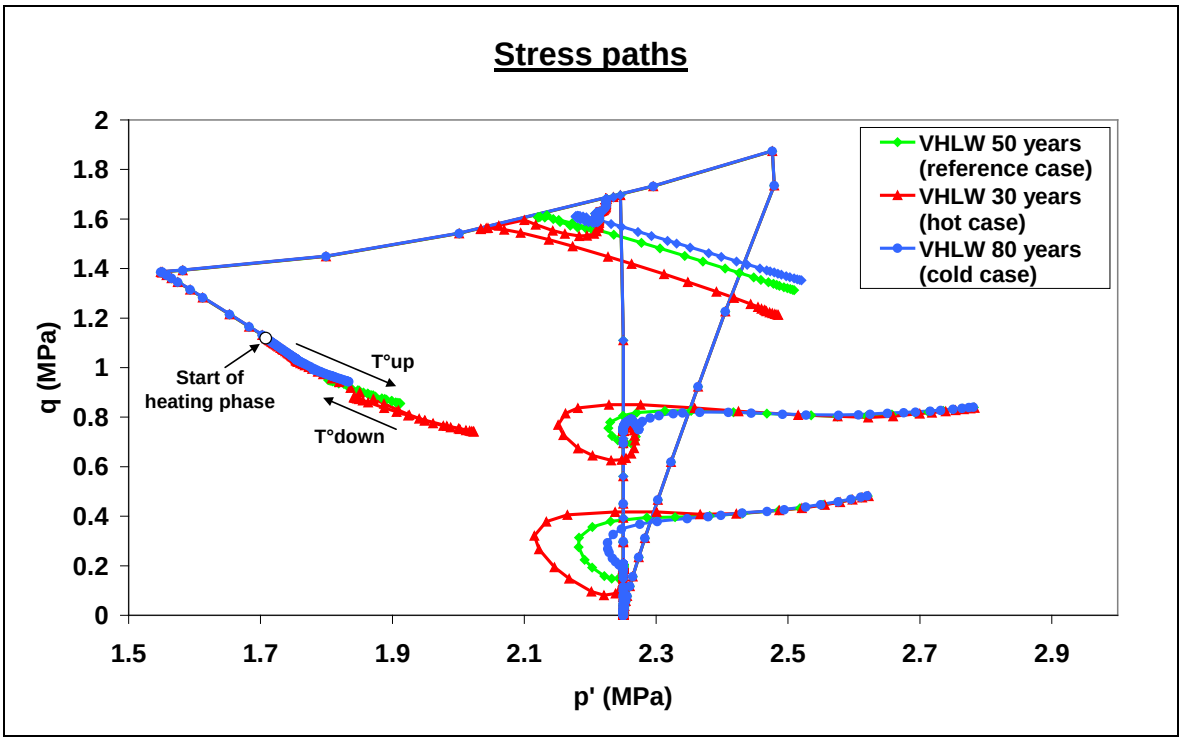

Figure 25 : Stress paths for VHLW after 30, 50 and 80 years of cooling at different radius

3.2 I1 CASE

3.2.1 RESULTS : REFERENCE CASE (I1A)

The excavation of the gallery and the liner installation are realized within 3 days. The water pressure at the tunnel face (AB) decreases linearly to the atmospheric pressure. Once the excavation is over, the liner is placed immediately.

The excavation is followed by a one-year open drift period during which the liner face (EF) is supposed to be under drained conditions : the pore water pressure is fixed to be equal to the atmospheric pressure. During the thousand-years heating phase, the gallery is still supposed to be drained : the pressure remains at 100 kPa. The heat flux considered is the HLW after 60 years. The conductibility parameter taken for the soil is λ = 1.75 W/(mK) and the permeability k = 5.10^{-14} m/s °. The elasto-plastic model used is a Mohr-Coulomb model.

Temperature, displacements, pore pressures and stress state are analysed during the excavation of the test drift and over a thousand-year period after the excavation. In particular, stress state are computed at r = R_1, r = $2R_1$, r = $5R_1$ and r = $10R_1$.

3.2.1.1 Temperature

Figure 26 presents the evolution of flux and temperature at the gallery wall. The first year, there is no heat injection and temperature in clay remains constant (T = 22 °C). Once the decreasing heat flux is applied (Q_0 = 57.2 W/m²), temperatures in the rock mass progressively

rise. At the gallery wall, the highest temperature (T_{max} = 58.8 °C) is reached after more or less 8 years of heating.

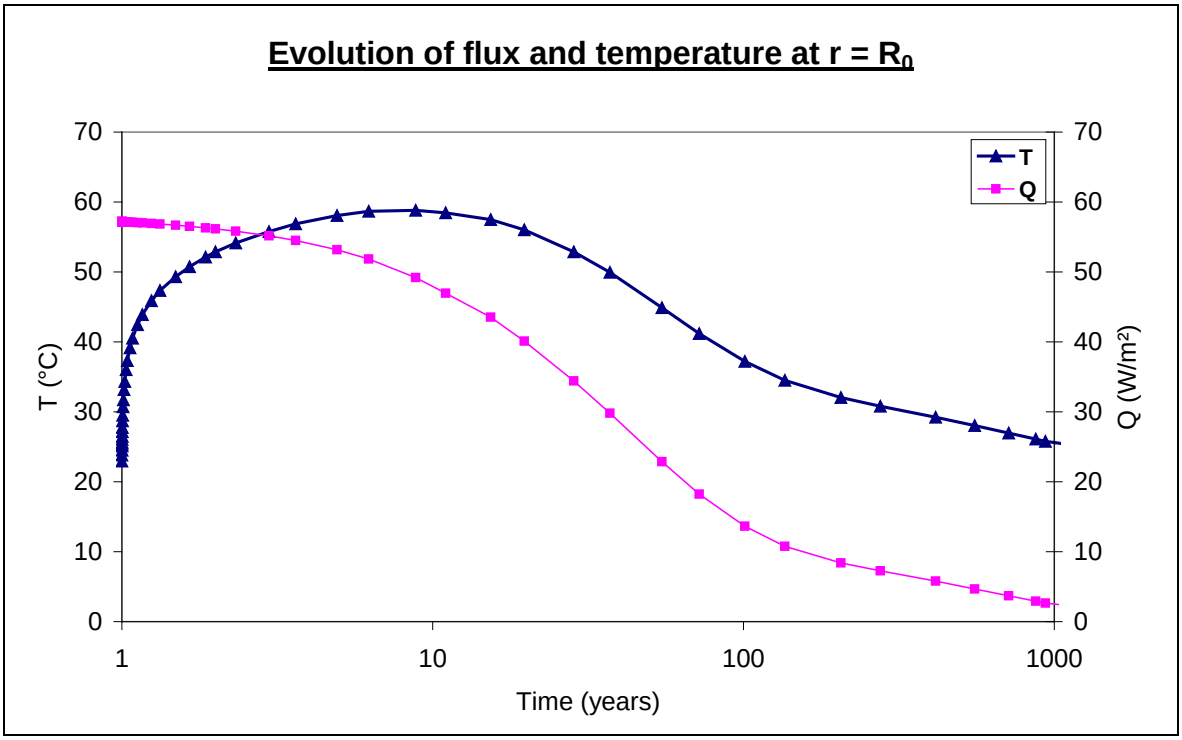

Figure 26 : Flux and temperature evolution at r = R_0 (semi-logarithmic scale)

Figure 27 presents temperature profile at different period of time during the heating stage. We note that significant changes in temperature are limited in space to a radius of 100 meters. Nevertheless, the far field is also slightly disturbed. At 1001 years, temperatures have nearly returned to their initial state (22°C) : the temperature at the gallery wall being equal to 26°C.

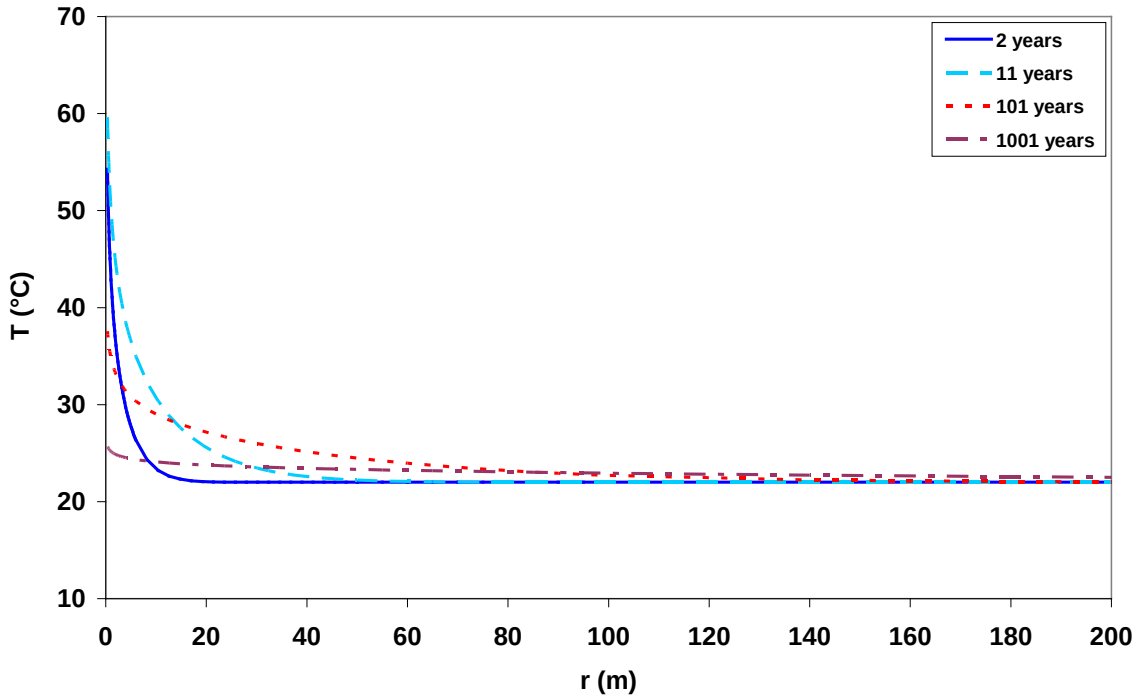

Figure 27 : Radial profile of temperature at different periods (heating)

3.2.1.2 Pore pressure

Figure 28 shows the radial profile of pore pressure during and at the end of excavation (3 days), after 15 days and 1 year of drained conditions a the lining. We note that during the excavation (day 1, 2 and 3), the pressure at the gallery wall decreases linearly to 100 kPa. With time, pore pressure distribution takes a profile corresponding to the fact that the gallery acts as a drain for the rock mass. For a radius higher than 4 meters, pore pressure distribution is not influenced.

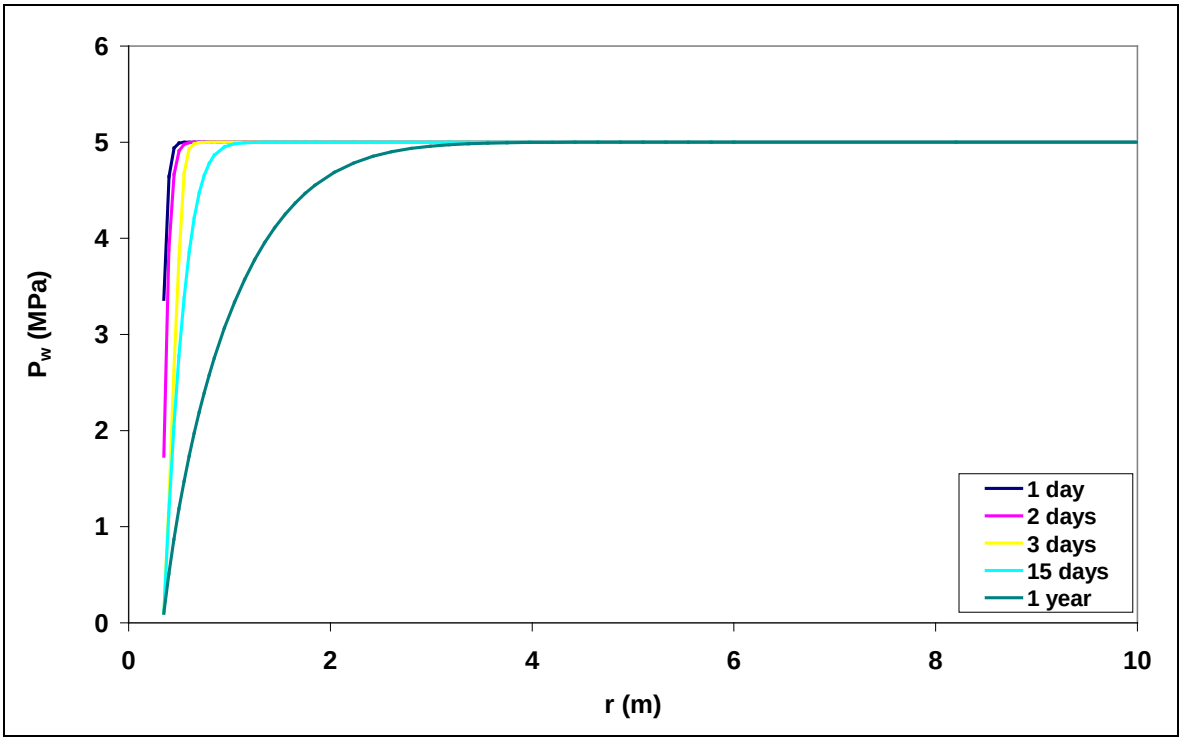

Figure 28 : Radial profile of pore water pressure at different periods during the excavation (3 days) and the drainage (1 year)

Figure 29 presents the radial profile of pore pressure at different periods (2 years, 11 years, 101 years and 1001 years) during the heating phase. From 2 years to 11 years, pore pressure increases with time near the gallery wall. This is due to the rise of temperature which causes a dilatation of grains and water. Consequently, as there is less pore space and that the water dilates, the pressure increases. The largest overpressure (2.6 MPa) at the time steps considered is observed at a radius of 6 m after 10 years of heating. After this period, as the temperature is decreasing until returning to its initial state, the pore water pressure drops. The outline after 1000 years of heating confirms that the gallery acts as a drain for the clay.

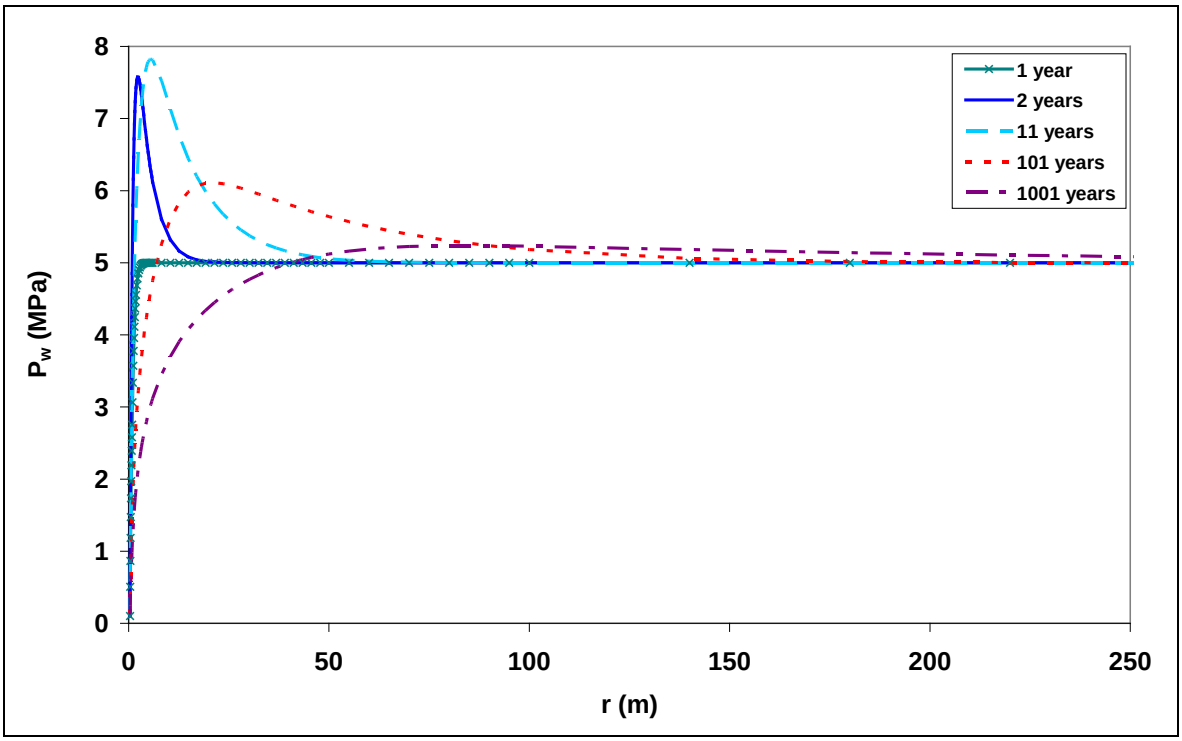

Figure 29 : Radial profile of pore water pressure at different periods during the heating phase

3.2.1.3 Displacement

When releasing total stress, the gallery wall converges and a negative radial displacement is measured α_{exc} = 1.4 mm (Figure 30). The lining is then placed. During the one-year drainage phase, no major change in displacements is observed.

During the heating phase, we observe on Figure 31 positive radial displacements from a radius of 1.35 meters until the far field which are due to the rise of temperature and pressure.

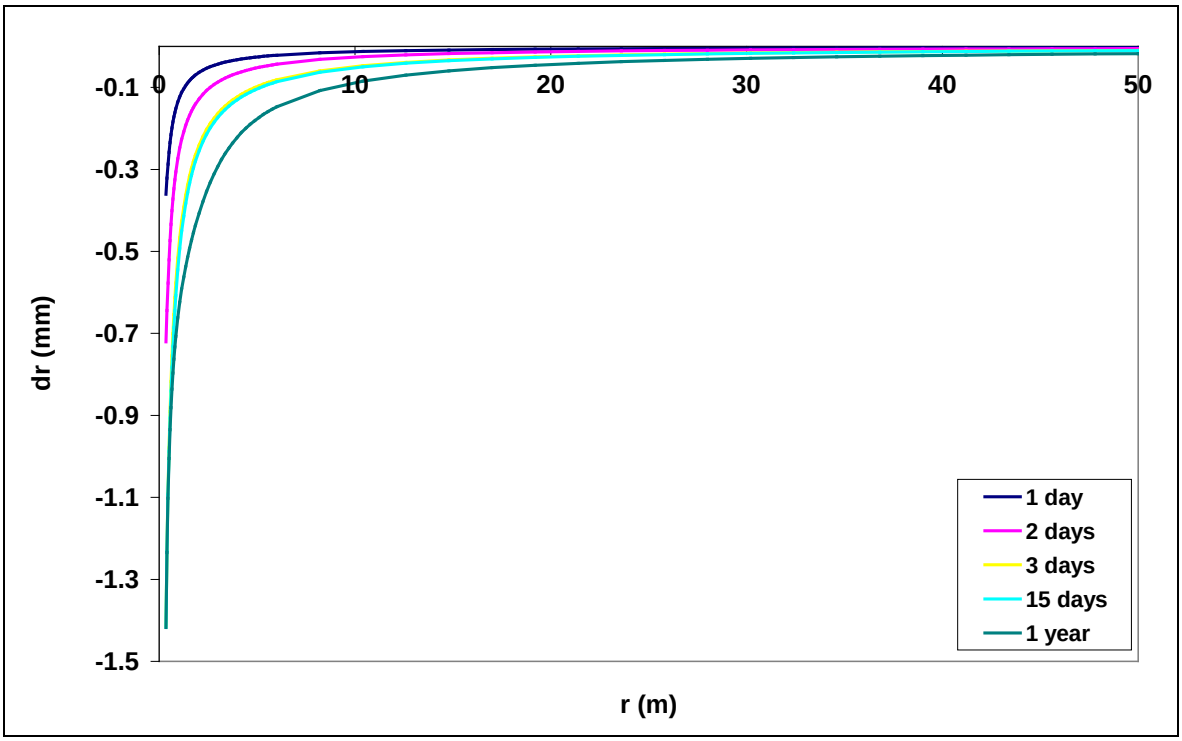

Figure 30 : Radial profile of radial displacement during excavation and open drift period

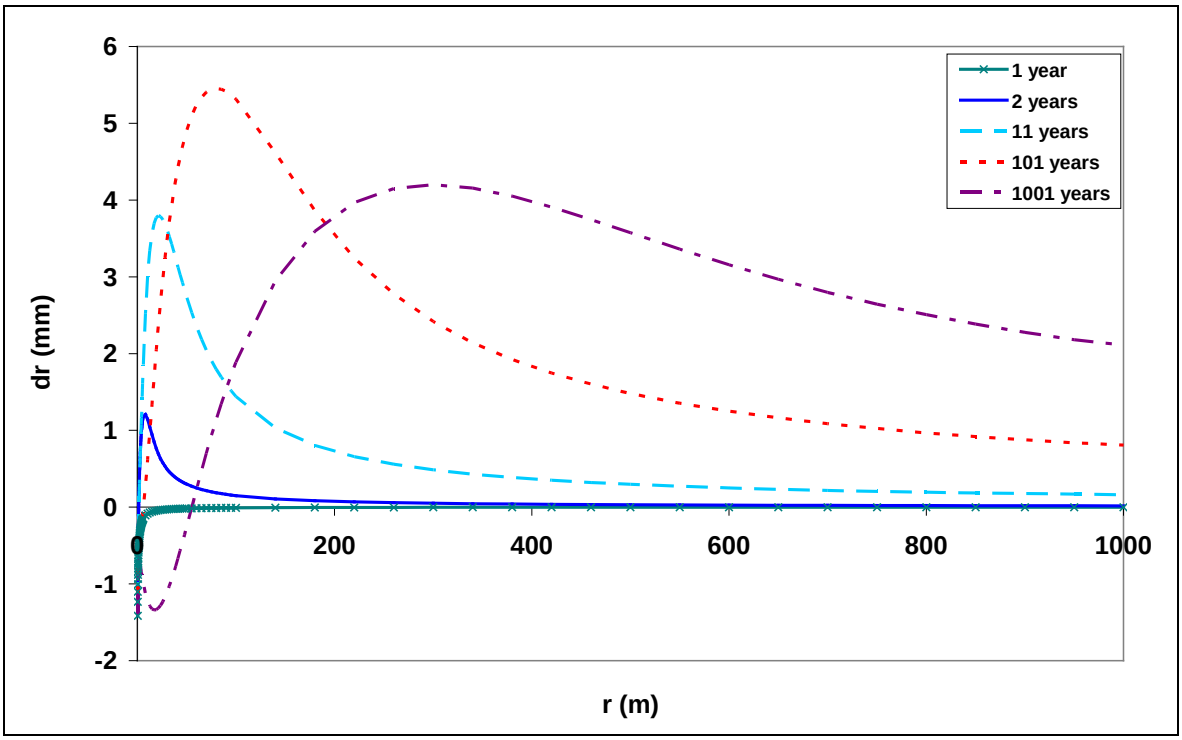

Figure 31 : Radial profile of radial displacement at different periods during heating phase

3.2.1.4 Stress paths

Figure 32 and Figure 33 show the effective stress path of clay at different radius R_0 = 2m, 2 R_0, 5 R_0 and 10 R_0 in the (p', q) stresses plane. Figure 33 relates in details the stress evolution during the excavation (3 days), during the drainage of the gallery, during the increase of temperature and finally during the temperature decrease. Figure 32 summarizes the different stress paths on the same graph. The initial Mohr-Coulomb yield limit is also plotted.

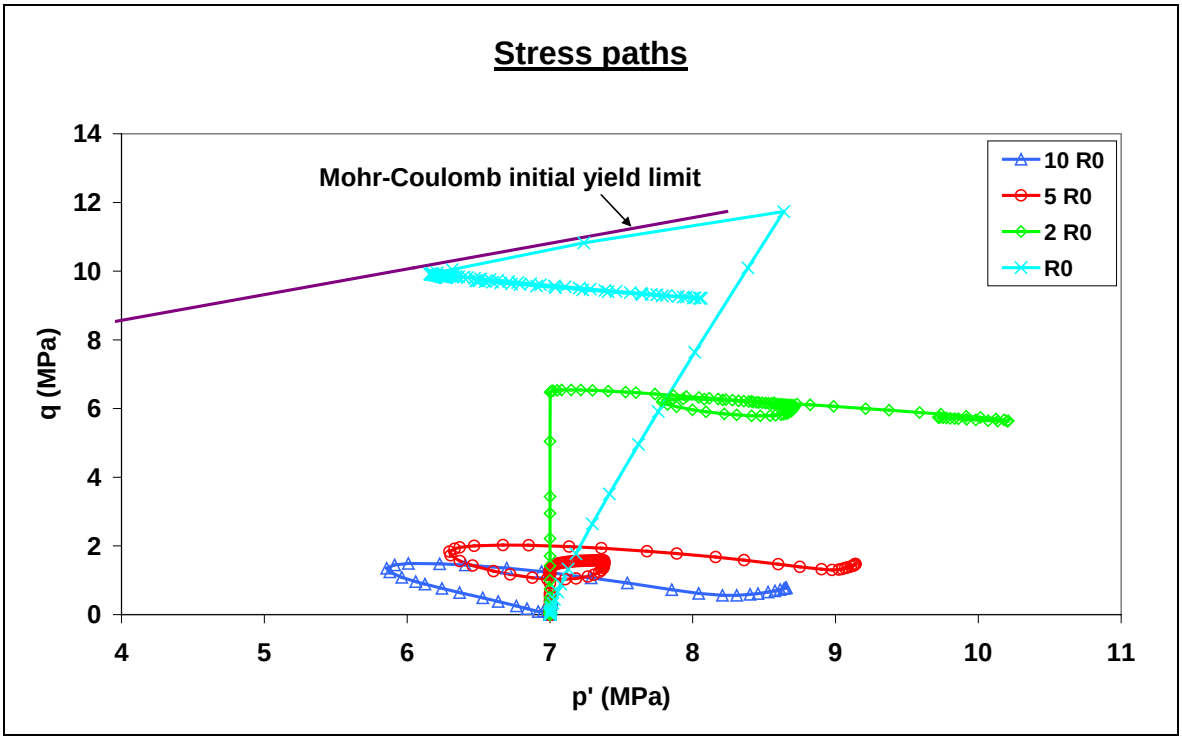

Figure 32 : Effective stress paths at r = R_0, r = 2R_0, r = 5R_0 and r = 10R_0

The initial stress state is isotropic and located in the elastic domain as shown on Figure 32.

Figure 33A : When total stress and pore pressure on the gallery wall start decreasing (excavation), the mean stress increases and the deviatoric stress increases until the stress state reaches the yield limit (stage 1). As there is no hardening possible, the stress path is then obliged to follow the yield limit. At this stage the plastic radius reaches its maximum and is equal to 0.51 m. Thus the clay is in a plastic state from 1 to 2. Once the temperature increases, there is a progressive stress release of the rock so that the stress state is elastic : the mean stress slightly increases and the deviatoric stress decreases. When the temperature of clay decreases, the stresses follow the inverse way (reversibility).

Figure 33B C and D: The stress states at r = 2 R_0, r = 5 R_0 and 10 R_0 stay elastic during the whole mechanical and thermal loading.

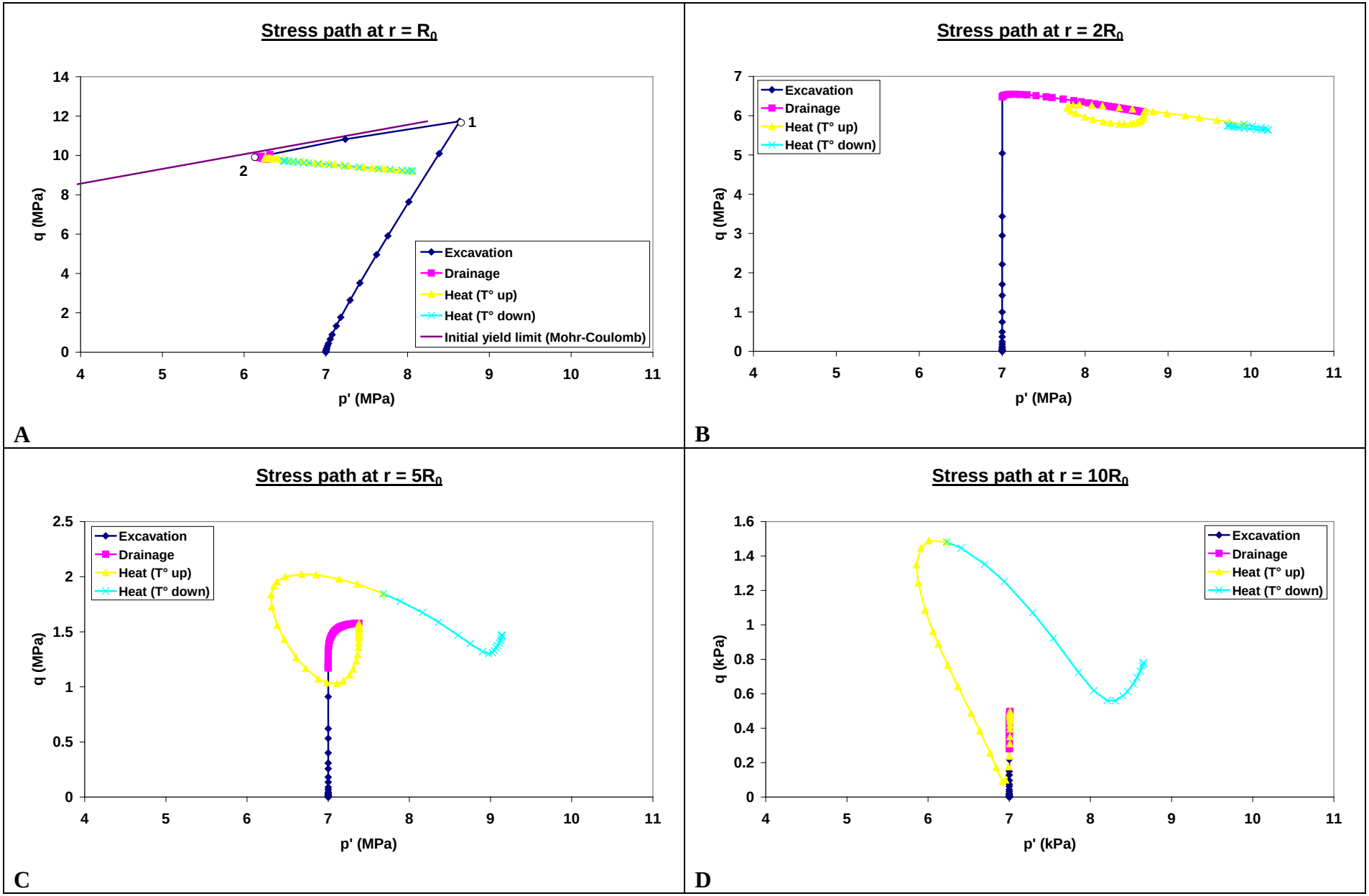

Figure 33 : Effective stress paths at r = R_0, r = $2R_0$, r = $5R_0$ and r = $10R_0$

3.2.2 COMPARISON OF RESULTS FOR DIFFERENT HEAT FLUXES

As it has been mentioned before, calculations for two different thermal source terms are realized, that is High Level Waste after 45 and 60 years (reference case) of cooling on surface.

3.2.2.1 Temperature

The evolution of temperature at the gallery wall is shown on the Figure 34 below. The maximum temperature reached for the hot case is now 71.8 °C instead of 58.8 °C for the normal case.

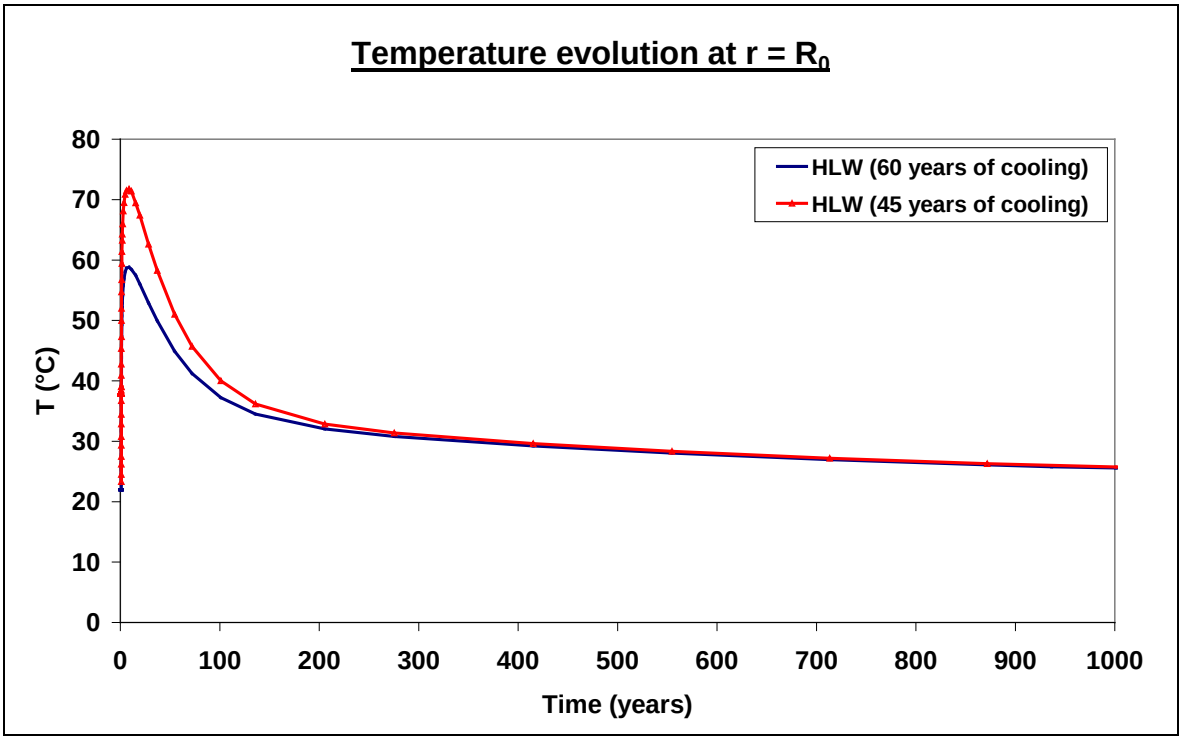

Figure 34 : Temperature evolution for 2 heat sources - Comparison

3.2.2.2 Pore pressure, displacement and stress paths

The conclusions stay identical as the one made for PC clay.

3.3 I2 CASE

3.3.1 RESULTS : REFERENCE CASE (I2A)

The excavation of the gallery is realized within 1 day. The water pressure at the tunnel face (AB) decreases linearly to the atmospheric pressure. There is no liner placed.

The excavation is followed by a one-year open drift period during which the tunnel face (AB) is supposed to be under drained conditions : the pore water pressure is fixed to be equal to the atmospheric pressure. During the thousand-years heating phase, the gallery is still supposed to be drained : the pressure remains at 100 kPa. The heat flux considered is the one from Spent Fuel BE container after 40 years of cooling on surface. The conductibility parameter taken for the soil is λ = 1.5 W/(mK), the permeability k = 2.10^{-13} m/s, the cohesion c =8.6 MPa and the friction angle ø = 24.6°. The elasto-plastic model used is a Mohr-Coulomb model.

Temperature, displacements, pore pressures and stress state are analysed during the excavation of the test drift and over a thousand-year period after the excavation. In particular, stress state are computed at r = R_1, r = $2R_1$, r = $5R_1$ and r = $10R_1$.

3.3.1.1 Temperature

Figure 35 presents the evolution of flux and temperature at the gallery wall. The first year, there is no heat injection and temperature in clay remains constant (T = 38 °C). Once the decreasing heat flux is applied (Q_0 = 26.7 W/m²), temperatures in the rock mass progressively rise. At the gallery wall, the highest temperature (T_{max} = 94.2 °C) is reached after more or less 10 years of heating.

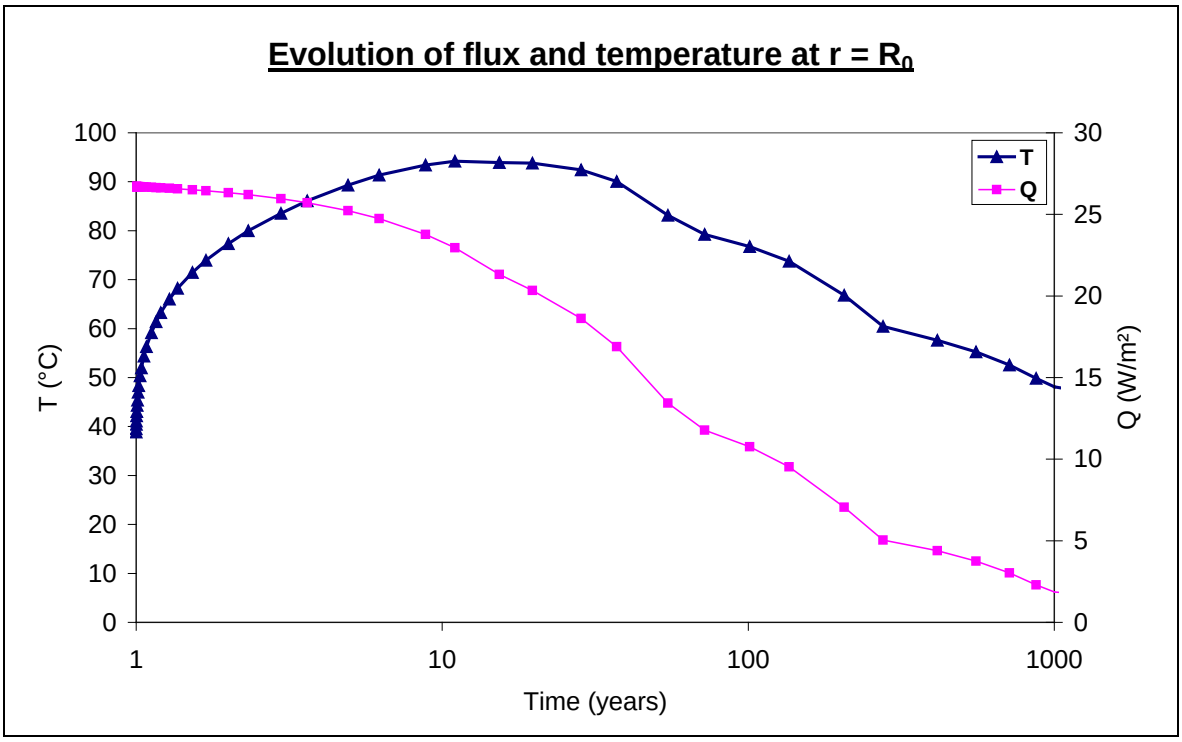

Figure 35 : Flux and temperature evolution at r = R_0 (semi-logarithmic scale)

Figure 36 presents temperature profile at different period of time during the heating stage. We note that significant changes in temperature are limited in space to a radius of 100 meters.

Nevertheless, the far field is also slightly disturbed. At 1001 years, temperatures have not yet returned to their initial state (38°C) : the temperature at the gallery wall being equal to 47.7°C.

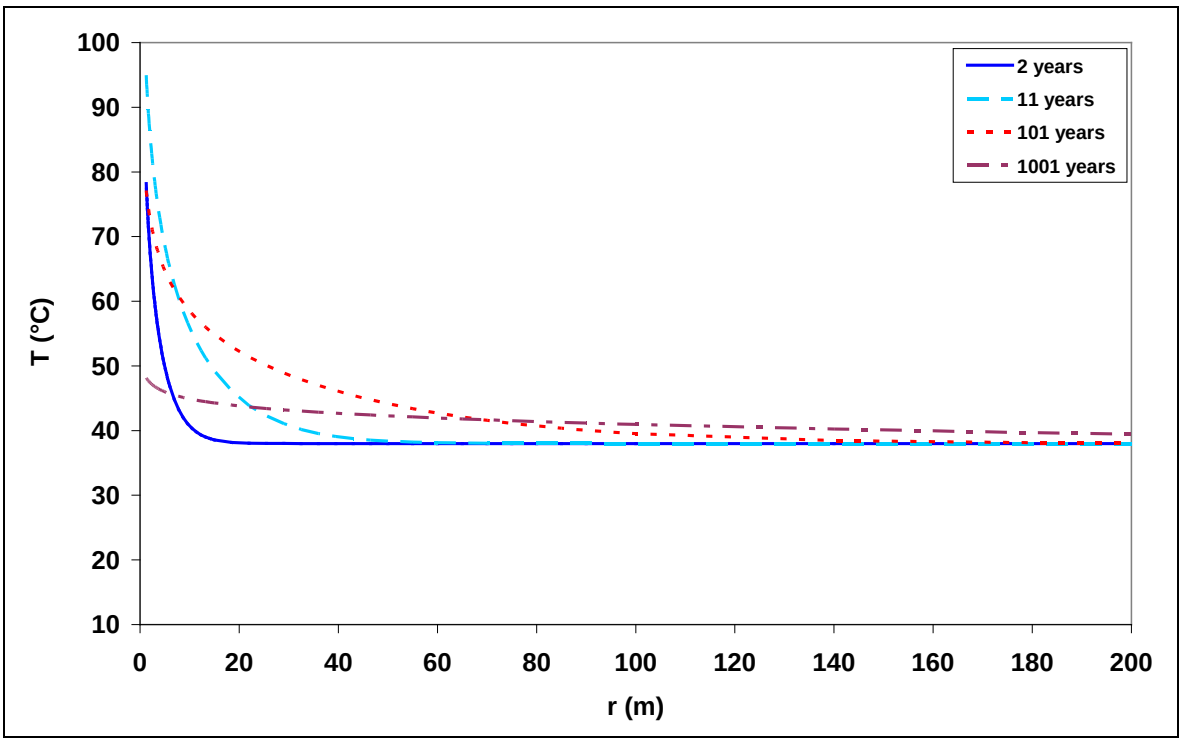

Figure 36 : Radial profile of temperature at different periods (heating)

3.3.1.2 Pore pressure

Figure 46 shows the radial profile of pore pressure during and at the end of excavation (1 day), after 15 days, 6 months and 1 year of drained conditions a the lining. With time, pore pressure distribution takes a profile corresponding to the fact that the gallery acts as a drain for the rock mass. For a radius higher than 8 meters, pore pressure distribution is not influenced.

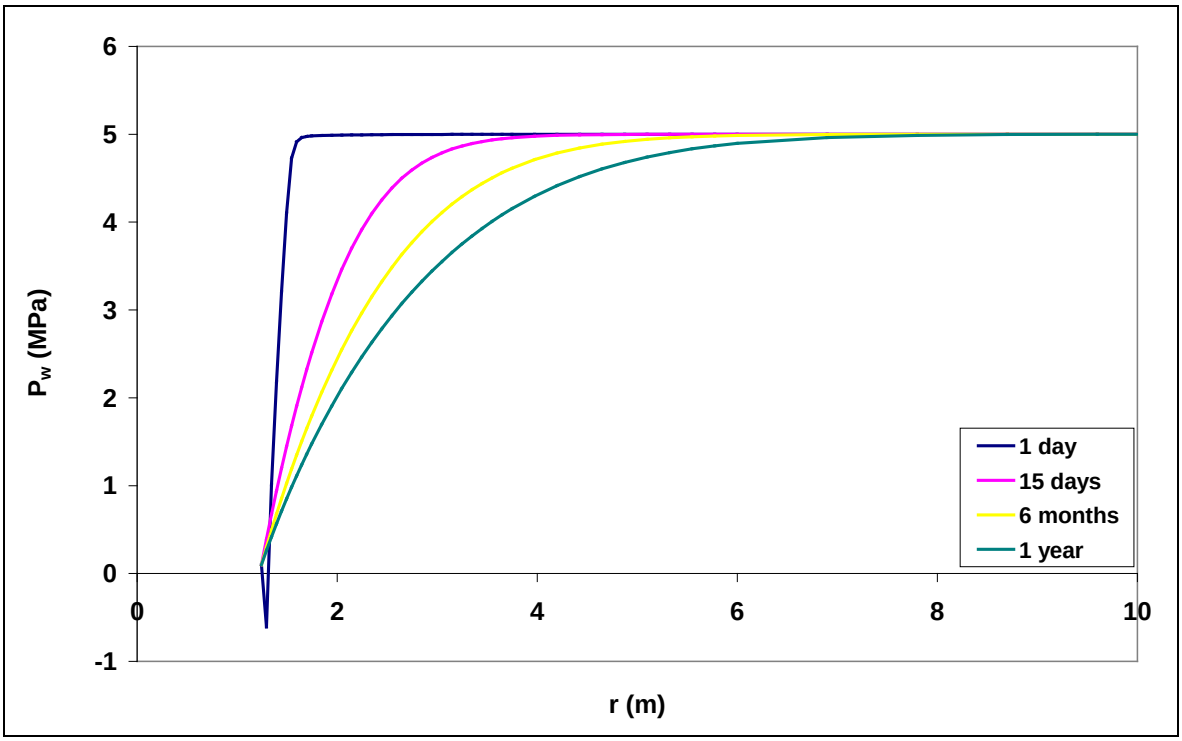

Figure 37 : Radial profile of pore water pressure at different periods during the excavation (1 day) and the drainage (1 year)

Figure 38 presents the radial profile of pore pressure at different periods (2 years, 11 years, 101 years and 1001 years) during the heating phase. From 2 years to 11 years, pore pressure increases with time near the gallery wall. This is due to the rise of temperature which causes a dilatation of grains and water. Consequently, as there is less pore space and that the water dilates, the pressure increases. The largest overpressure (3.2 MPa) at the time steps considered is observed at a radius of 11.4 m after 10 years of heating. After this period, as the temperature is decreasing until returning to its initial state, the pore water pressure drops. The outline after 1000 years of heating confirms that the gallery acts as a drain for the clay but there is still a small over-pressure observed until 400 m.

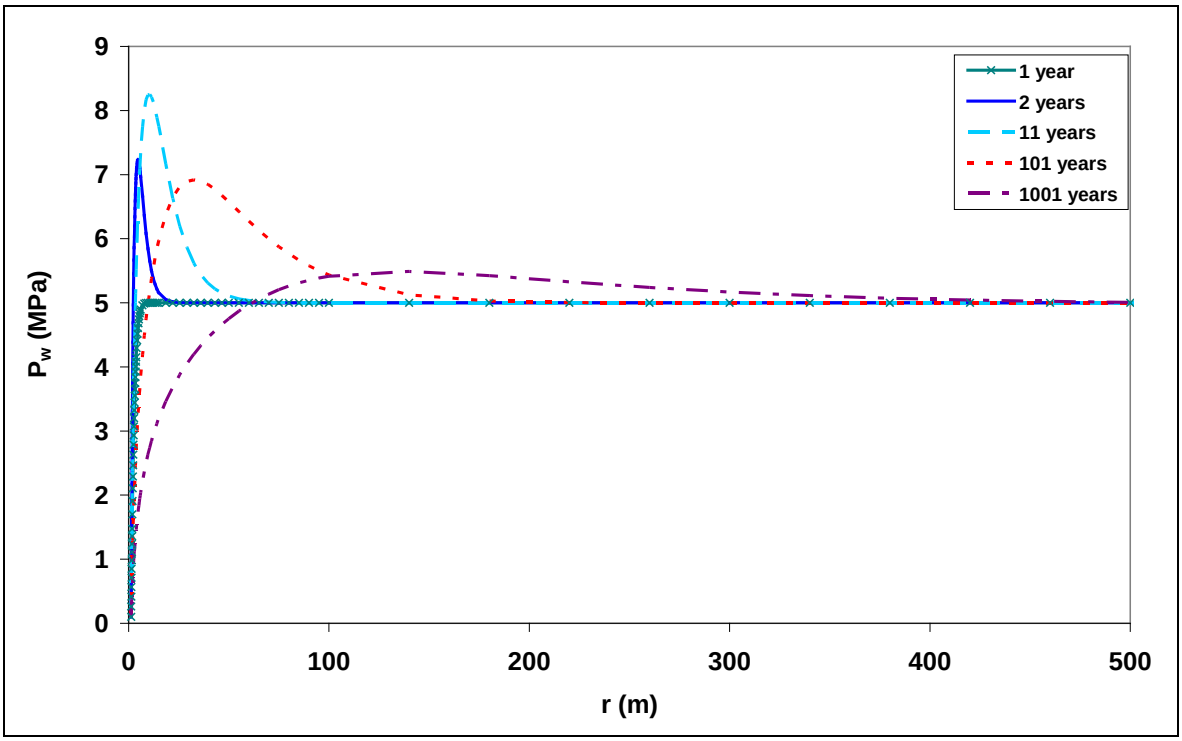

Figure 38 : Radial profile of pore water pressure at different periods during the heating phase

3.3.1.3 Displacement

When releasing total stress, the gallery wall converges and a negative radial displacement is measured α_{exc} = 7.45 mm (Figure 39). During the one-year drainage phase, no major change in displacements is observed.

During the heating phase, we observe on Figure 40 positive radial displacements from a radius of 4 meters until the far field which are due to the rise of temperature and pressure.

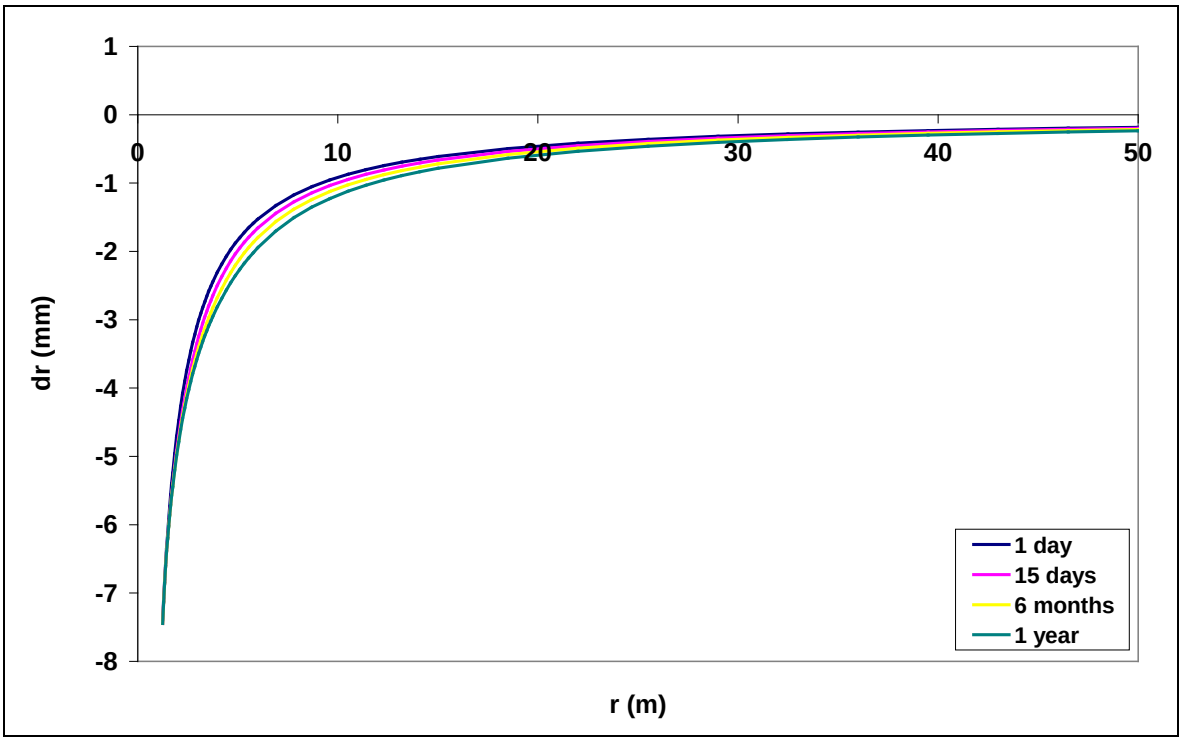

Figure 39 : Radial profile of radial displacement during excavation and open drift period

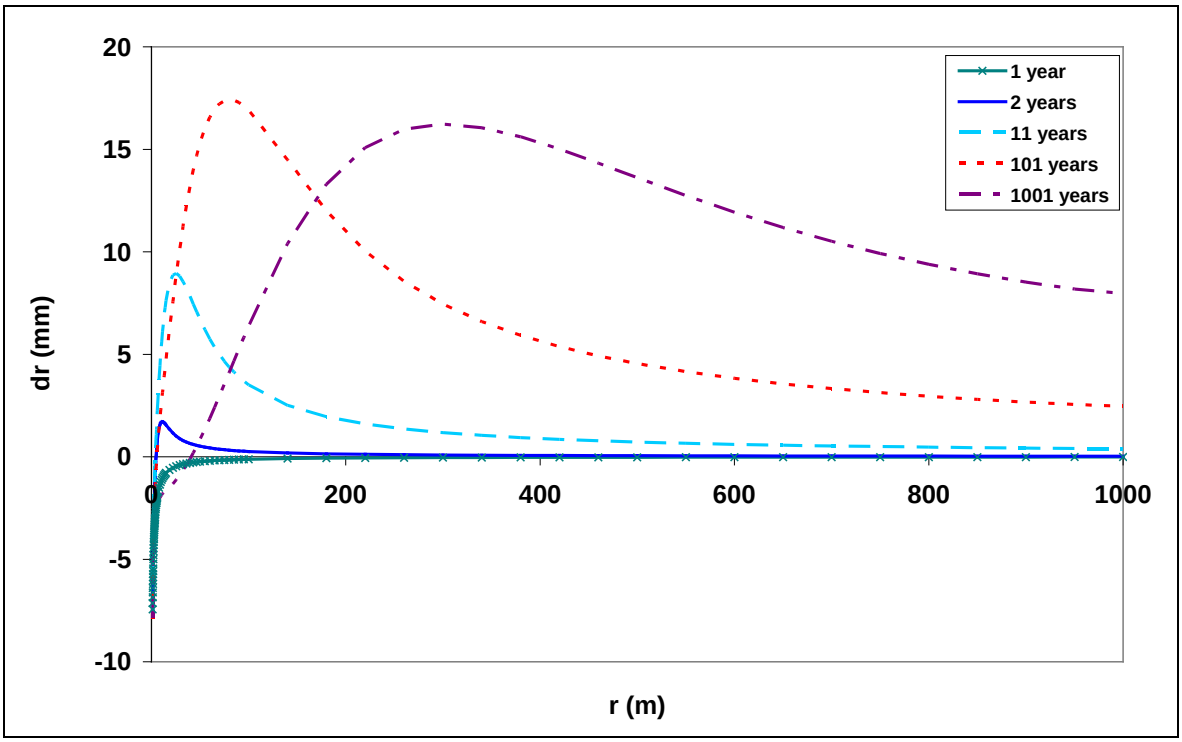

Figure 40 : Radial profile of radial displacement at different periods during heating phase

3.3.1.4 Stress paths

Figure 50 and Figure 42 show the effective stress path of clay at different radius R_0 = 2m, 2 R_0, 5 R_0 and 10 R_0 in the (p', q) stresses plane. Figure 42 relates in details the stress evolution during the excavation (1 day), during the drainage of the gallery, during the increase of temperature and finally during the temperature decrease. Figure 41 summarizes the different stress paths on the same graph. The initial Mohr-Coulomb yield limit is also plotted.

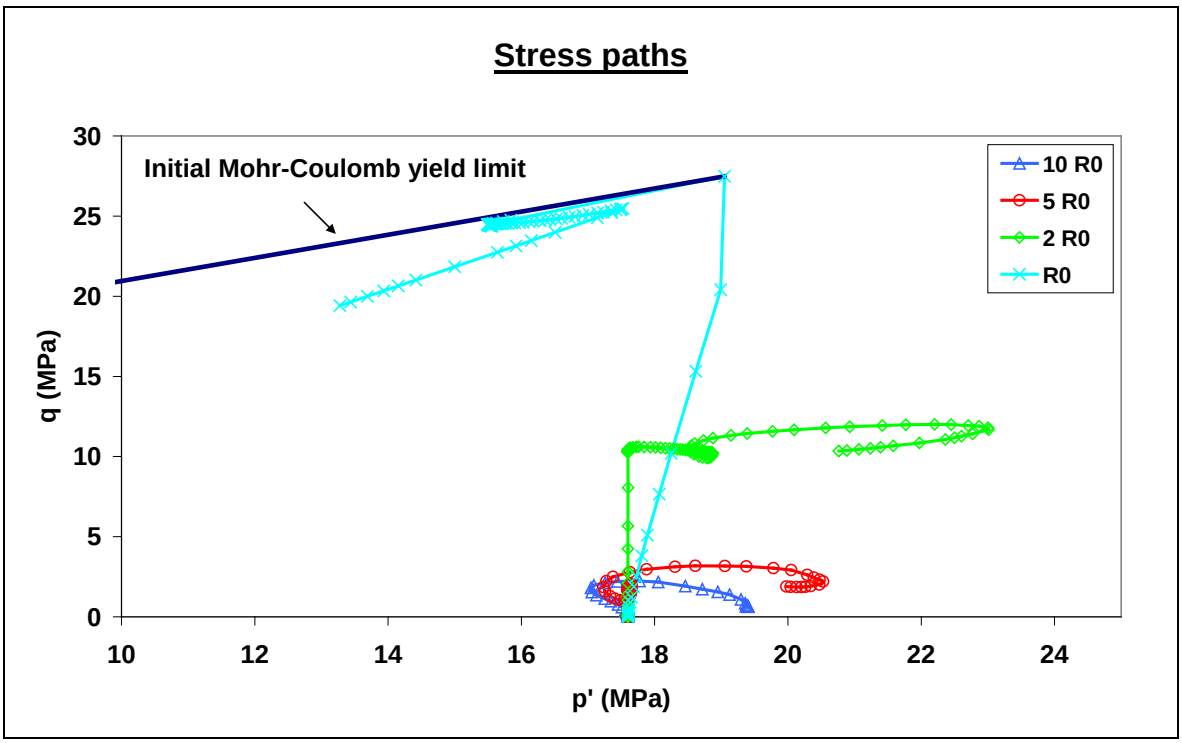

Figure 41 : Effective stress paths at r = R_0, r = 2R_0, r = 5R_0 and r = 10R_0

Figure 42A : When total stress and pore pressure on the gallery wall start decreasing (excavation), the mean stress increases and the deviatoric stress increases until the stress state reaches the yield limit (stage 1). As there is no hardening possible, the stress path is then obliged to follow the yield limit. At this stage the plastic radius reaches its maximum and is equal to 1.5 m. Thus the clay is in a plastic state from 1 to 2 (end of the one-year drainage phase) but at the point 2, the plastic radius has decreased. Once the temperature increases, the stresses increase so that the sate remains plastic until point 3 : the mean stress increases from 15.5 MPa to 17.5 MPa and the deviatoric stress slightly increases. At this stage the plastic radius returns to its maximum and is equal to 1.5 m. When the temperature of clay decreases, there is a progressive stress release so that the stress state is elastic.

Figure 42B C and D: The stress states at r = 2 R_0, r = 5 R_0 and 10 R_0 stay elastic during the whole mechanical and thermal loading.

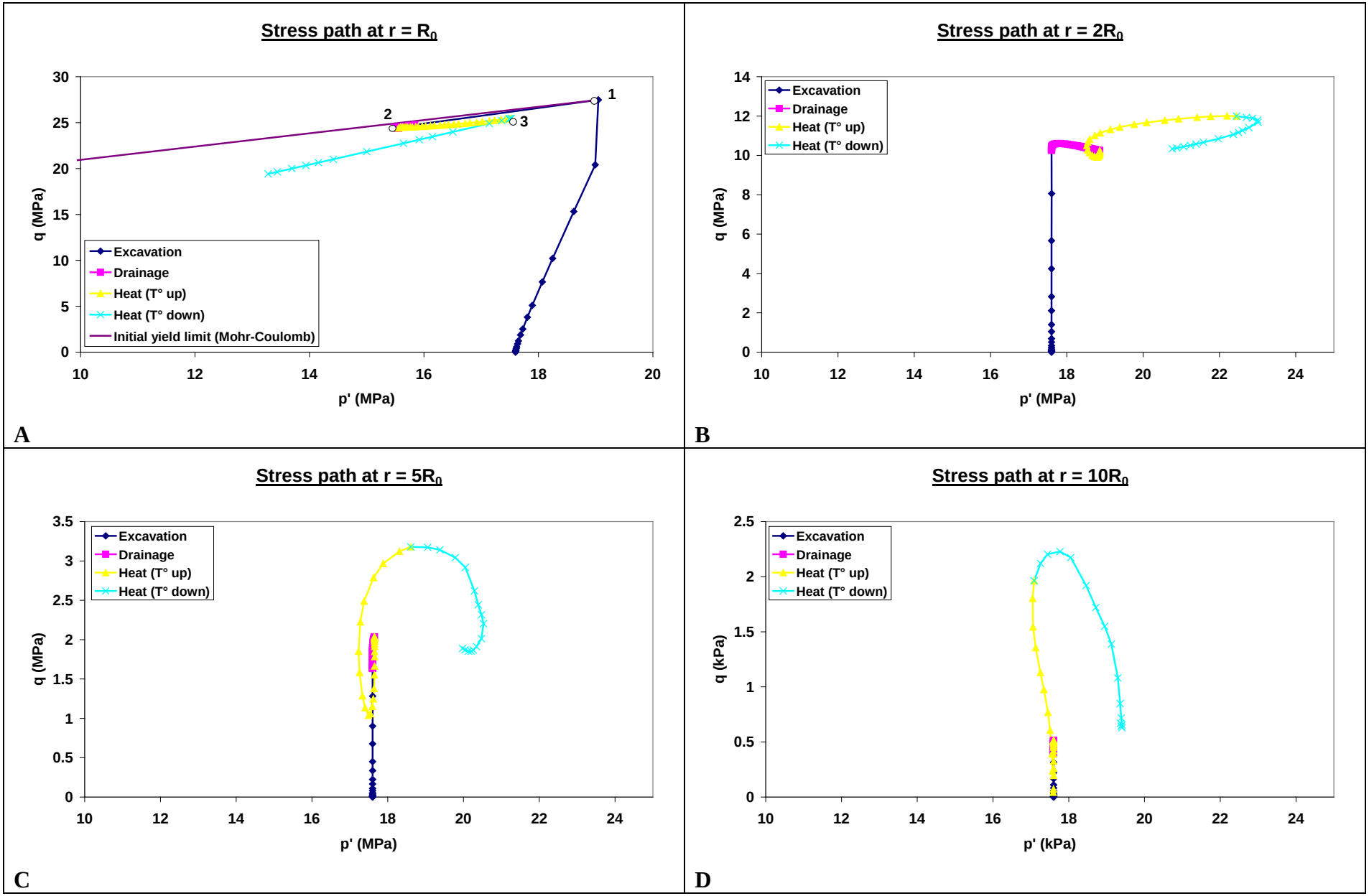

Figure 42 : Effective stress paths at r = R_0, r = $2R_0$, r = $5R_0$ and r = $10R_0$

3.3.2 COMPARISON OF RESULTS FOR DIFFERENT HEAT FLUXES

As it has been mentioned before, calculations for two different thermal source terms are realized, that is Spent fuel (BE container) after 30 and 40 years (reference case) of cooling on surface.

3.3.2.1 Temperature

The evolution of temperature at the gallery wall is shown on the Figure 43 below. The maximum temperature reached for the hot case is now 103.7 °C instead of 94.2 °C for the normal case.

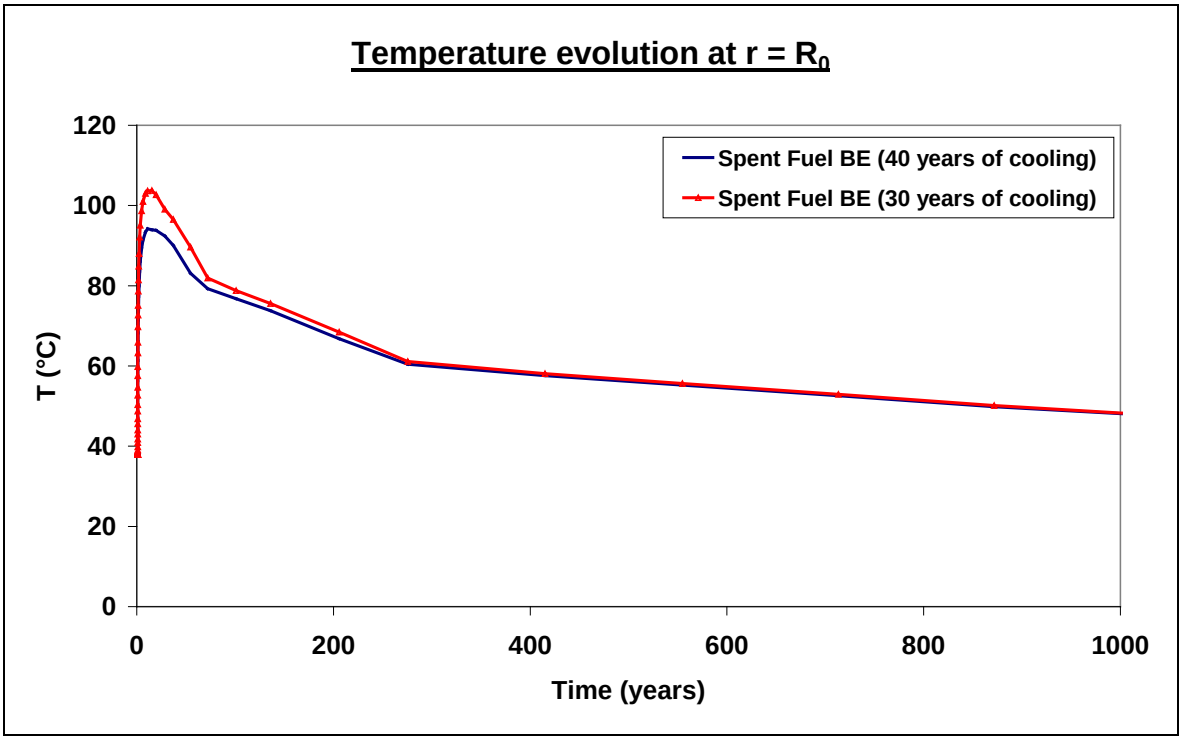

Figure 43 : Temperature evolution for 2 heat sources - Comparison

3.3.2.2 Pore pressure, displacement and stress paths

The conclusions stay identical as the one made for PC clay.

4 TEST CASE 2 : HEATING UNDER UNDRAINED CONDITION

For test case 2, the excavation and drainage phase are identical as for the test case 1. That is first, releasing the total radial stress and the pore pressure on the gallery wall down to zero simulates the excavation (3 days). Within these three days, the clay comes in contact to the rigid lining initially located at 9 cm far from the clay. The excavation is followed by a one-year open drift period where the tunnel face is supposed to be under drained conditions : the pore water pressure at it is fixed to be atmospheric pressure. The results related to this period are not analysed since they are identical at the TC1.

During the thousand-years heating phase, the tunnel face is now supposed to be undrained : the pore pressure is not fixed The heat flux considered is the VHLW after 50 years. The conductibility parameter taken for the soil is $\lambda = 1.35$ W/(mK) and the dilatancy angle $\psi = 0°$.

Temperature, displacements, pore pressures and stress state are analysed during the excavation of the test drift and over a thousand-year period after the excavation. In particular, stress state are computed at $r=R_1$, $r=2R_1$, $r=5R_1$ and $r=10R_1$.

Each time we will compare the results obtained with those of the reference case (PCA drained).

4.1 RESULTS FOR PC CLAY

4.1.1 TEMPERATURE

The evolution of temperature in the rock mass is identical at the test case 1. That is an increase of temperature at the gallery wall until 68.3°C after 10 years of heating then a decrease of temperature until 19°C after 1000 years.

4.1.2 PORE PRESSURE

Figure 44 presents the radial profile of pore pressure at different periods (2 years, 11 years, 101 years and 1001 years) during the heating phase. We observe that pore pressure increases with time. This is due to two factors: the first one is that the rock mass is now undrained and that the pressure tends to return to its initial state, the second one is that the rise of temperature causes a dilatation of grains and water. Consequently, as there is less pore space and that the water dilates, the pressure increases.

The largest overpressure (390 kPa) at the time steps considered is observed at a radius of 6 m after 10 years of heating. After this, as the temperature is decreasing, the pore water pressure decreases and return slowly to a uniform value corresponding to the hydraulic boundary condition. The outline of pore pressure after 1000 years of heating confirms that the gallery is undrained.

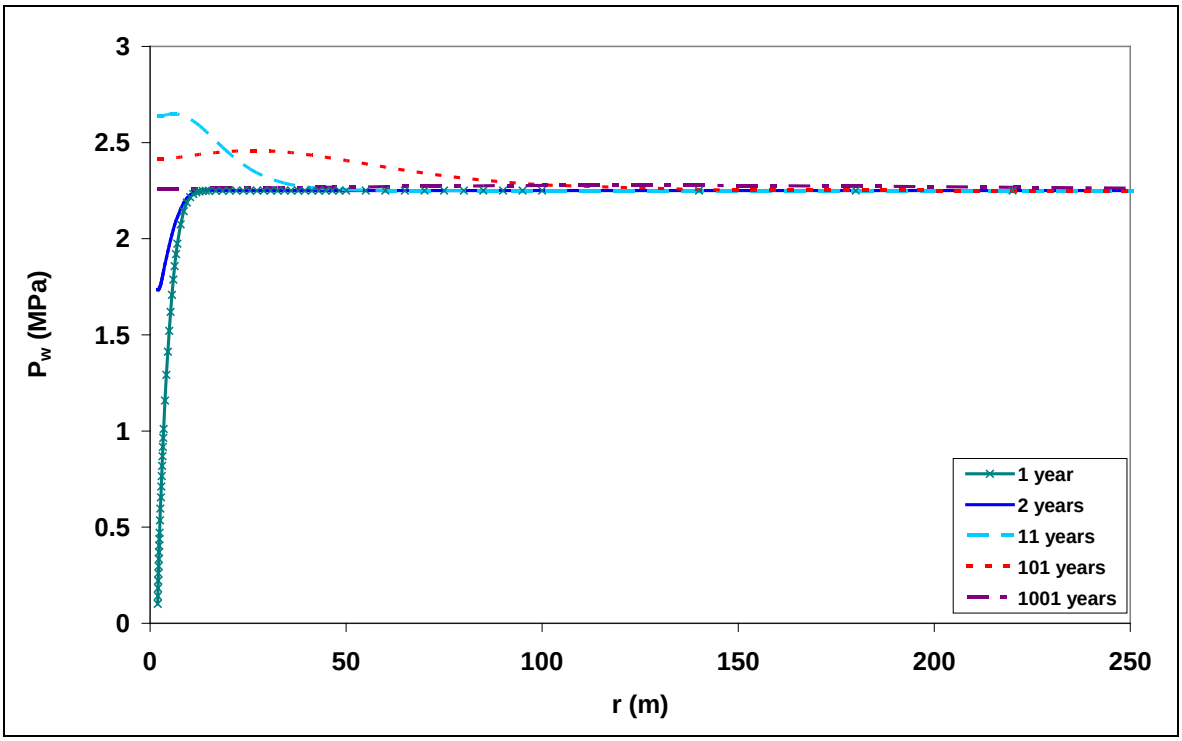

Figure 44: Radial profile of pore water pressure at different periods during the heating phase – undrained case

4.1.3 DISPLACEMENT

We observe positive radial displacements from a radius of 10 meters until the far field. These are due to the rise of temperature and pressure. After 1000 years, the profile of radial displacement tends towards the profile before heating.

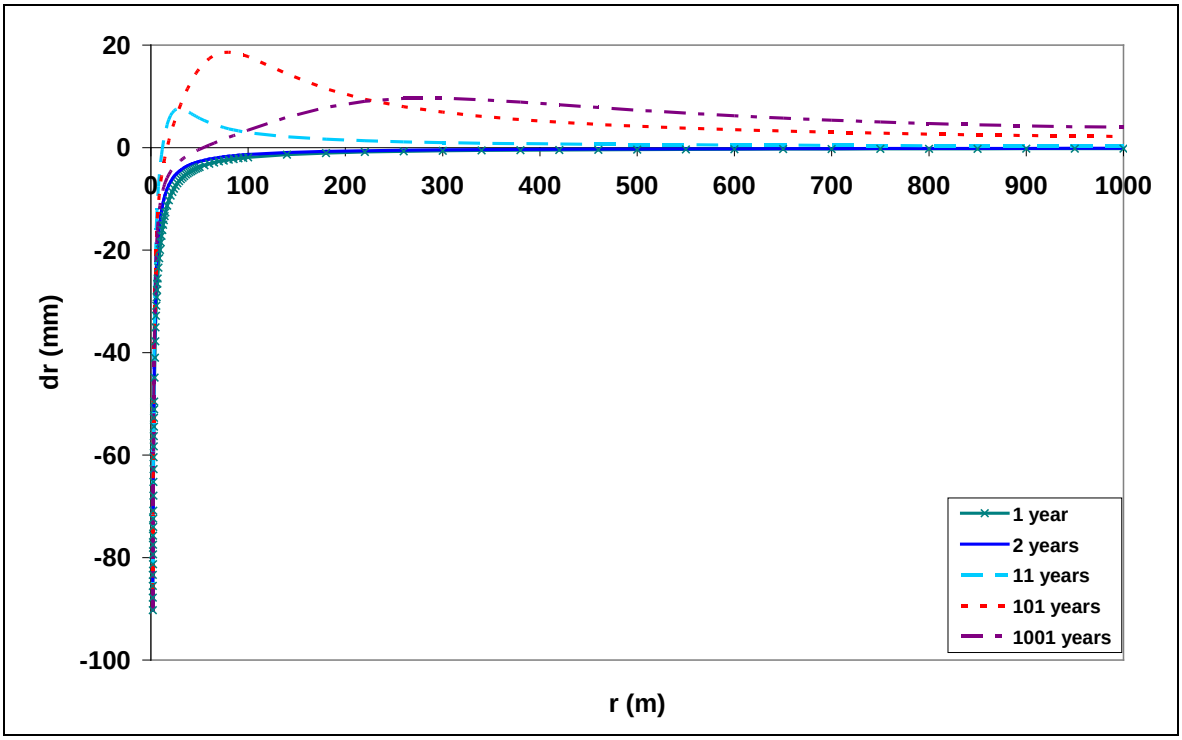

Figure 45 : Radial profile of radial displacement at different periods – undrained case

4.1.4 STRESS PATHS

Figure 45 shows the deviatoric stress at the gallery wall in function of the time. Figure 46 and Figure 47 show radial profiles of radial and orthoradial effective stress at different periods. We observe that, given the mechanical boundary condition (liner placed at a radial distance of 9 cm from the initial gallery surface) and the hydraulic conditions (waterproof condition) during the heat injection, the radial effective stresses at the gallery wall enter slightly in traction but there is no detachment between the liner and the soil.

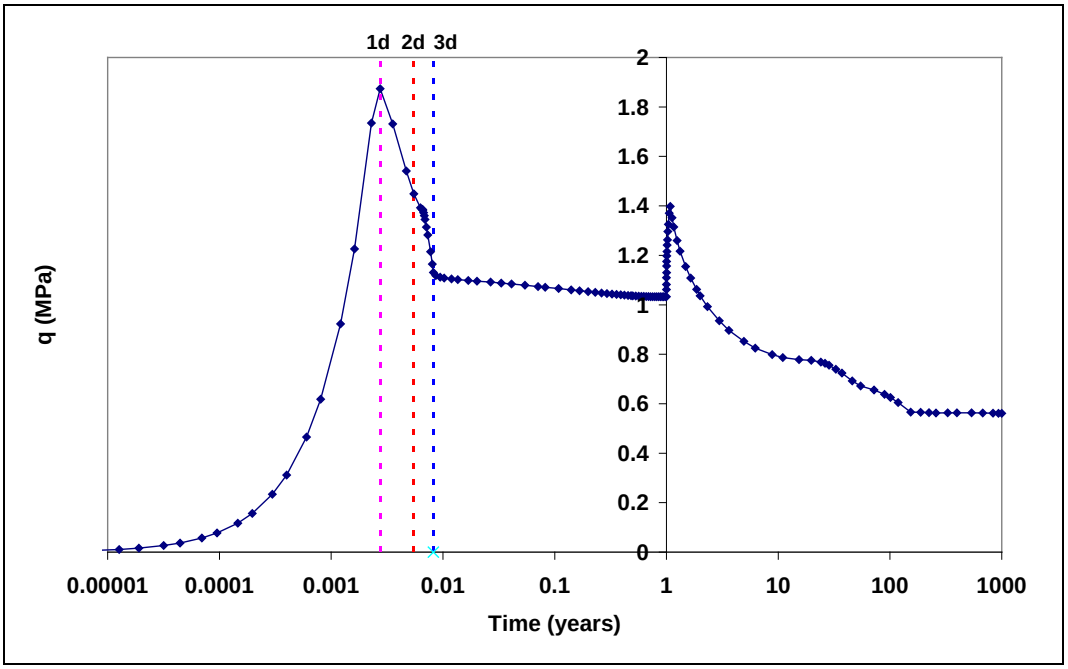

Figure 46 : Deviatoric stress at the gallery wall in function of the time – undrained case

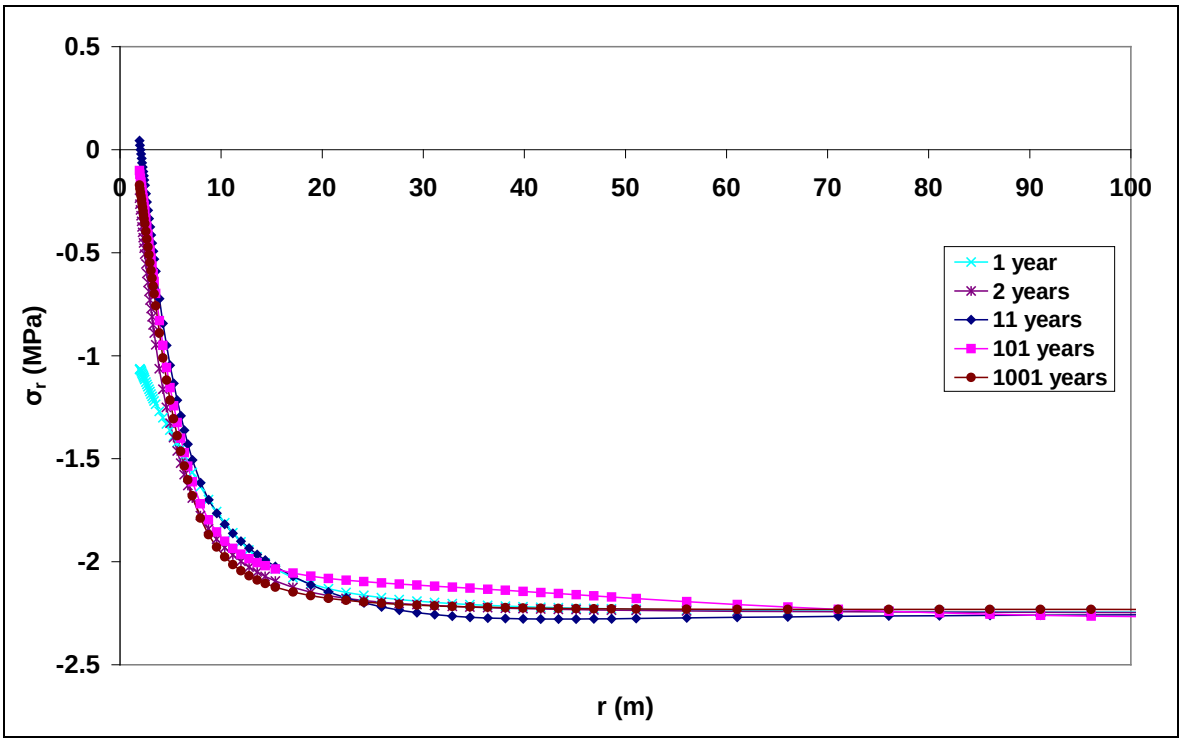

Figure 47 : Radial profile of radial effective stress at different periods- undrained case

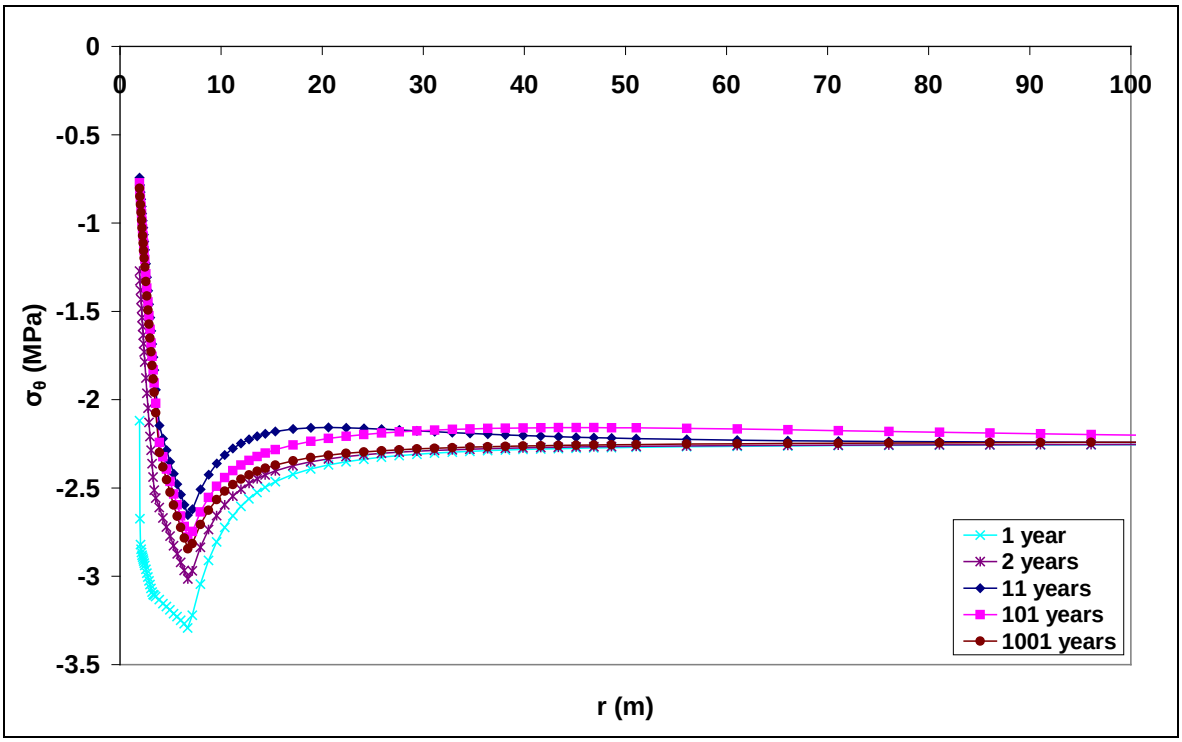

Figure 48 : Radial profile of orthoradial effective stress at different periods - undrained case

Figure 49 and Figure 50 show the effective stress path of clay at different radius R_0 = 2m, 2 R_0, 5 R_0 and 10 R_0 in the (p', q) stresses plane. Figure 50 relates in details the stress evolution during the excavation (3 days), during the drainage of the gallery, during the increase of temperature and finally during the temperature decrease. Figure 49 summarizes the different stress paths on the same graph. The initial Mohr-Coulomb yield limit is also plotted. Let's remind that this latter varies in the (p', q) plane, thus the stress state from point 1 to 2 is plastic.

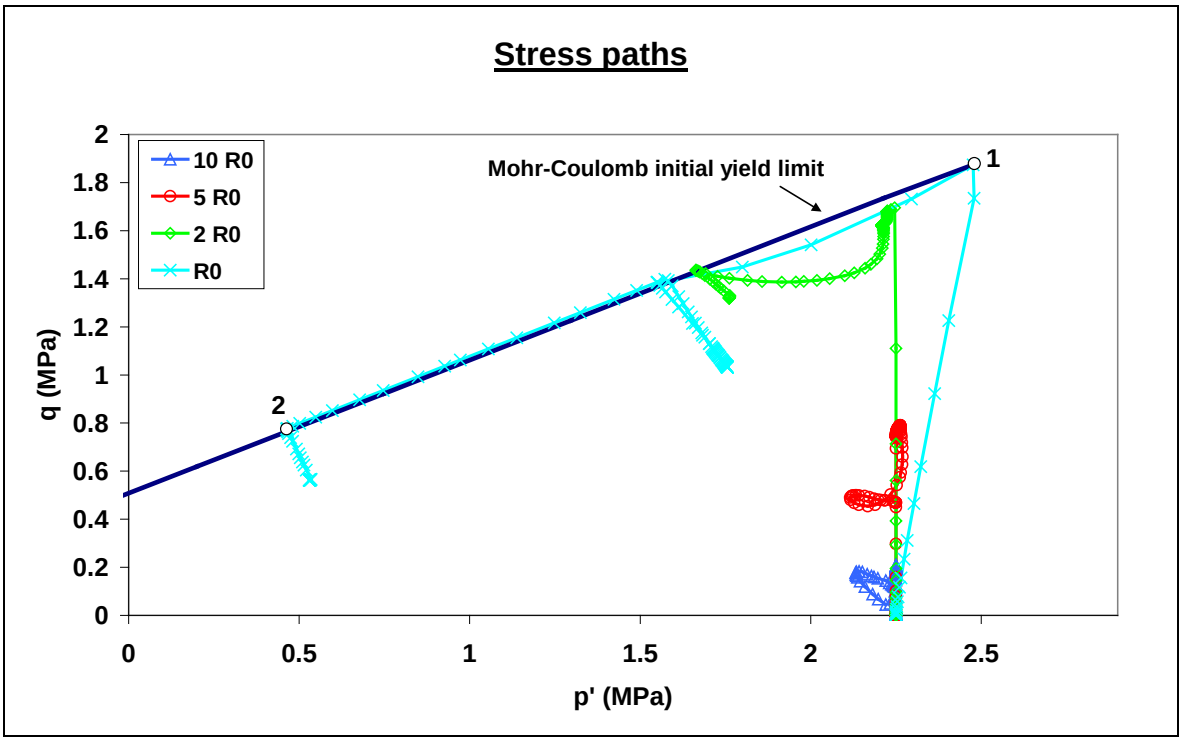

Figure 49 : Effective stress paths at r = R_0, r = $2R_0$, r = $5R_0$ and r = $10R_0$ - undrained case

Figure 50A : At the end of excavation, the stress state at the gallery wall is plastic and the plastic radius is equal to 6.7 m. The drainage of the gallery (from 3 days to 1 year) is characterised by a progressive stress release of the rock mass and the stress state after a year is elastic. Once the temperature increases, the deviatoric stress increases too but quickly meet the yield limit which is then obliged to follow as there is no hardening possible of the yield limit. The plastic radius after 10 years of heating is then 3.6 m. The temperature decrease state is characterised by a progressive stress release of the rock mass.

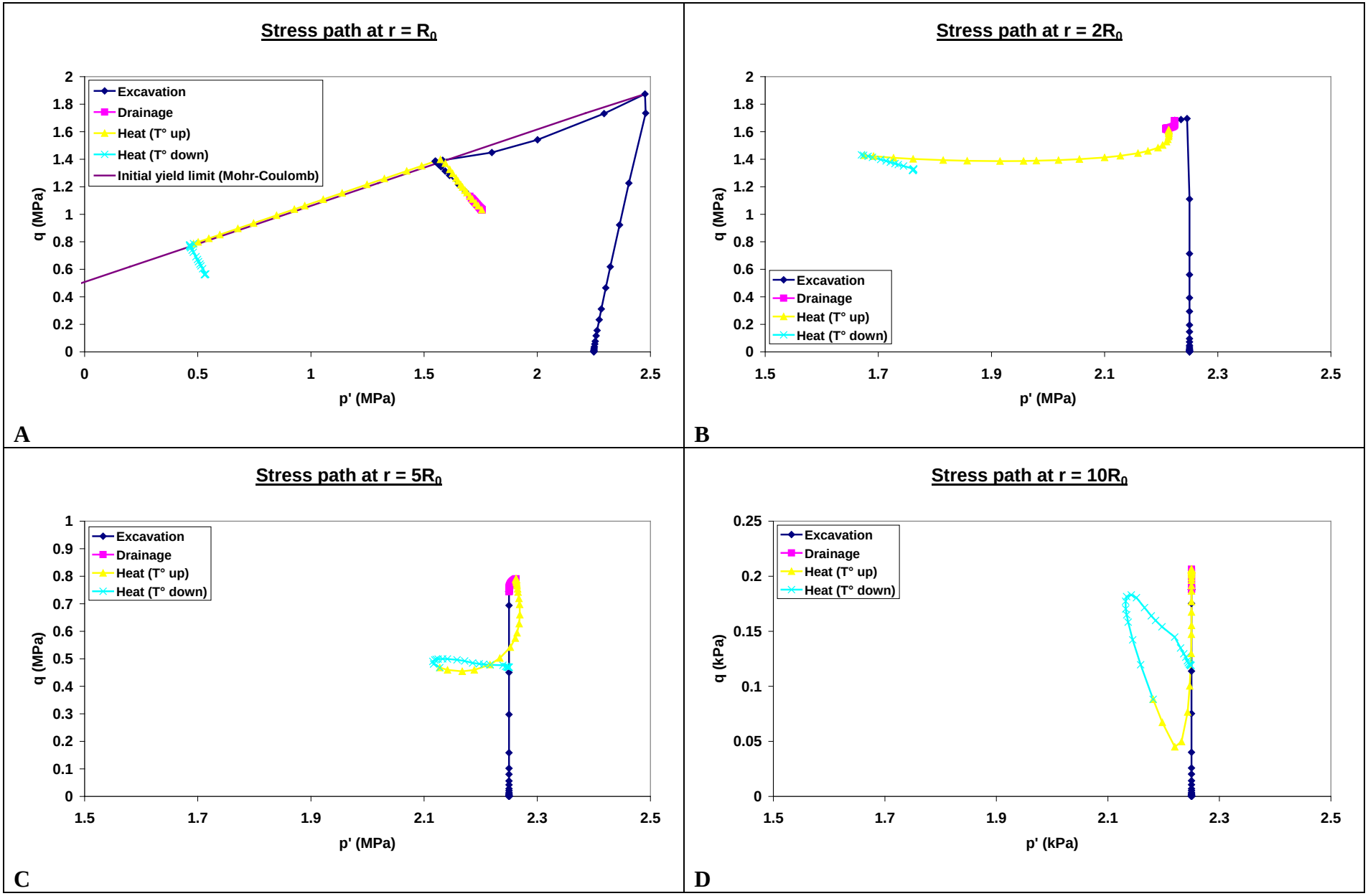

Figure 50 : Effective stress paths at r = R_0, r = $2R_0$, r = $5R_0$ and r = $10R_0$ – undrained case

4.2 COMPARISON BETWEEN THE DRAINED AND UNDRAINED CASES

4.2.1 PORE PRESSURE

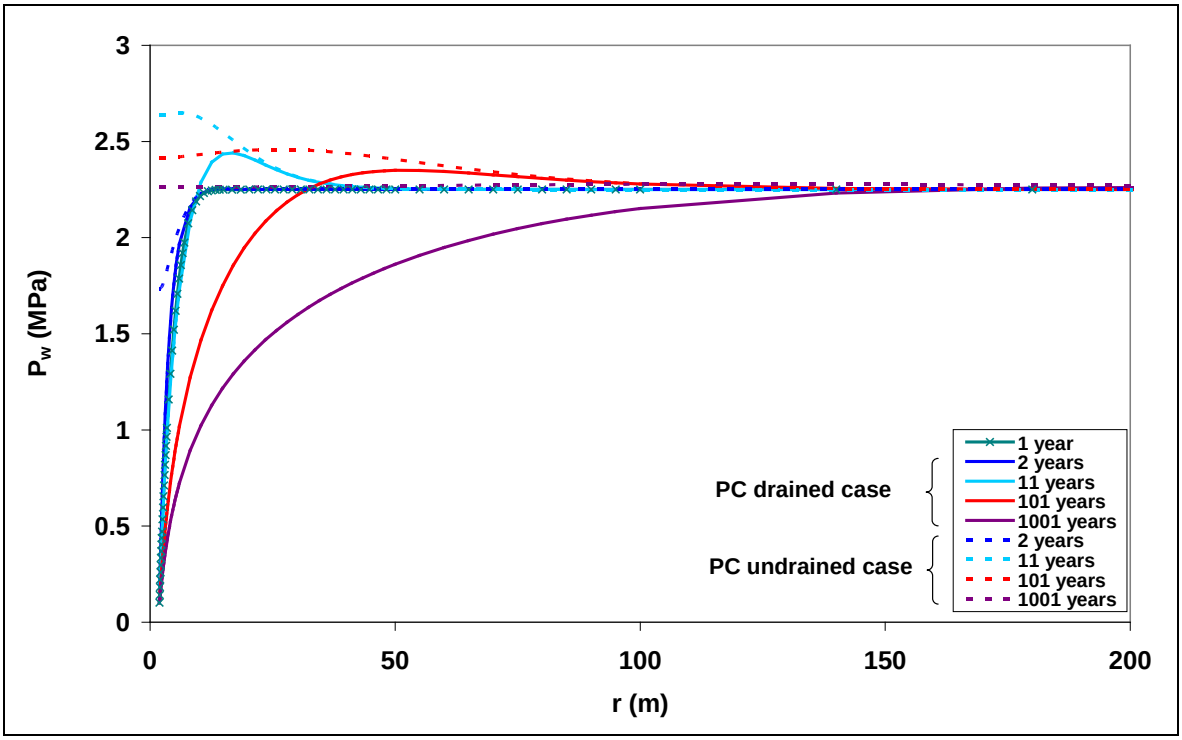

Figure 51 : Pore pressure profiles - comparison between drained and undrained conditions

4.2.2 DISPLACEMENT

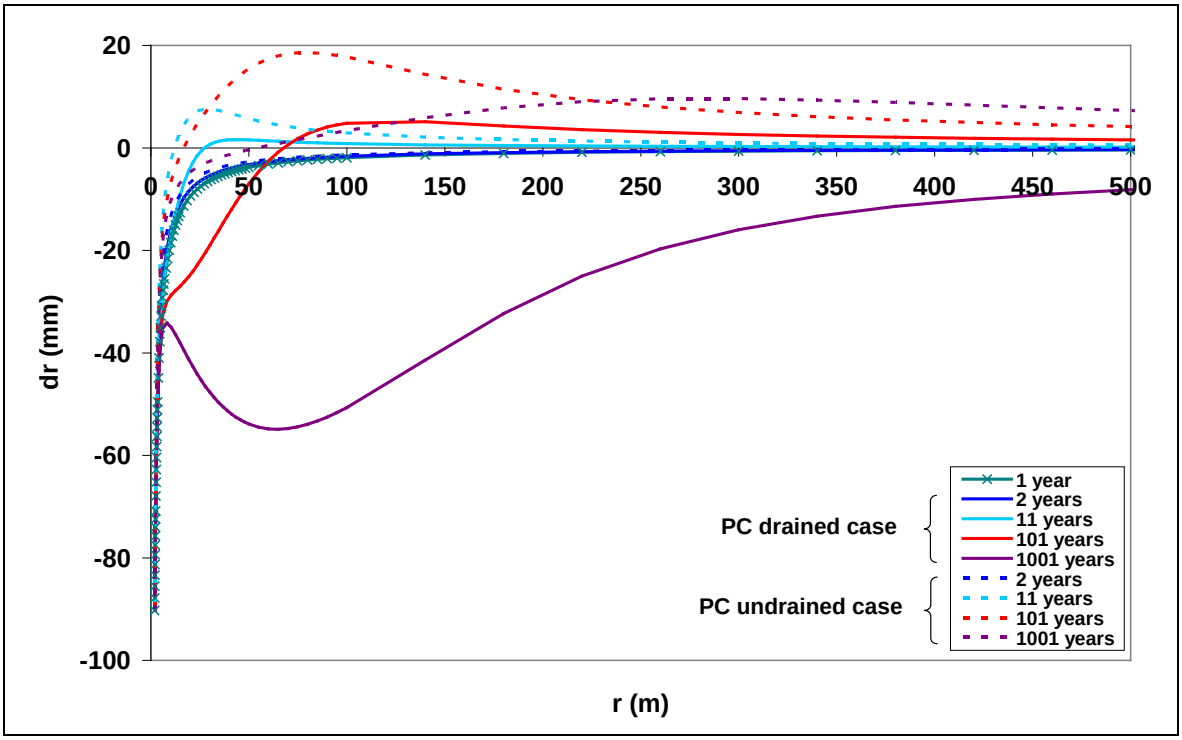

Figure 52 : Displacement profiles - comparison between drained and undrained conditions

4.2.3 STRESS PATHS

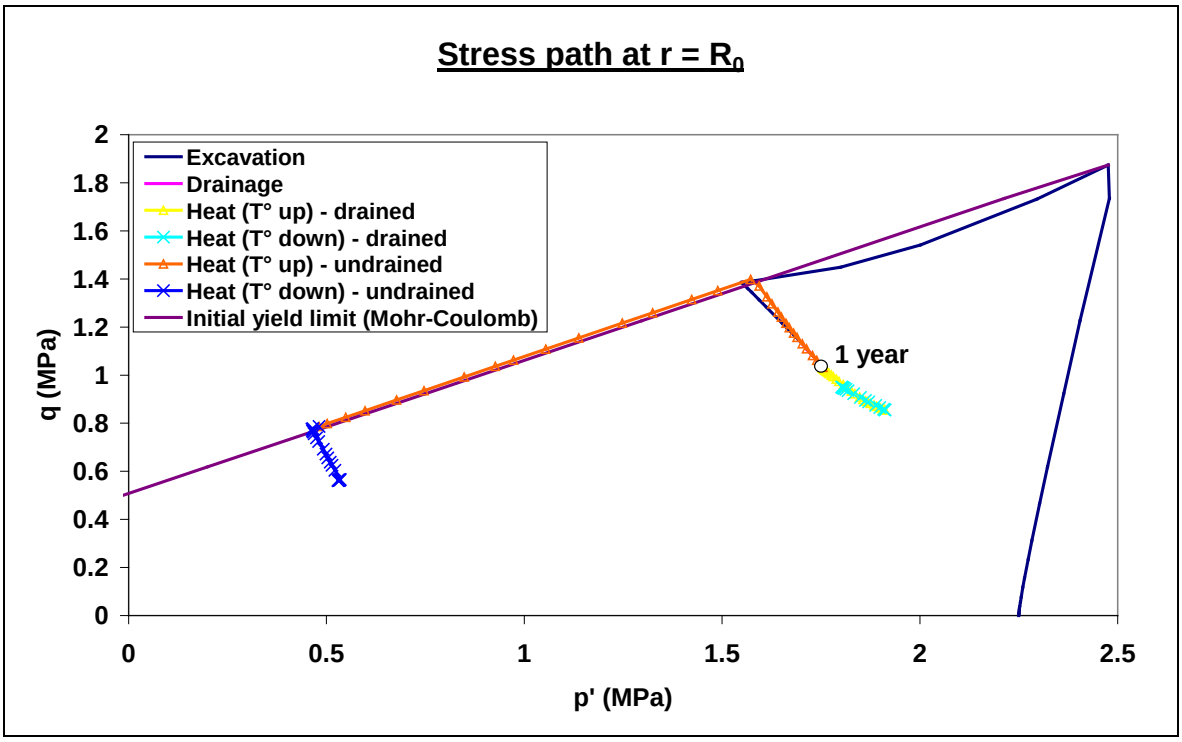

Figure 53 : Stress paths at the gallery wall- comparison between drained and undrained boundary conditions

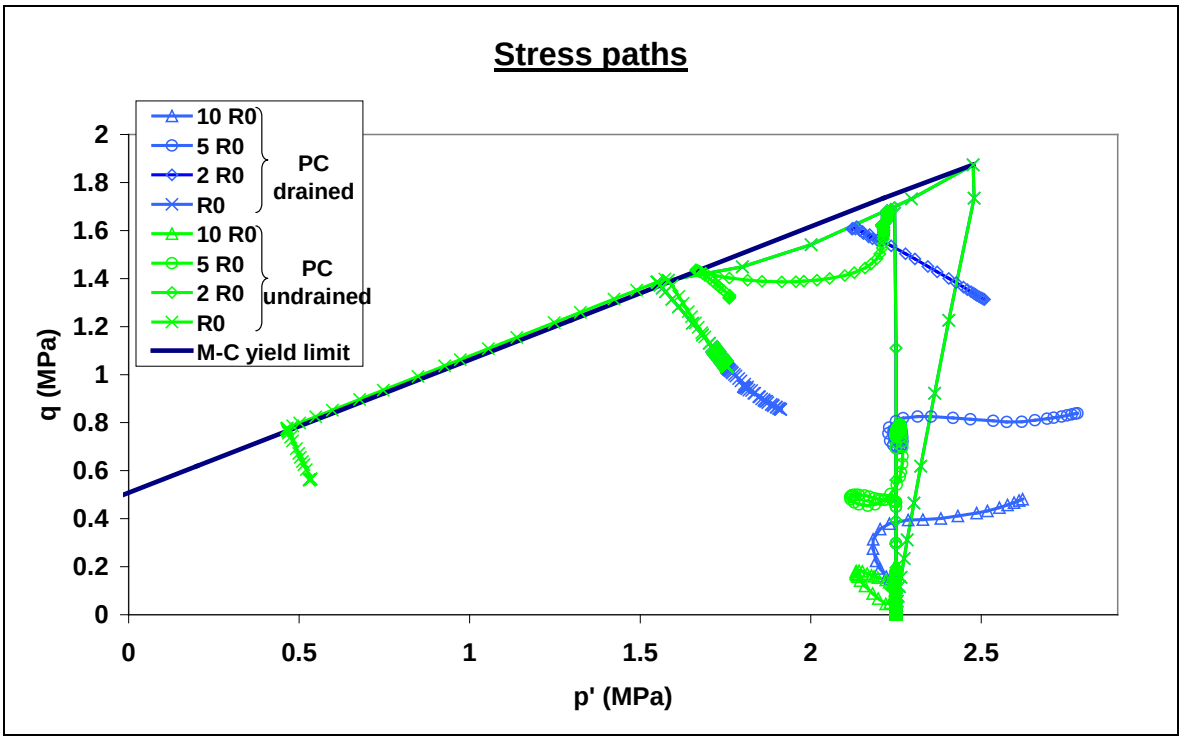

Figure 54 : Stress paths at r = R_0, r = $2R_0$, r = $5R_0$ and r = $10R_0$ - comparison between drained and undrained boundary conditions

All the figures in this chapter show the importance of the hydraulic boundary conditions on the deformation and stresses. In particular, we observe that the effect is really marked on the stress paths at the gallery wall : for the drained boundary conditions stresses in the plastic state varied from (p', q) = (2480,1870) kPa to (1550, 1380) kPa while for the undrained boundary conditions stresses varied from (p', q) = (2480,1870) kPa to (470, 760) kPa. As the stress sate in the undrained case remains plastic for a longer period, the undrained case looks more critic than the drained case.

4.3 RESULTS FOR I1 CLAY

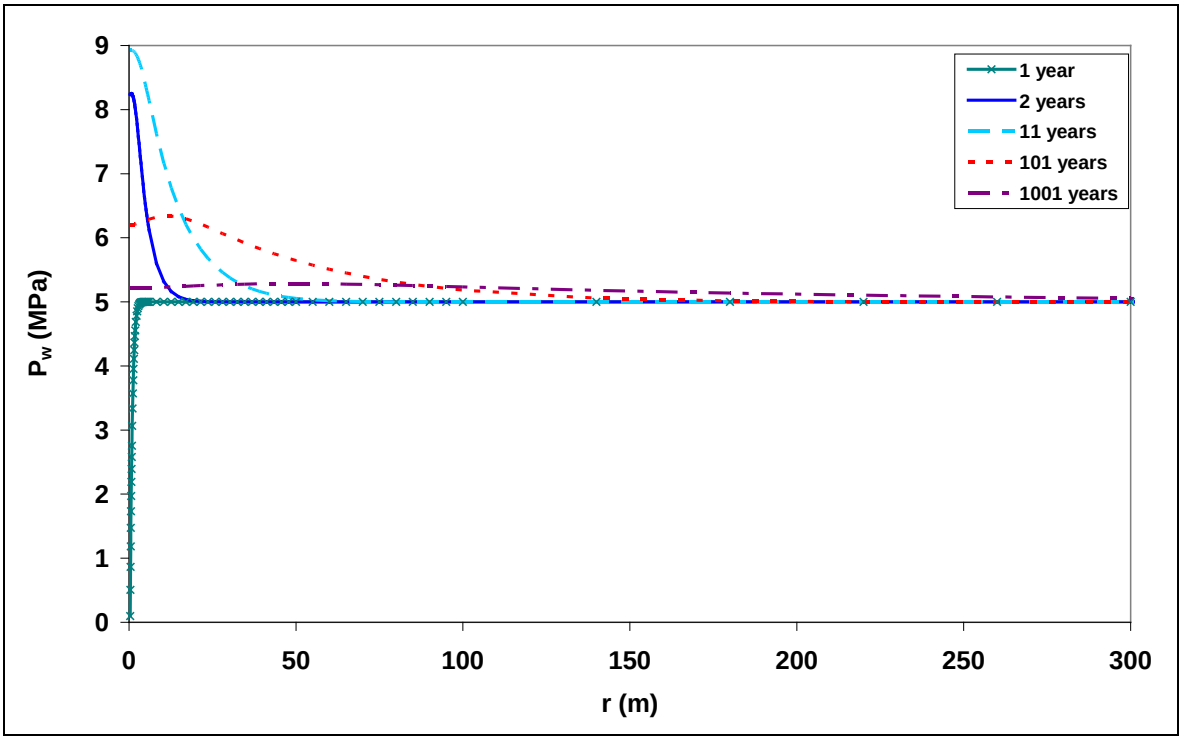

Figure 55 : Radial profile of pore water pressure at different periods during the heating phase – undrained case (I1)

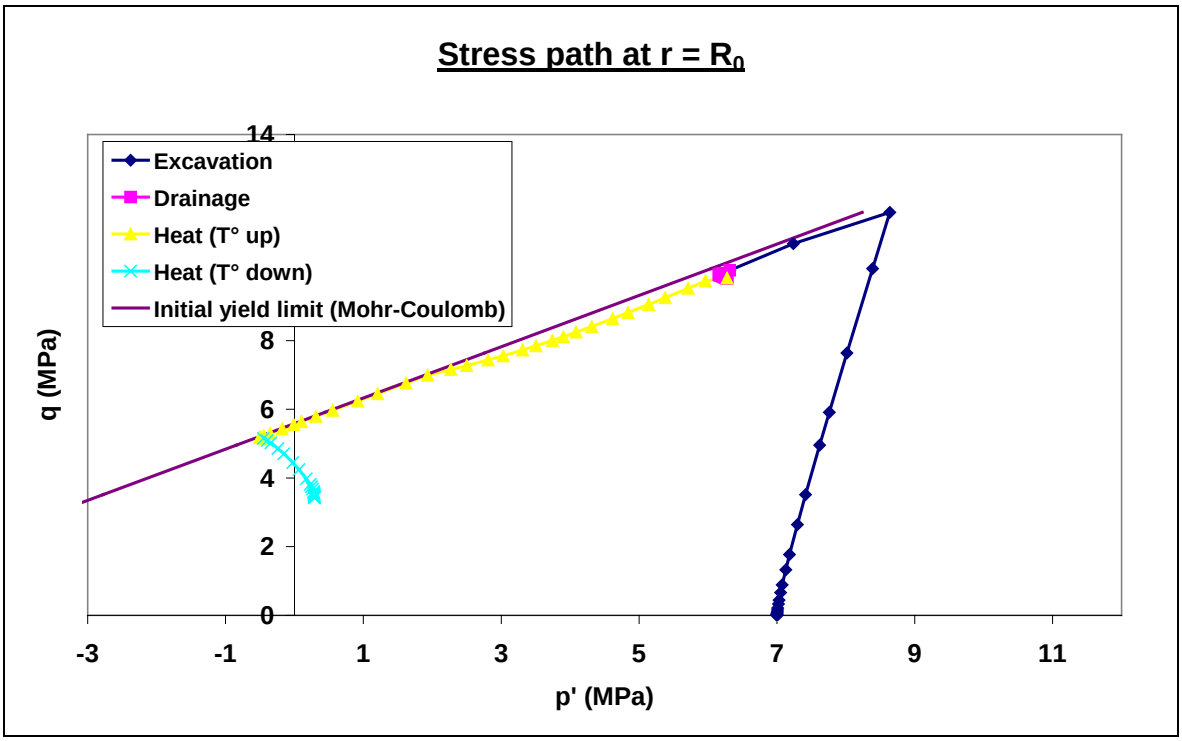

Figure 56 : Effective stress paths at r = R_0– undrained case (I1)

4.4 RESULTS FOR I2 CLAY

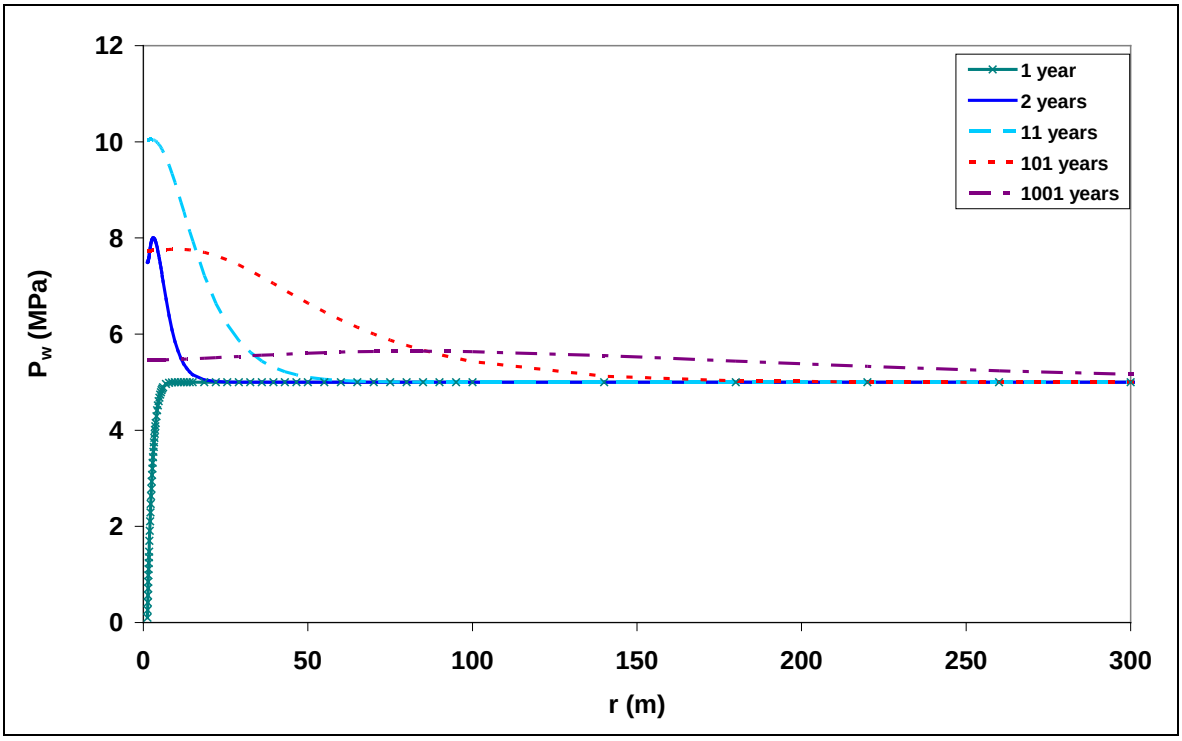

Figure 57 : Radial profile of pore water pressure at different periods during the heating phase – undrained case (I2)

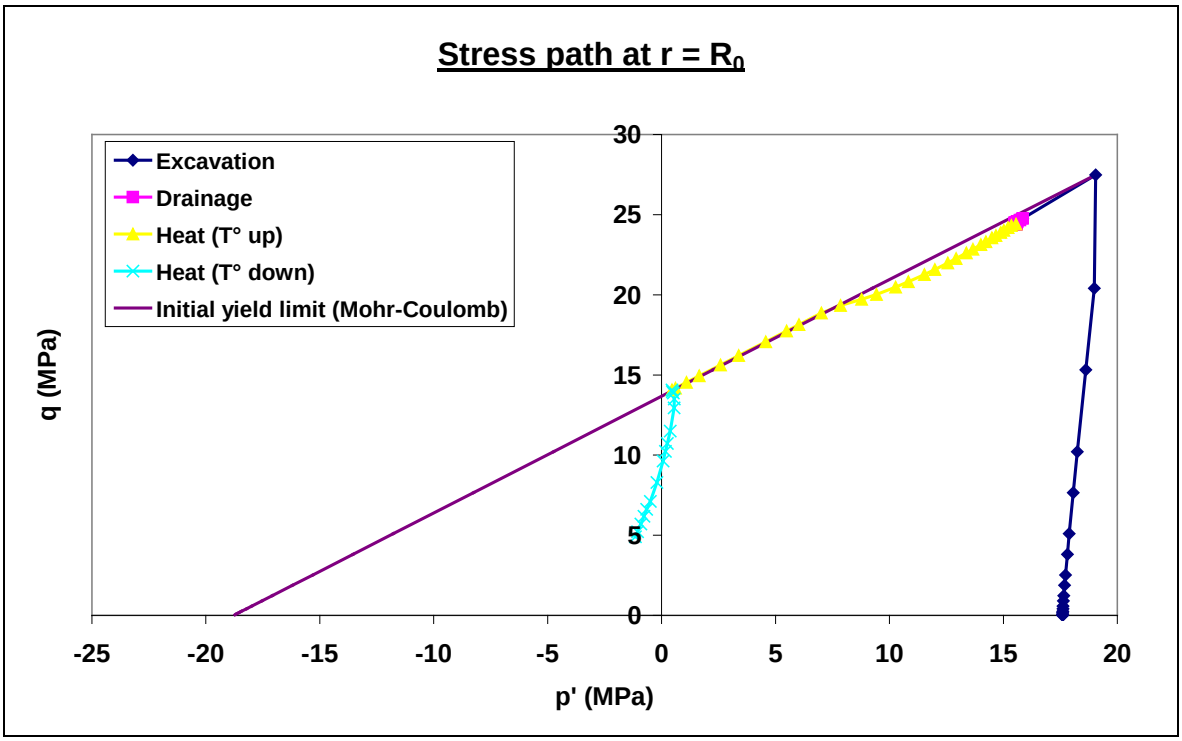

Figure 58 : Effective stress paths at r = R_0– undrained case (I2)

5 TEST CASE 3 : HEATING UNDER DRIPPING CONDITION

A more realistic hydraulic condition is a dripping boundary condition : a water flow can be created only if the pore pressure in the formation is greater than the atmospheric pressure (unilateral flow condition) as shown by Figure 59.

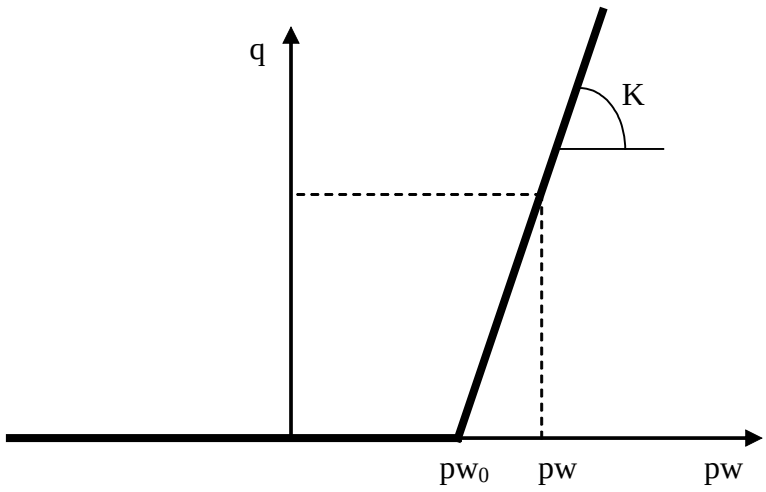

Figure 59 : Dripping condition

Where q : output or input flow at the boundary

K : a penalty coefficient

if $p_w < p_{w0}$: $q = 0$

if $p_w > p_{w0}$: $q = K (p_{w0} - p_w)$

p_{w0} can be equal to the air pressure in the gallery (we assume p_{air} = 100 kPa)

In this test case, we assume that during the whole procedure from excavation to the heating, the hydraulic boundary condition is a dripping condition : the water flow will be created only when the pore pressure is larger than the atmospheric pressure.

A simulation has been done with a value of the parameter $K = 10^{-7}$. We will only realized a simulation for the I2 case with c = 1.9 MPa and ø = 24.1° since the pressures are negative during the excavation in the drained case.

Two simulations are done : the first one with the hypothesis of a completely saturated soil and the second one with unsaturated parameters (retention curve and permeability curve).

5.1 SATURATED CASE

We still consider that the rock mass is saturated. Figure 60 shows the comparison between the drained case and the dripping saturated case for I2 clay with c = 1.9 MPa and ø = 24.1.

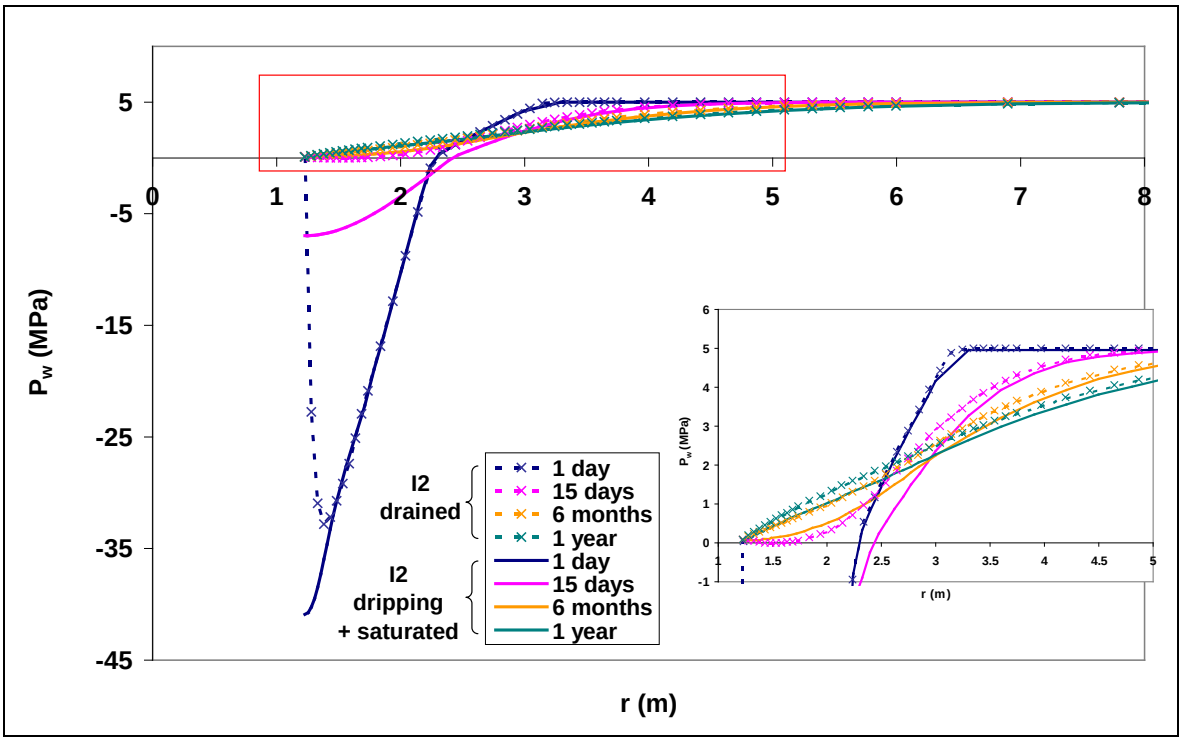

Figure 60 : Pressure profile comparison for drained and dripping conditions (I2 c = 1.9 MPa and ø = 24.1)

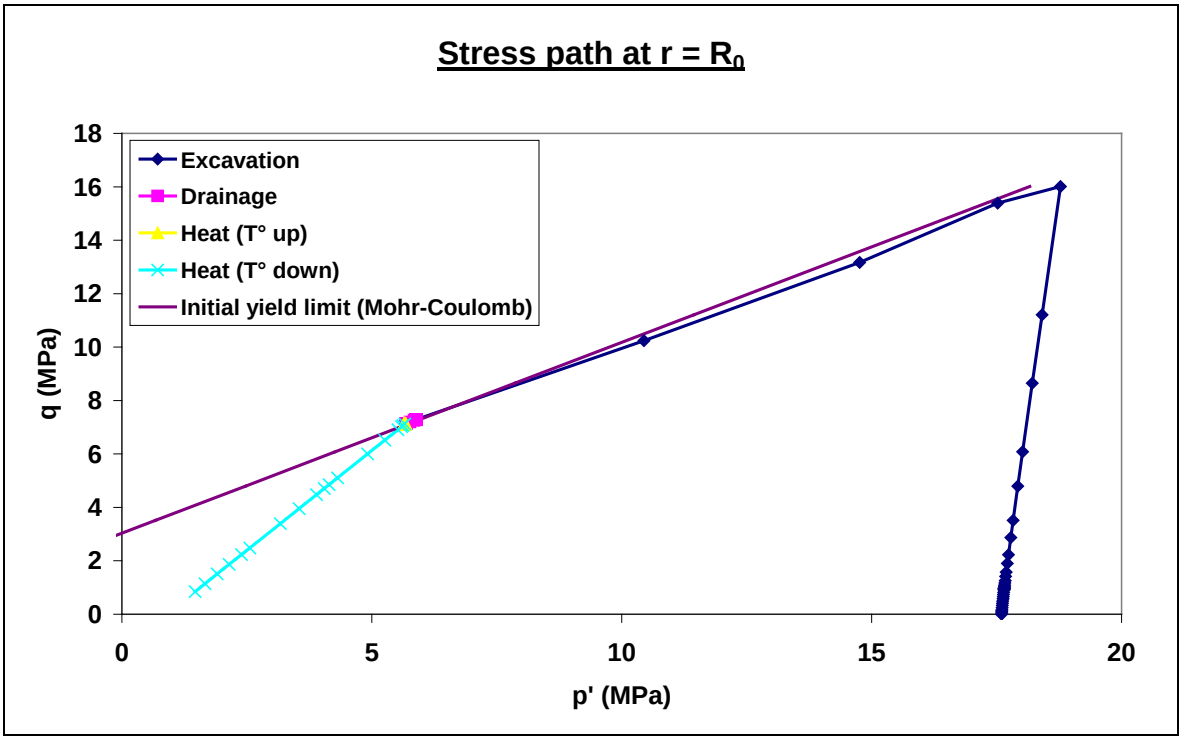

Figure 61 : Effective stress paths at r = R_0 – undrained case (I2 c = 1.9 MPa and ø = 24.1)

5.2 UNSATURATED CASE

We considered here that the rock mass can be unsaturated and we introduce a permeability curve and a water retention curve.

The following laws have been used:

- Van-Genuchten parameters (Gens 2000)

$$S_r = S_{r0} + \left[1 + \left(\frac{s}{P_0}\right)^{1/(1-\lambda)}\right]^{-\lambda}$$ with $S_{r0} = 0.007$, $\lambda = 0.403$ and $P_0 = 20.65$ MPa

- Relative permeability (from EC RESEAL report)

$$k_{rw} = \sqrt{S_r}\left[1 - \left(1 - s_e^{1/\lambda}\right)^{\lambda}\right]^2$$ with $\lambda = 0.6$

Here are the comparison between the saturated and unsaturated case for I2 clay with c = 1.9 MPa and ø = 24.1.

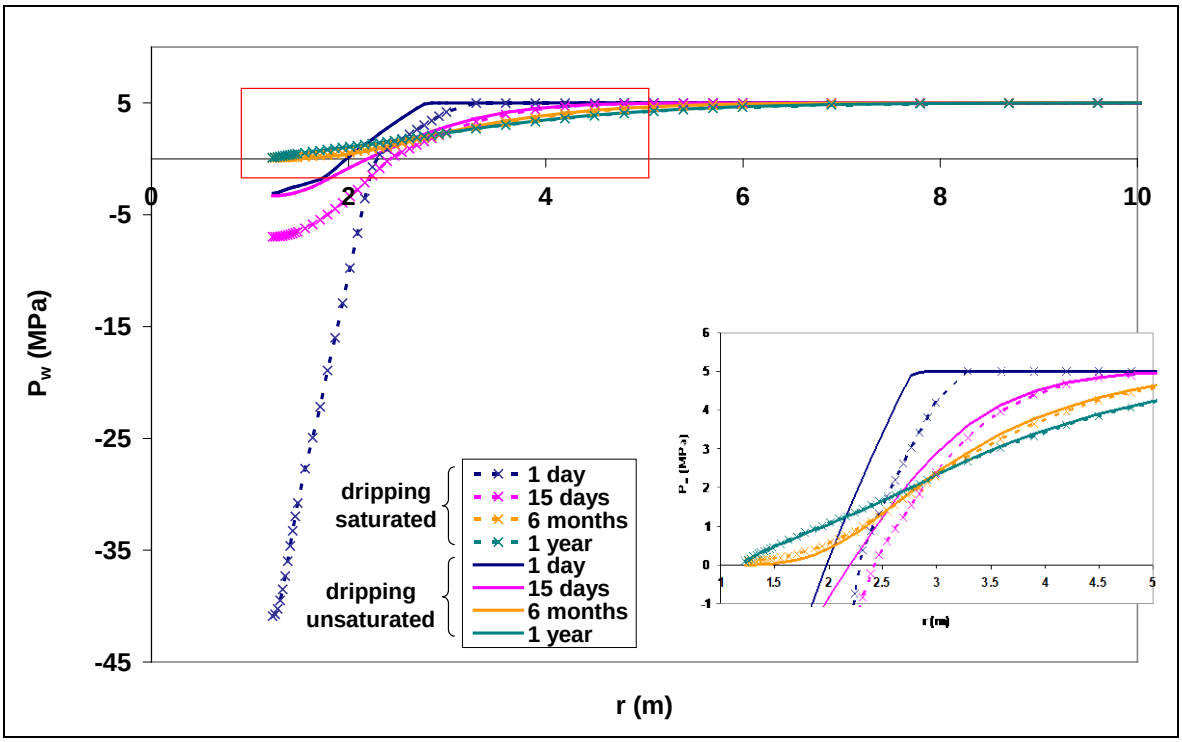

Figure 62 : Pressure profile comparison for saturated and unsaturated dripping conditions (I2 c = 1.9 MPa and ø = 24.1)

6 PARAMETRIC SENSITIVITY STUDY

Without doubt, uncertainties on some parameters exist. Parametric sensitivity study is thus interesting. The Table 13 below lists the variants which have been studied. The values in bold are those used in the normal cases.

Variants	PC case	I1 case	I2 case
Thermal conductivity	**1.35** - 1.7 [W/mK]	**1.75** [W/mK] (mean value) 1.3 [W/mK] (⊥ to bending) 2.0 [W/mK] (// to bending)	
Dilation angle	**0** - 10 [°]		
Cohesion			**8.6** [MPa] (Matrix) 1.9 [MPa] (Bedding)
Frictional angle			**24.6** ° (Matrix) 24.1 ° (Bedding)
Biot coefficient		**1** – 0.6	
Permeability		**5.10^{-14}** [m/s] (⊥ to bending) 5.10^{-13} [m/s] (// to bending)	**2.10^{-13}** [m/s] (// to bending) 6.10^{-14} [m/s] (⊥ to bending)

Table 13 : Parametric sensibility study

6.1 THERMAL CONDUCTIVITY COEFFICIENT

In the reference cases PC, we change the thermal conductibility coefficient λ value from 1.35 W/(mK) (value obtained in ATLAS) to 1.7 W/(mK) (SAFIR2) to check its influence on the results. As well, in the I1 case, we realize the simulation with λ equals to 1.3 (⊥ to bending) and 2 W/(mK) (// to bending).

6.1.1 PC

As it was predicted (Figure 63), the maximum temperature reached at the gallery is smaller (-12.9 %) when the thermal conductivity coefficient increases (+26 %), that is when the material is more conductive. However, for the same heat flux, the maximum is reached more or less after the same time (10 years of heating).

On the Figure 64, we observe that this decrease of temperature induced by a higher conductivity is limited in space. The thermal disturbed zone is, in both cases, around 100 meters. This reduction of temperature induces, of course, all the consequences on pore water pressure, displacement and stresses which have been mentioned before.

	T_{max} (°C)	t (years)
λ = 1.35 W/(mK)	68.3	11
λ = 1.7 W/(mK)	59.5	11

Table 14 : Maximum temperature for different values of thermal conductivity (PC)

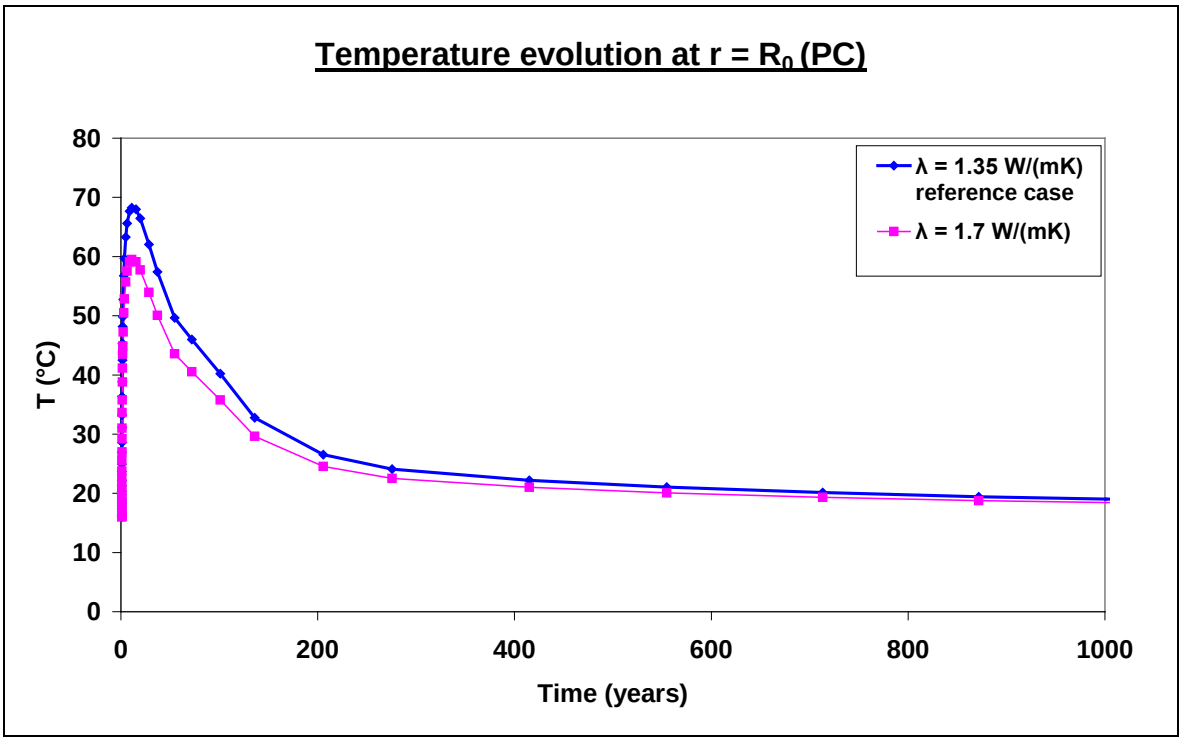

Figure 63 : Comparison of temperature evolution for different value of conductivity (PC)

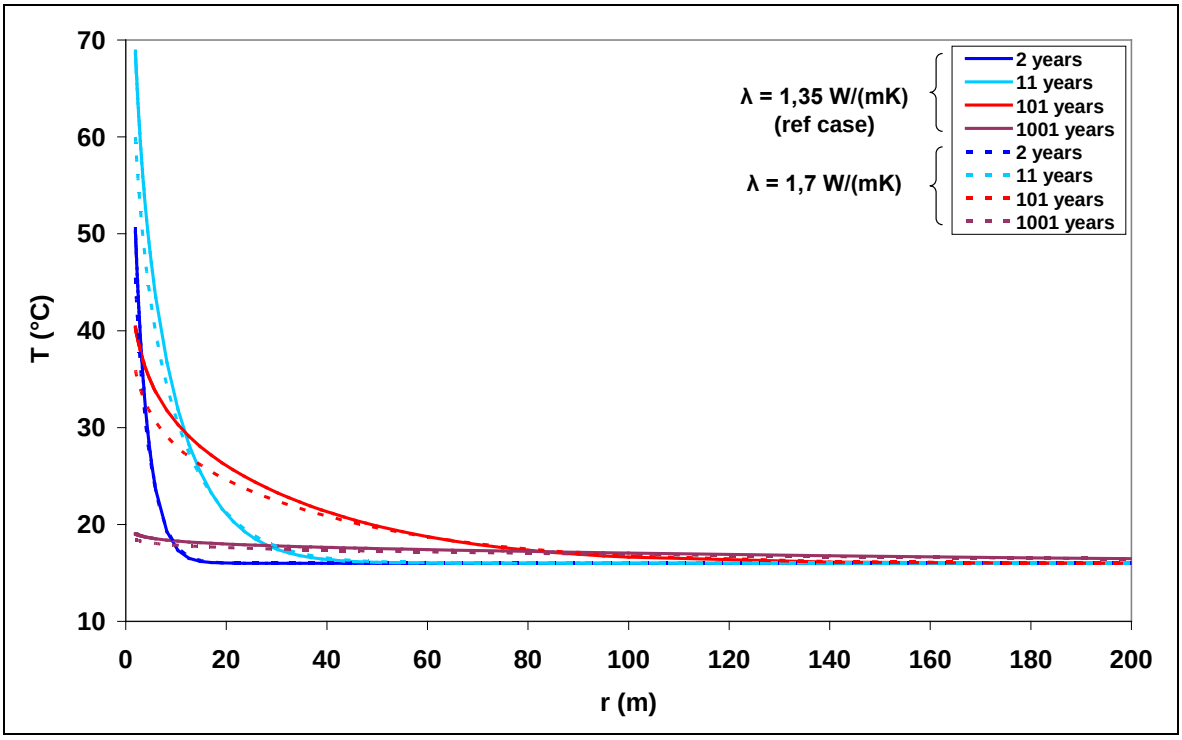

Figure 64 : Temperature profile during the heating stage for different value of conductivity (PC)

6.1.2 I1

Here are the results for I1 case.

	T_{max} (°C)	t (years)
λ = 1.75 W/(mK)	58.8	8.8
λ = 2 W/(mK)	54.7	8.8
λ = 1.3 W/(mK)	69.7	8.8

Table 15 : Maximum temperature for different values of thermal conductivity (I1)

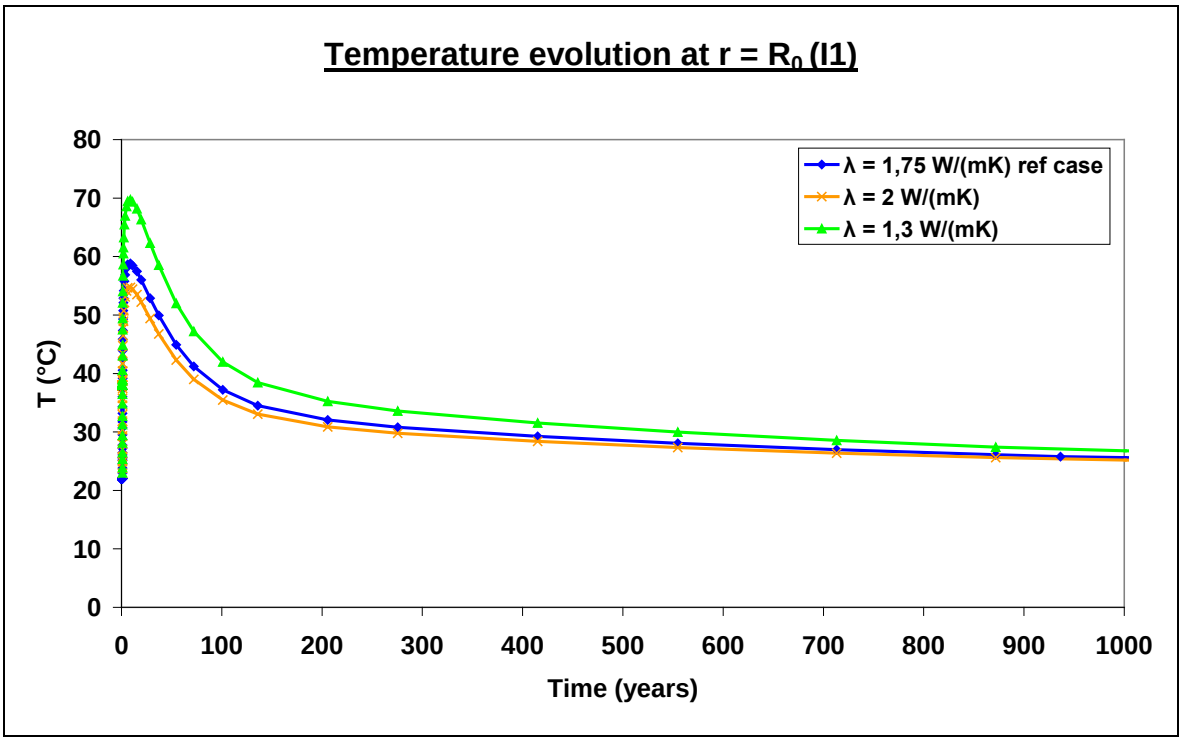

Figure 65 : Comparison of temperature evolution for different value of conductivity (I1)

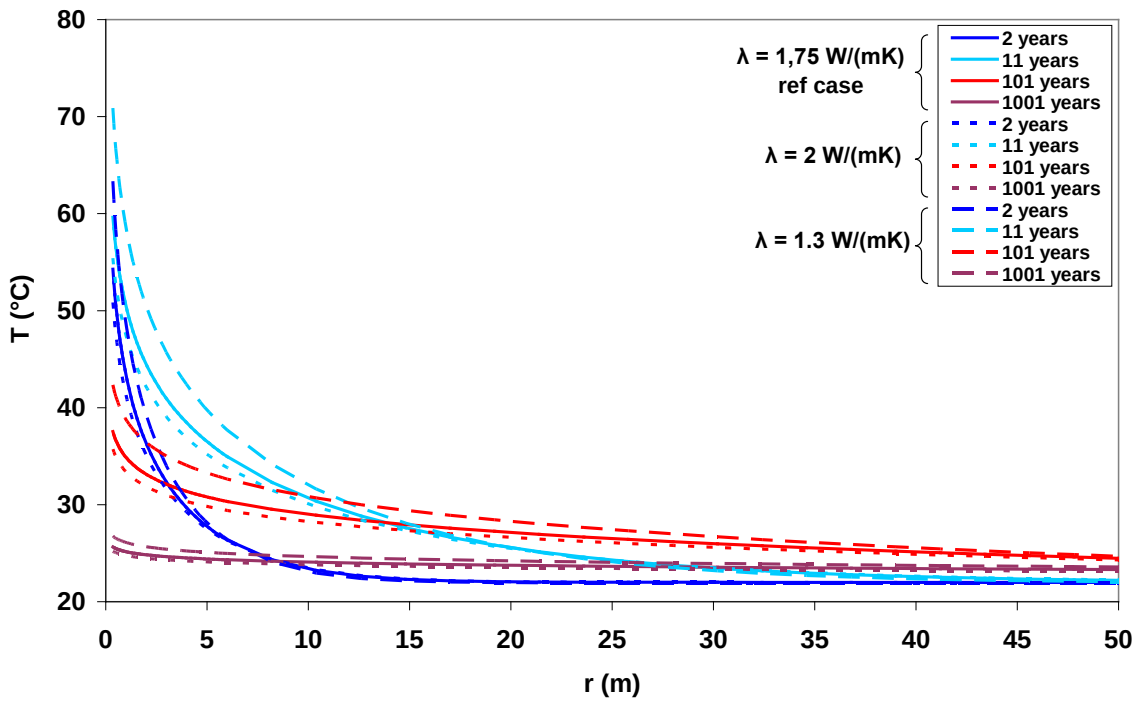

Figure 66 : Temperature profile during the heating stage for different value of conductivity (I1)

6.2 DILATATION ANGLE (PC)

We change the dilatation angle ψ value from 0° (reference case PC) to 10° to analyse its influence on the results. Temperature profiles and evolution are identical to the reference case, whereas the stress paths are slightly modified (Figure 68). Let's remind that only the initial Mohr-Coulomb yield limit is plotted and that this one changes in the (p', q) axes. The highest difference consists in the pore water pressure profiles (Figure 67). Indeed, higher is the dilatation angle higher is the dilatation during the excavation. This causes higher "negative pressure". After one year of drainage at the gallery wall, the pressure profiles for the two values of ψ are identical. This stays true during the heating phase.

In this case, it must be interesting to study the dripping boundary conditions.

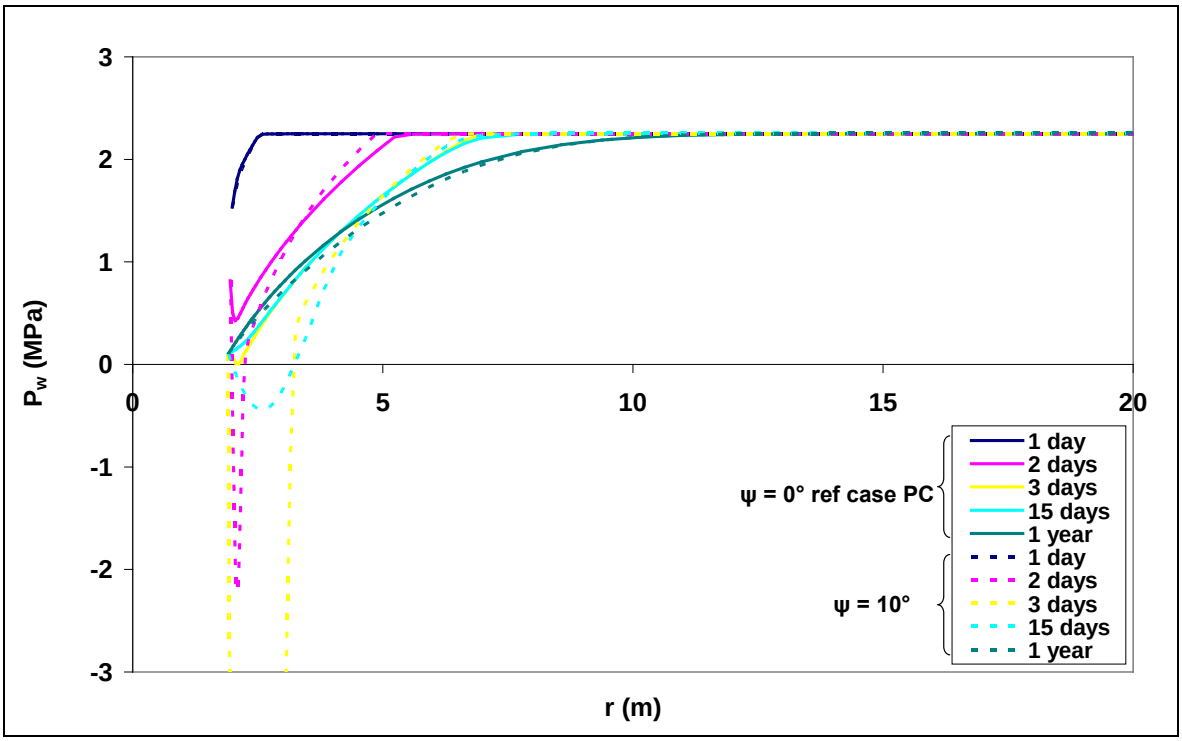

Figure 67 : Comparison of the pore water pressure profiles during the excavation and the drainage phases for different value of the dilatation angle (PC)

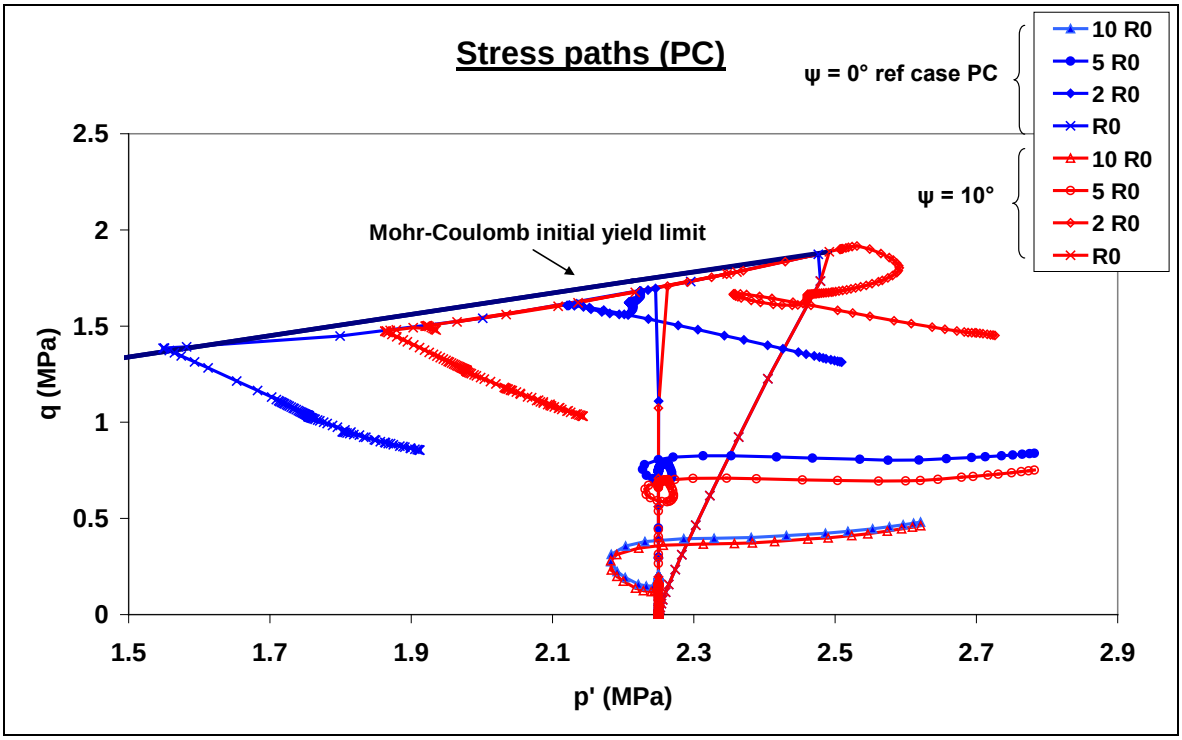

Figure 68 : Comparison of the stress paths for VHLW after 50 years of cooling for 2 dilatation angles (ψ = 0° and ψ = 10°) (PC)

6.3 MECHANICAL PARAMETERS (C,Φ) (I2)

In this section we test the influence of the resistance parameters, which are the cohesion and the frictional angle. In the reference case (I2), the parameters for the matrix were c = 8.6 MPa and ø = 24.6 °. There are now those for the bedding : c = 1.9 MPa and ø = 24.1 °.

There is of course no influence on the temperature. The influence is observed on displacement, pore pressure and stresses. The following figures compare the results obtained for the reference case and the parametric sensitivity case.

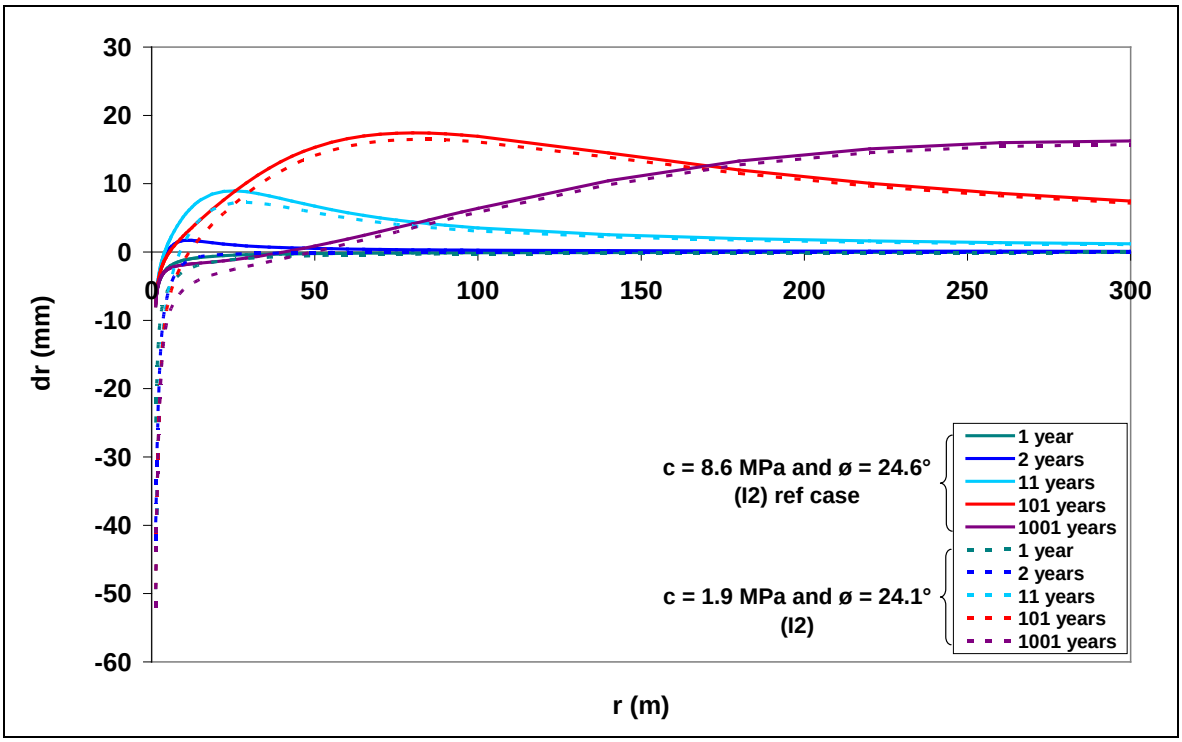

Figure 69 : Displacement profiles - comparison for various mechanicals parameters (I2)

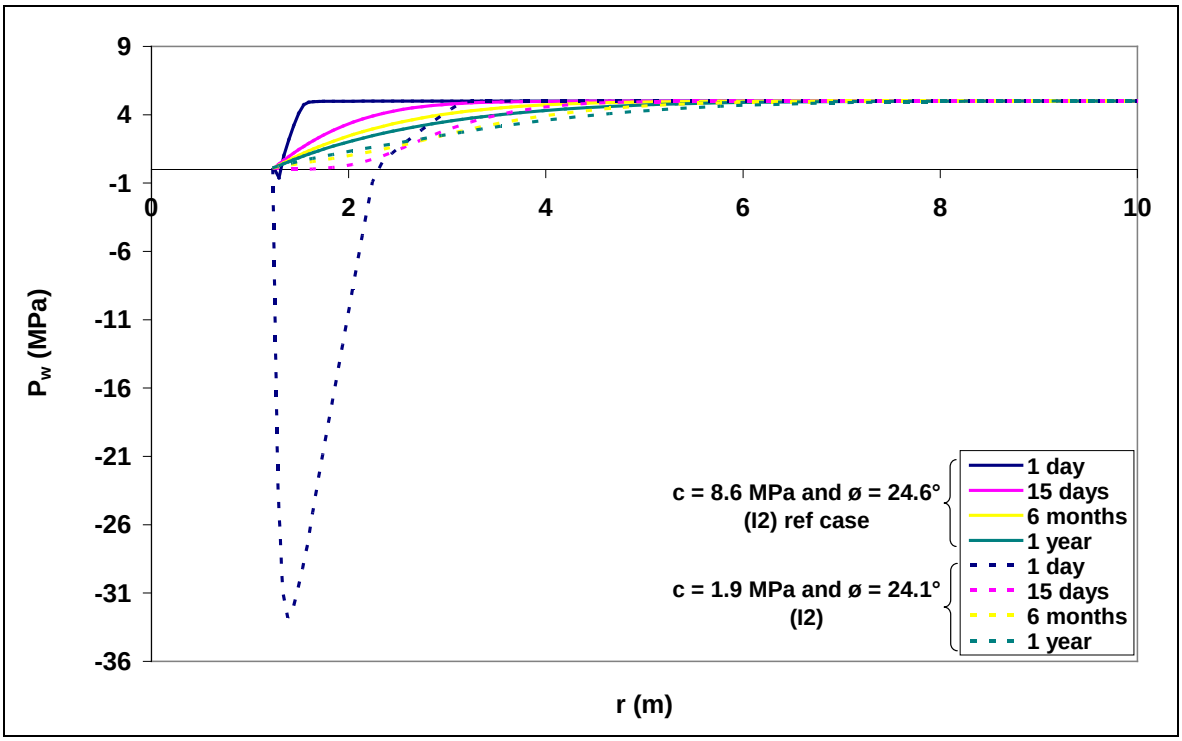

Figure 70 : Pressure profiles - comparison for various mechanicals parameters (I2)

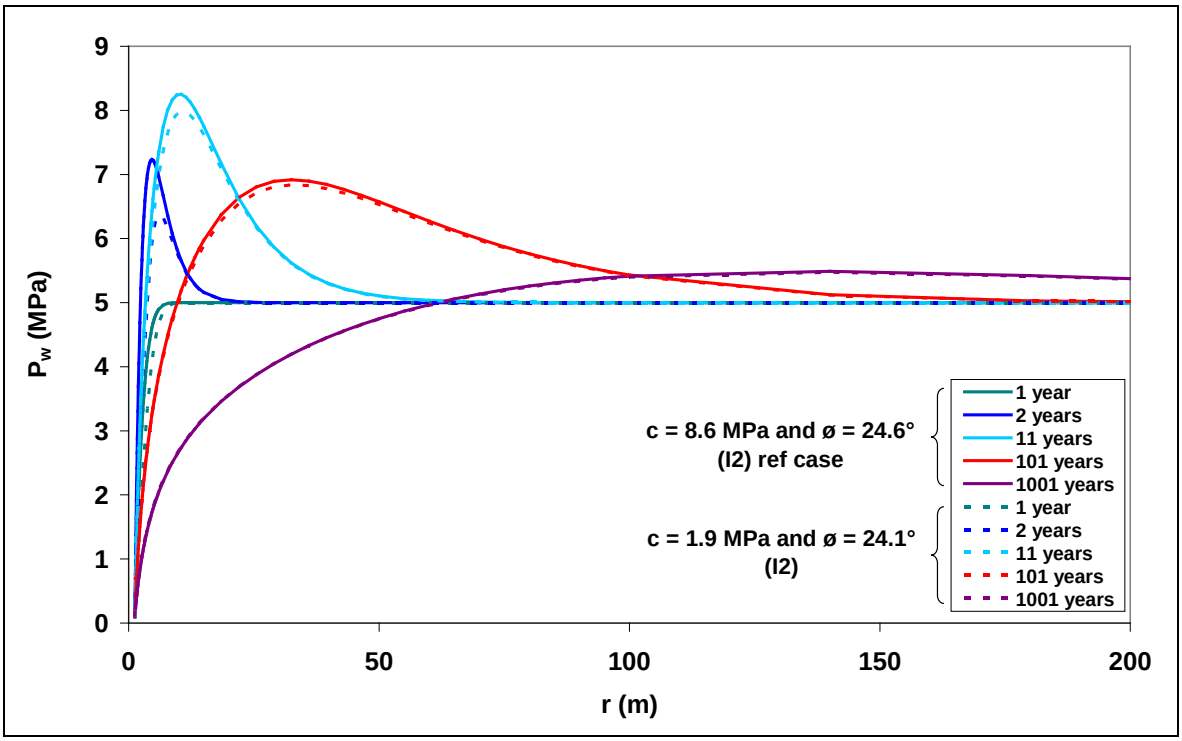

Figure 71 : Pressure profiles - comparison for various mechanicals parameters (I2)

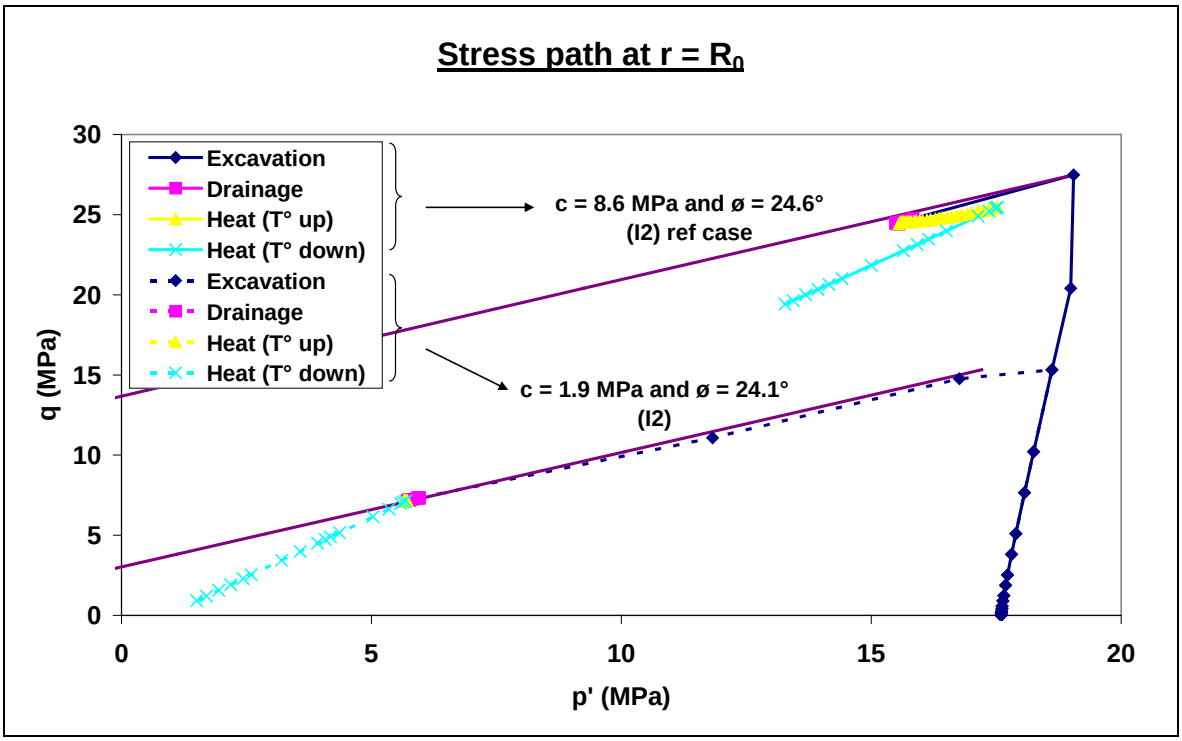

Figure 72 : Comparison of the stress paths for various mechanicals parameters (I2)

6.4 BIOT COEFFICIENT (I1)

In this section we test the influence of the Biot coefficient. For I1 reference case, the Biot coefficient was equal to 1, it is now equal to 0.6.

There is of course no influence on the temperature. The influence is observed on displacement, pore pressure and stresses. The following figures compare the results obtained for the reference case and the parametric sensitivity case.

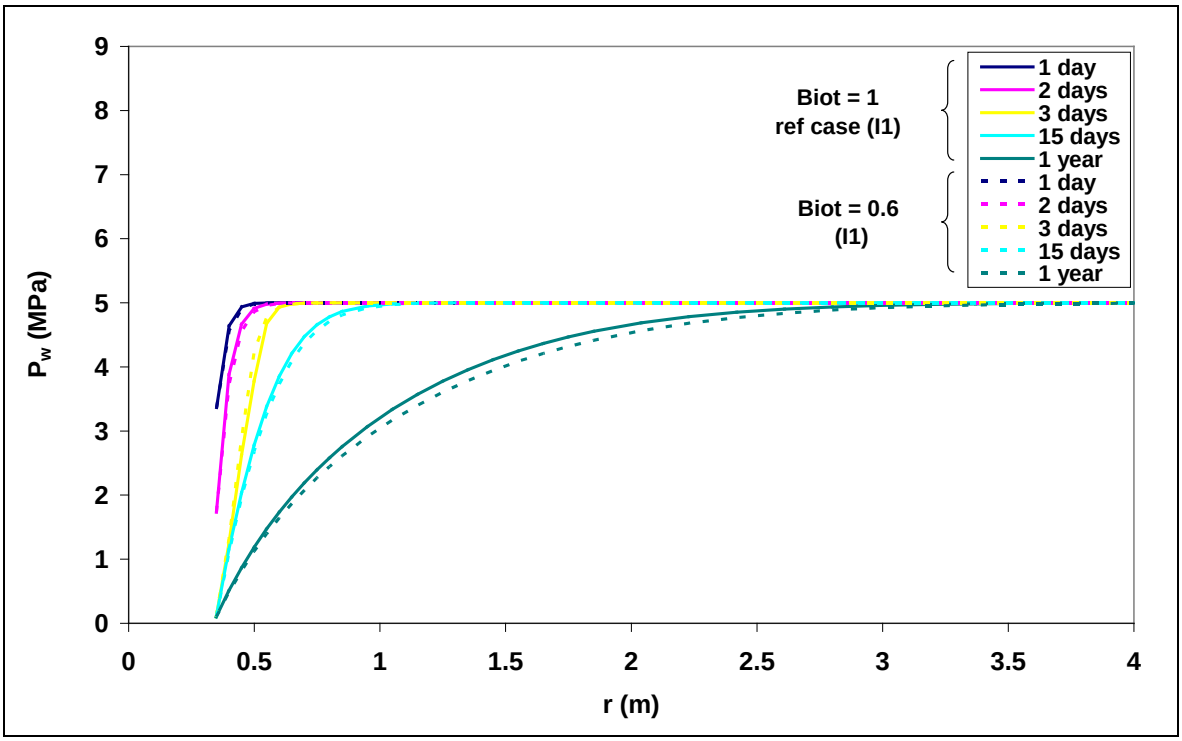

Figure 73 : Pressure profiles - comparison for various Biot coefficient (I1)

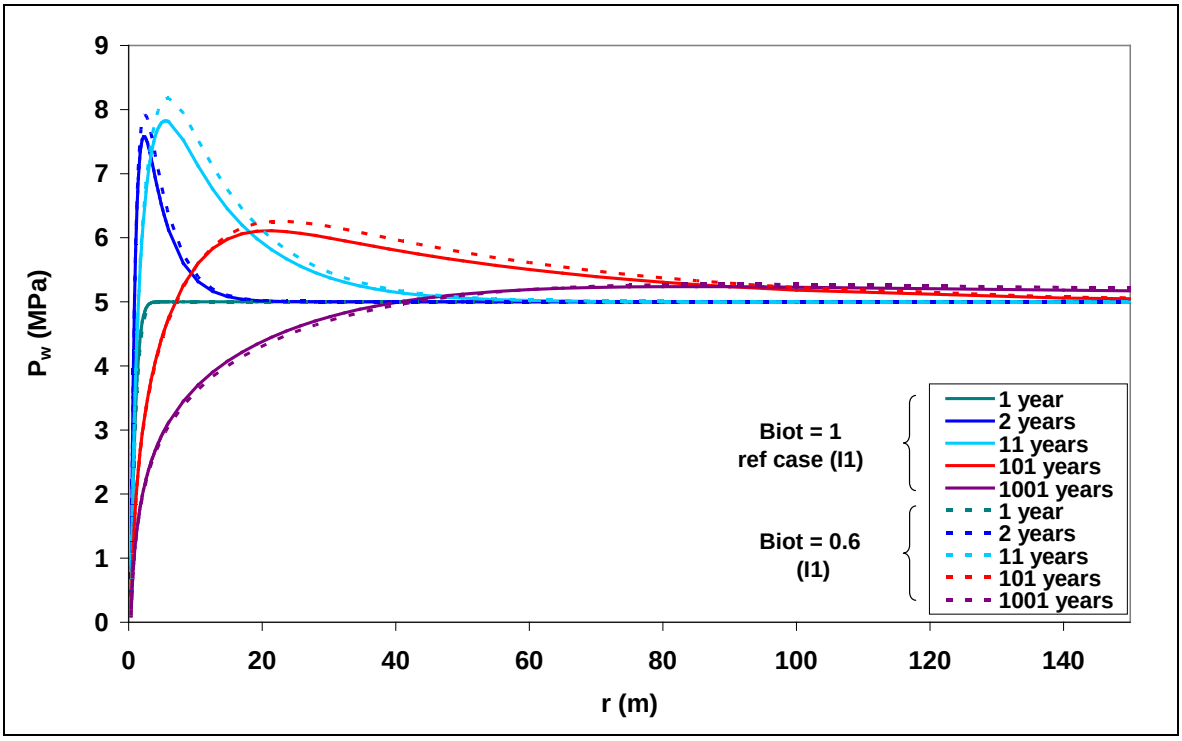

Figure 74 : Pressure profiles - comparison for various Biot coefficient (I1)

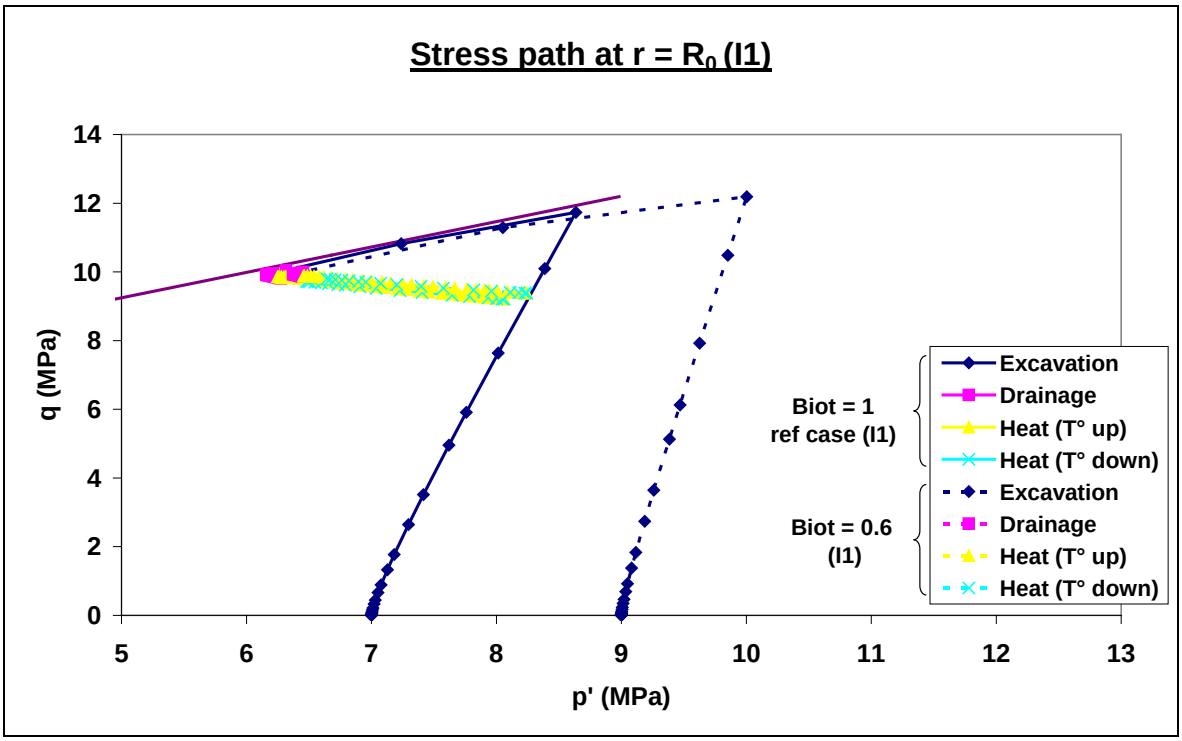

Figure 75 : Comparison of the stress paths for various Biot coefficient (I1)

6.5 PERMEABILITY (I2)

In this section we test the influence of the permeability. We will only show the results for I2 since the one for I1 show the same tendencies.

In the reference case (I2), the permeability was k = 2.10^{-13} m/s (// to bending). The simulation is now realized with the permeability perpendicular to the bending k = 6.10^{-14} m/s.

The variation of permeability mainly acts on pore water pressure and thus on effective stress. There is of course no influence on the temperature. The following figures compare the results obtained for the reference case and the parametric sensitivity case.

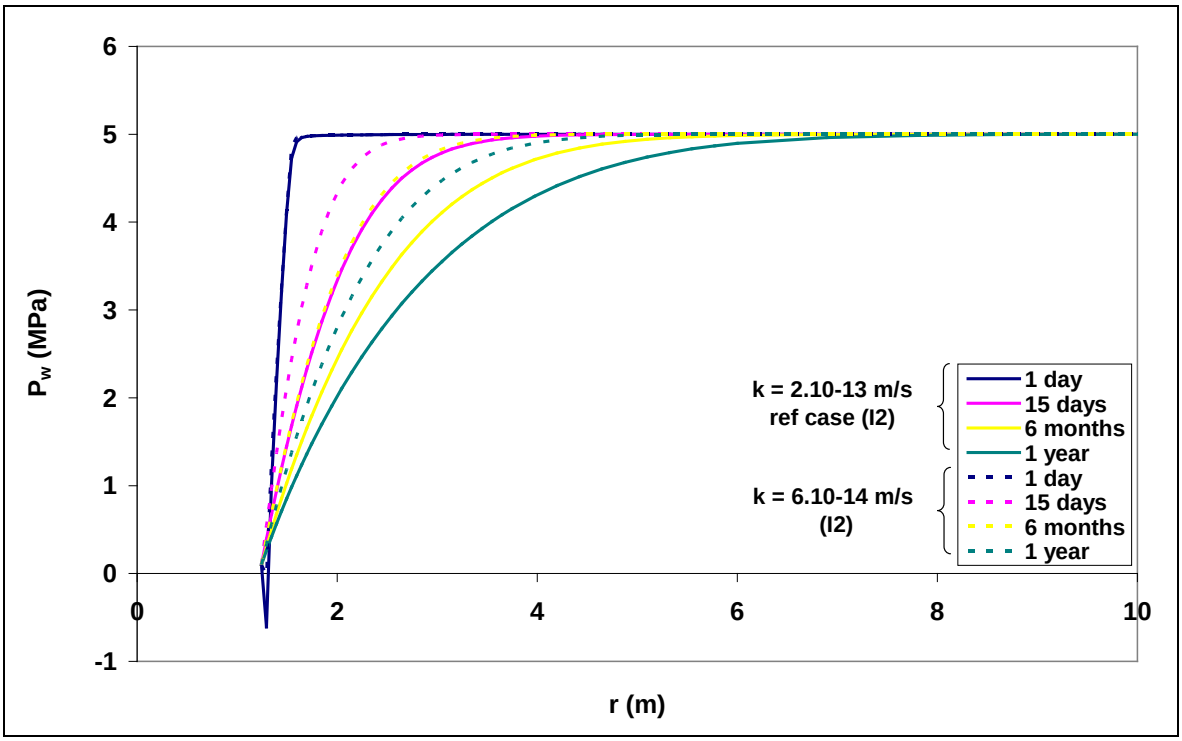

Figure 76 : Pressure profiles - comparison for various permeabilities (I2)

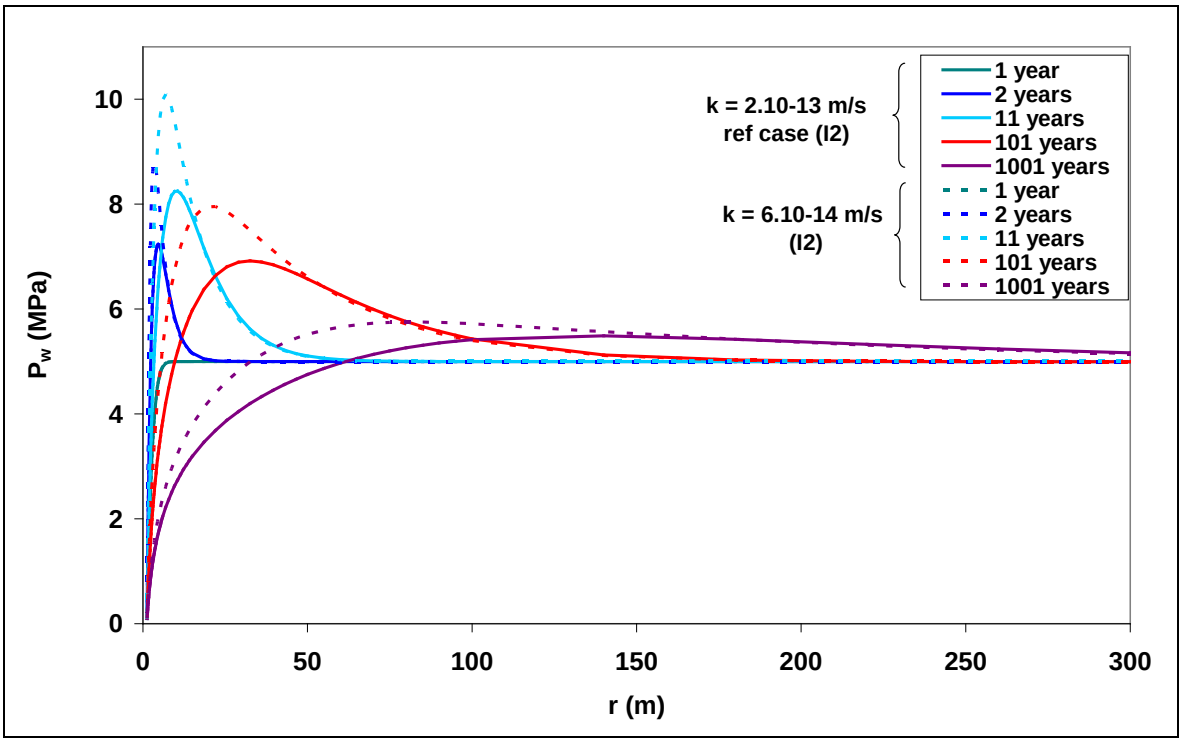

Figure 77 : Pressure profiles - comparison for various permeabilities (I2)

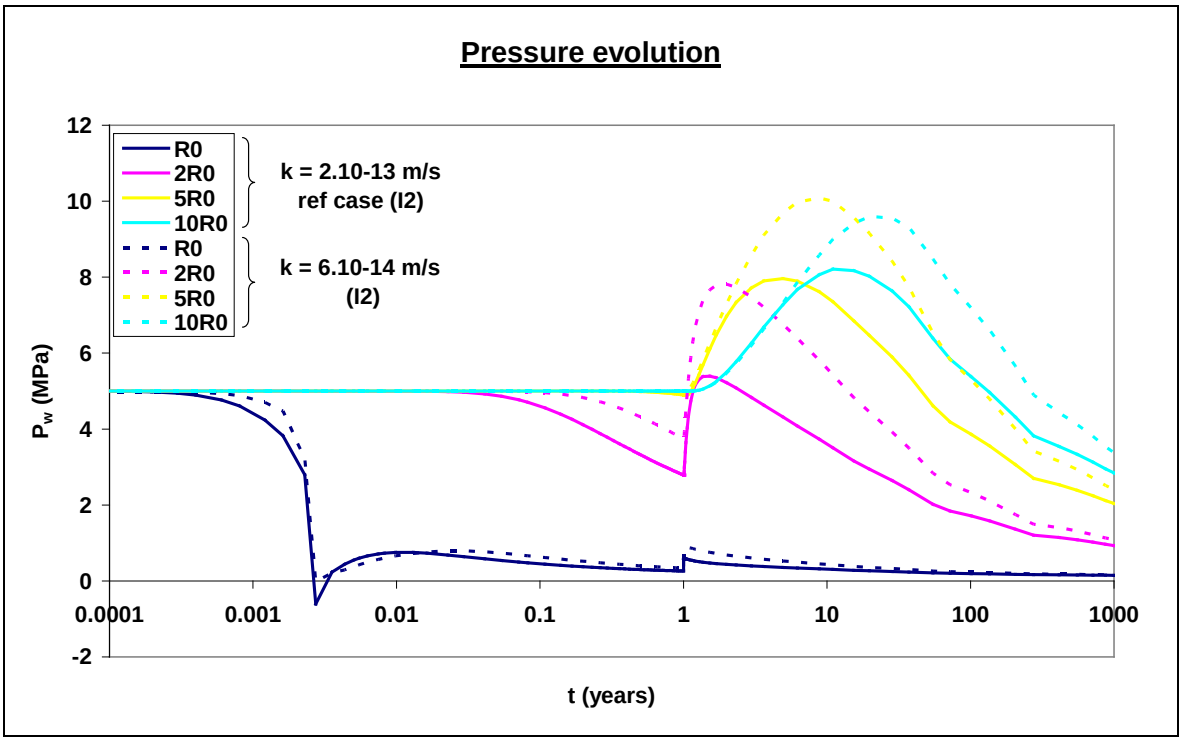

Figure 78 : Pressure evolution at various radius - comparison for various permeabilities (I2)

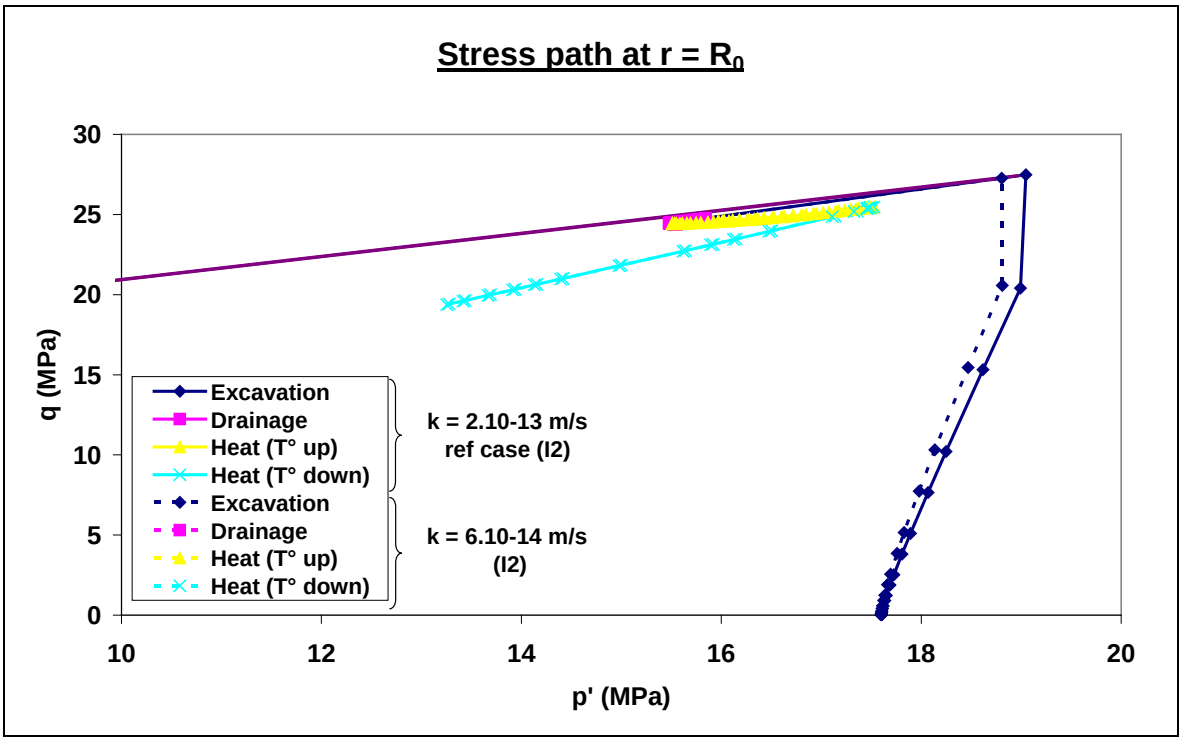

Figure 79 : Comparison of the stress paths for various permeabilities (I2)

6.6 CONSTITUTIVE LAW SENSIBILITY STUDY (PC)

In this chapter we propose to test the influence of the constitutive law on the stress paths. The reference case used a Mohr-Coulomb model where only the thermo-elasticity was considered. We are now looking at a model where the internal friction yield limit is a Van Eekelen criterion. The second law analysed is a CapSol model taking into account a thermal softening.

6.6.1 VAN EEKELEN

Figure 80 shows the stress paths at different radius for the reference case and the Van Eekelen one. We note that the extreme deviatoric and mean stresses are slightly different. For the reference case: p_{min} = 1800 kPa, p_{max} = 2745 kPa, q_{min} = 0 kPa and q_{max} = 1838 kPa and for the Van Eekelen one : p_{min} = 1530 kPa, p_{max} = 2745 kPa, q_{min} = 0 kPa and q_{max} = 2230 kPa.

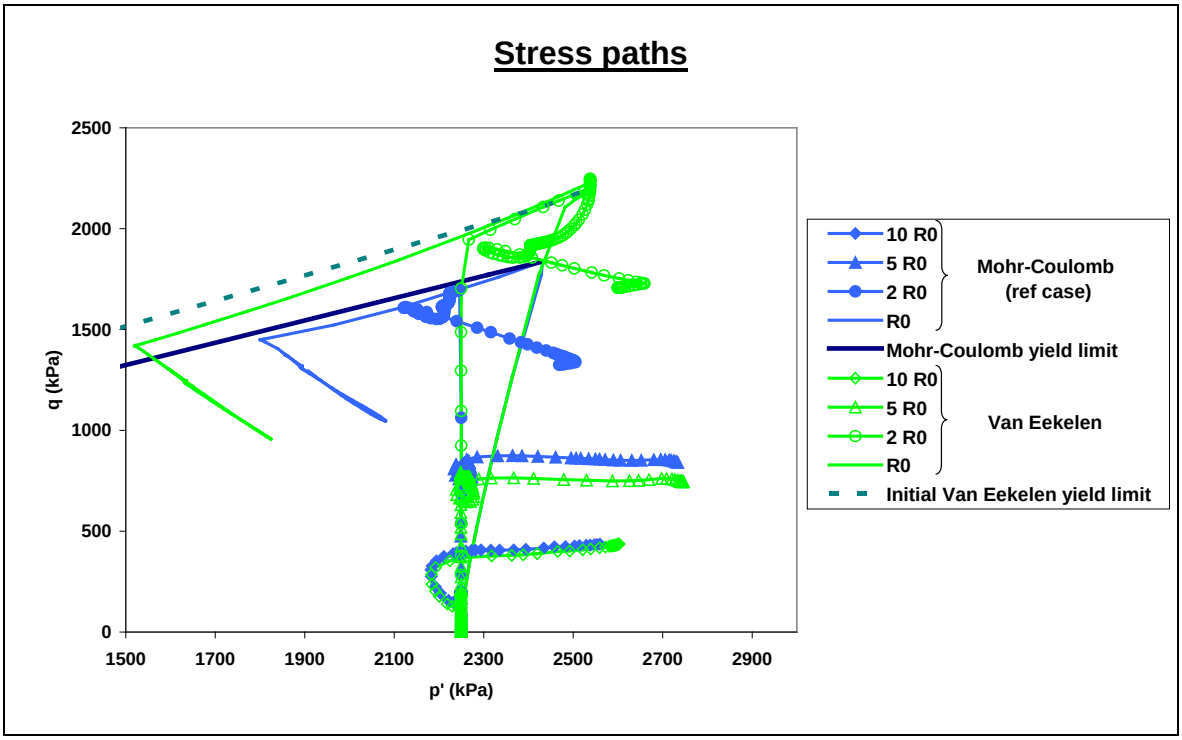

Figure 80 : Comparison of the stress paths for VHLW after 50 years of cooling for 2 constitutive laws (Mohr-coulomb and Van Eekelen)

6.6.2 CAPSOL MODEL WITH THERMAL SOFTENING

Table 16 presents the characteristics of the Capsol model including a thermal softening (Laloui & al., 2003), that is a variation of the preconsolidation pressure with temperature. This model can also take into account a variation of cohesion and friction angle with temperature. The CapSol model presented hereafter is a combination, within a cap yield surface, of a modified CamClay and a frictional mechanism.

TIM2EA : Thermo-elasto-plastic law (Liège)

CAP MODEL : 3 coupled yield limit (traction + isotropic + deviotaric) including thermal hardening, reversible thermal dilatation and irreversible contraction

- Preconsolidation pressure σ'_c variation with temperature T° (Laloui & al., 2003) :

$$\sigma'_{c0}(T) = \sigma'_{c0}(T_0)\left\{1 - \gamma \log\left\{\left[T_0 + \Delta T\right]/T_0\right\}\right\}$$

With $\sigma'_c(T_0) = \sigma'_{co}(T_0)\exp\left(\beta\varepsilon_v^p\right)$

- Friction angle and cohesion variation with temperature T° :

$\phi(T) = \phi_0 - g\left(T - T_0\right)$ and $c(T) = c_0 - k_c\left(T - T_0\right)$

- Deviatoric yield limit : internal friction model (Plasol)

$$f_d = II_{\hat{\sigma}} - m\left(I_{\hat{\sigma}} + 3\frac{c(T)}{\tan\phi_c}\right) = 0$$

with $m = \dfrac{2\sin\phi_c}{\sqrt{3}(3 - \sin\phi_c)}$ (Drucker-Prager)

or $m = a(1 + b\sin\beta)^n$ (Van Eekelen)

- Isotropic yield limit : Modified Cam Clay model

$$f_i = II_{\hat{\sigma}}^2 + m^2\left(I_\sigma + 3\frac{c(T)}{\tan\phi_c}\right)\left(I_\sigma - 3\sigma'_{c0}(T)\right) = 0$$

- Traction yield limit

$$f_t = II_{\hat{\sigma}}^2 - m^2\left(I_\sigma + \left(3\frac{c(T)}{\tan\phi_c}\right)^2 / 3\sigma_t\right)\left(I_\sigma - 3\sigma_t\right) = 0$$

Or $f_t = I_\sigma - 3\sigma_t = 0$

Table 16 : Characteristics of the CapSol model including thermal softening

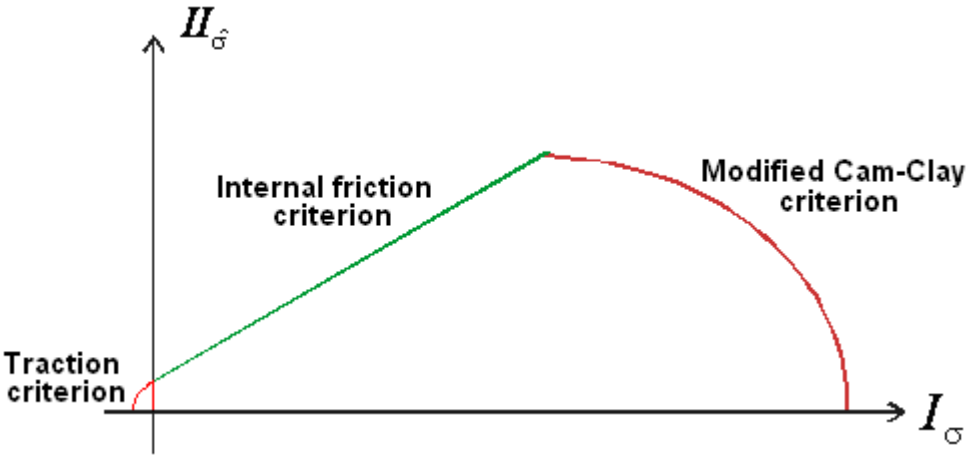

Figure 81 : CapSol model in the $(I_{\sigma}, II_{\hat{\sigma}})$ plane

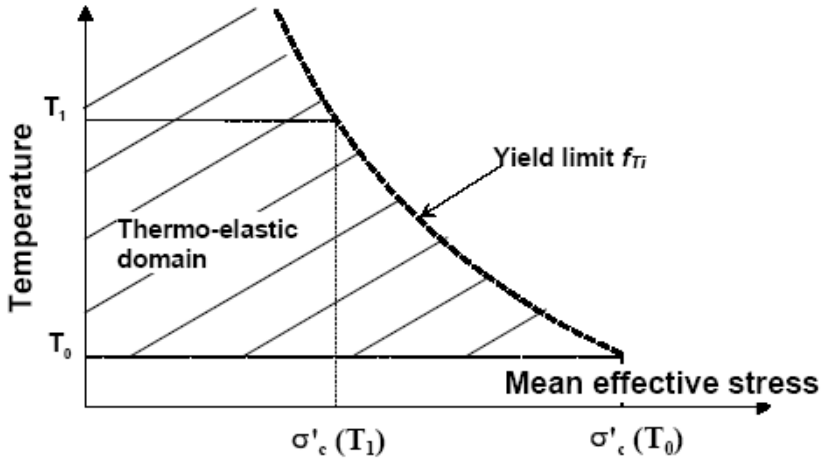

Figure 82 : Thermo-plastic yield limit - Variation of the preconsolidation pressure with temperature (Laloui & al., 2003)

The simulation is realized with the same parameters than the reference case. The only new parameters are the preconsolidation pressure (σ_c' = 6 MPa), the volumetric hardening parameter (β = 14) and the parameter γ which gives the evolution of the preconsolidation pressure with temperature (γ = 0.18 : Laloui & al., 2003). The internal friction model used is a Drucker-Prager criterion. We admit that there are no variations of friction angle nor cohesion.

Figure 83 shows the stress path at the gallery wall obtained with the TIM2EA law. We observe the deviatoric and the isotropic yield limit. The first one (f1) does not depend of the thermal hardening, thus is constant during the all simulation. On the other hand, the second one (f2) depends of it. So, when the temperature reaches its maximum at the gallery wall (T_{max} = 68.57°C after 11 years), the preconsolidation pressure is equal to 5.32 MPa (compared to 6 MPa initially) and the yield limit creeps (f2 interm). Once the temperature decreases, the yield limit returns to its initial state.

Let's note that in this case, the thermal softening does not influence the stress path since only the deviatoric yield limit is reached.

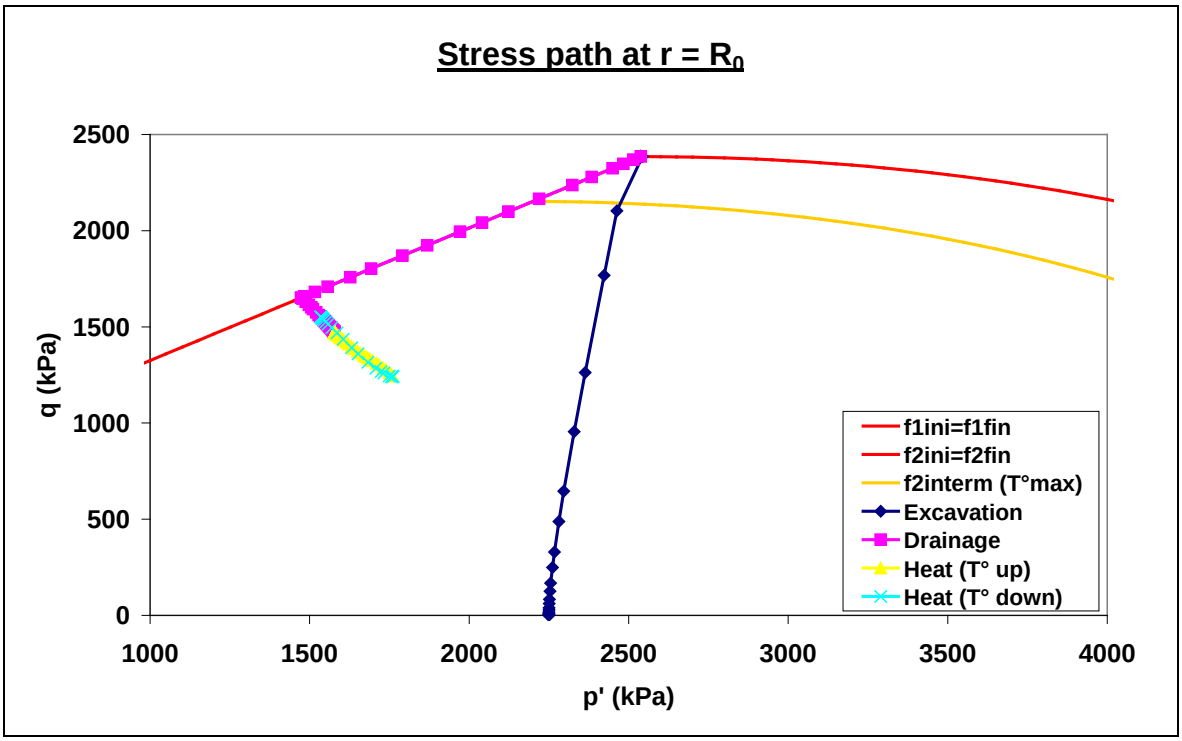

Figure 83 : Stress path at the gallery wall for VHLW after 50 years of cooling (Tim2EA)

The following figure shows the comparison of the stress paths between the reference case (Mohr-coulomb) and the CapSol model with thermal hardening (Tim2EA).

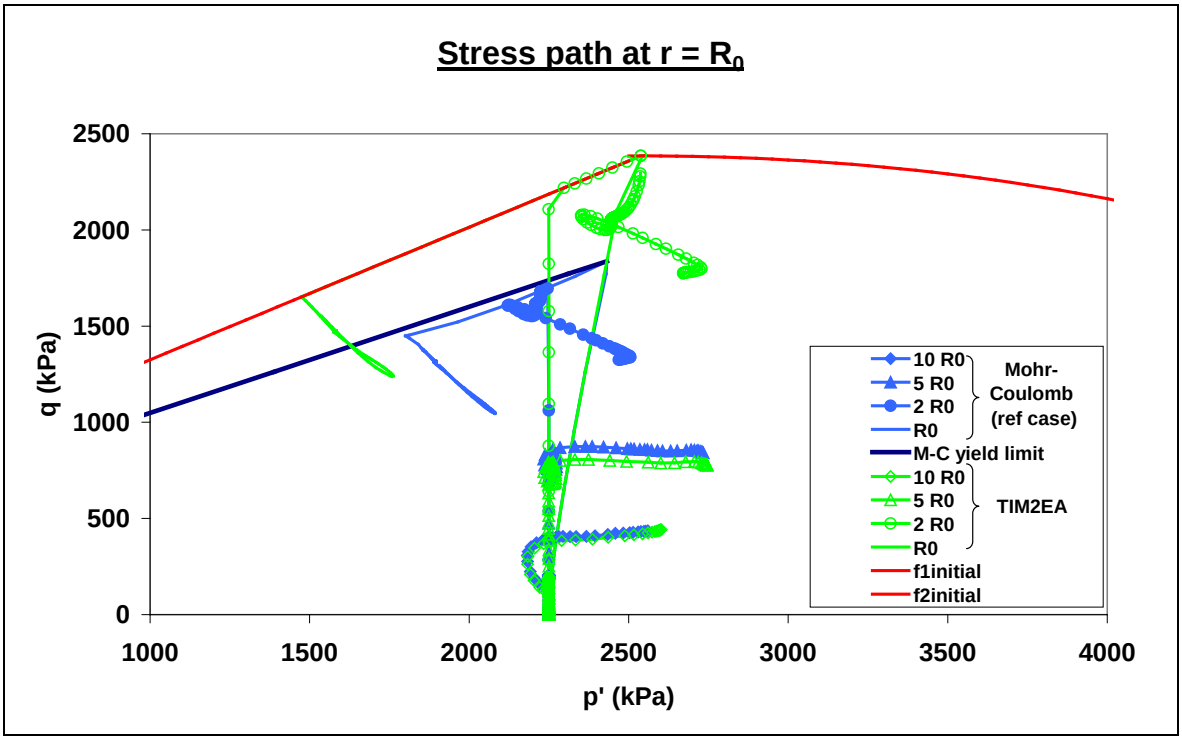

Figure 84 : Comparison of the stress paths for VHLW after 50 years of cooling for 2 constitutive laws (Mohr-Coulomb and Tim2EA)